LBL--14138

DE82 013860

WORKSHOP ON NUCLEAR DYNAMICS

22-26 February 1982
Granlibakken, Tahoe City, California

ORGANIZERS: W. D. Myers, J. J. Griffin, J. R. Huizenga, J. R. Nix, F. Plasil and V. E. Viola

April 1982

This work was supported by the Director, Office of Energy Research, Division of Nuclear Physics of the Office of High Energy and Nuclear Physics of the U.S. Department of Energy under Contract No. DE-AC03-76SF00098.

PREFACE

The Nuclear Dynamics Workshop again proved to be an excellent medium for the presentation and exchange of ideas focusing on a close interaction between theoretical calculations and experimental results. The workshop format enabled the participants to gather informally for many lively discussions, and, as usual, the proceedings tell only half the story. Some of the controversial issues raised at this meeting involved Pauli blocking; a "soggy saddle" model intended to shore up weaknesses of the statistical model; the concept and definition of central collisions; and the amount of deviation from energy conservation a model can be allowed.

The organizers wish to thank Susan Ovuka and Loretta Lizama of TID for their respective work in the advance planning of the conference and the editing of the proceedings. All of us connected with the conference also wish to thank the management and staff of Granlibakken, whose mixture of friendliness and professionalism allowed the workshop to run smoothly and pleasantly.

Jeannette Mahoney

Conference Coordinator

PROGRAM

Page

Monday, February 22, 1982

Morning Session

W.J. Swiatecki, "The Nature of Nuclear Dynamics" 1

C-Y. Wong, "The Viscoelastic Properties of the Nucleus" 12

R. Hasse, "Long-Mean-Free-Path Nuclear Fluid Dynamics to All Orders in the Moments" 17

P. Shuck, "A Boltzmann Equation Approach to the Damping of Zero Sound Modes in Nuclei" 23*

Evening Session

H. Feldmeier, "Dissipation and Fluctuation Caused by Statistical Exchange of Particles" 31

M. Dworzecka, "The 'Wall Formula' for Nuclear Dissipation as Classical Limit of the Damping of Collective Motion in the Time-Dependent RPA" 40

H. Sann, "Dynamics of the Fusion Process Pb+Mg-Ni" . . . . . --+

Tuesday, February 23, 1982

Morning Session

V. Viola, "Linear Momentum Transfer in Nucleus-Nucleus Collisions" 45

T. Awes, "Pre-Equilibrium Light Particle Emission in ^{16}O-Induced Reactions" 50

J. Natowitz, "Fragmentation at 20 to 43 MeV/n" 56

F. Plasil, "Heavy-Ion-Induced Fission in the Rare Earth Region and the Statistical Model" 61

---

*No talk given; written contribution only.
+No written contribution.

Tuesday, February 23, 1982

Evening Session

S. Shlomo, "Pauli Blocking in Finite Nuclei" 67

L. Moretto, "Pre-Fission Neutrons: A Major Failure of the Statistical Model" . . . . . --*

A. Mignerey, "Mass and Charge Distributions in the Reactions of ^{40}Ca and ^{209}Bi with ^{37}Cl" 70

Wednesday, February 24, 1982

Morning Session

K. Frankel, "Deuteron Production in High Energy Heavy Ion Collisions" 74

K. Frankel, "Flow of Nuclear Matter in Heavy Ion Collisions" . . . . . 80+

J. Harris, "Analysis of Relativistic Heavy Ion Collisions Using Collective Variables" . . . . . --‡

J. Randrup, "Complete Events in Medium-Energy Nuclear Collisions" 84

C-Y. Wong, "Particle Production in High-Energy, Heavy-Ion Reactions" . . . . . 88+

Evening Session

P. Danielewicz, "Quantum Description of the Heavy-Ion Collision Process" 93

J. Griffin, "A Physically Asymptotic Hartree-Fock Stationary Phase Approximant to the Many Body S Matrix" 99

E. Bartnik, "Friction and Diffusion in Feynman's Path Integral Method" . . . . . 102+

B. Grammaticos, "RHI and TDHF: The Evolution of the Target" . . . . . 105+

---

*Published as LBL-13880; talk also published in the Proceedings of the Nuclear Excitations Workshop, Hirschegg, Kleinwalsertal, Austria, January 18-23, 1982.

+No talk given; written contribution only.

‡Published as LBL-14255.

Thursday, February 25, 1982

Morning Session Only

A. Warwick, "Target Fragment Production Mechanisms in Relativistic Nuclear Collisions" 110

H. Wieman, "Multiplicities of Slow Target Fragments in Relativistic Heavy Ion Collisions" 116

H. Ritter, "First Experiments with the Plastic Ball" 124

Friday, February 26, 1982

Morning Session Only

P. Hecking, "Pion Production from Heavy-Ion Collisions at 80-400 MeV/n" 131

A. Klar, "Density Fluctuations in Nuclei: Consequences for Relativistic Heavy-Ion Collisions" 135

K-H. Müller, "Subthreshold K^- Production by Coherently Produced ϕ-Meson in Nuclear Collisions" 139

List of Participants 143

THE NATURE OF NUCLEAR DYNAMICS*

W. J. SWIATECKI

Nuclear Science Division
Lawrence Berkeley Laboratory
University of California
Berkeley, California 94720

Several important advances in the description of nuclear dynamics have taken place in the past few years. There are the TDHF calculations, including recent attempts to treat residual interactions, statistical Master Equation approaches and equations of motion with dissipation. To me, one of the clarifying messages, which is coming through the multitude of different approaches that have been taken, is the following:

> "The nature of nuclear dynamics is dominated by the presence or absence of symmetries."

I have prepared a transparency in which I try to put together a number of insights into the nature of nuclear statics and nuclear dynamics and in which the presence or absence of symmetries plays a dominant role.

I will explain the word "Plastodynamics" in the title of the transparency (Fig. 1) at the end of my talk.

The transparency is in two parts, the upper referring to statics, the lower to dynamics. In each part I have isolated two limiting cases: The "Chaotic Regime" at the top and the "Ordered Regime" at the bottom, with a Transitional Regime in between. The Ordered Regime is further subdivided into cases corresponding to Fast and Slow deformations.

---

*This work was supported by the Director, Office of Energy Research, Division of Nuclear Physics of the Office of High Energy and Nuclear Physics of the U.S. Department of Energy under Contract No. DE-AC03-76SF00098.

The Chaotic Regime corresponds to the limiting case in which there are no degeneracies in the single-particle spectrum of the system. Insofar as degeneracies are associated with symmetries, this implies an absence of symmetries.

The Ordered Regime is the limiting case dominated by symmetries of various kinds, leading to strong degeneracies in the single-particle spectrum. (This is actually the more familiar situation on which, for two reasons, a lot of stress has been laid in the past. First, nuclei in their ground states usually seek out symmetric configurations in order to make use of the extra stability associated with a completely filled set of degenerate levels. Second, we only know how to solve the Schrodinger equation analytically in simple situations, characterized by a high degree of symmetry.)

A typical example of a situation dominated by symmetries is the famous Hill-Wheeler Box --an infinitely deep, sharp, box-like potential well, filled with eigenfunctions given by products of three sines: $\sin k_x x \cdot \sin k_y y \cdot \sin k_z z$. (Refs. (1), (2).) It is a prototype of an independent-particle model of a nuclear system. If you fill the Hill-Wheeler potential well with A particles up to a Fermi energy E_F, and then plot the total energy,

$$V = \sum_{i=1}^{A} \varepsilon_i ,$$

against a volume-preserving stretching deformation $1+\alpha$, you find a result shown in the middle of the transparency. (The longitudinal dimension is stretched by a factor $1+\alpha$, the transverse dimensions are compressed by a factor $1+\frac{1}{2}\alpha$.) Each steep, parabola-like curve is the energy $\Sigma\alpha_i$ corresponding to the case when the particles stay

in their original orbitals and the wavelengths are simply stretched in one dimension and compressed in the other, following the deformation of the box. In other words, the nodal structure of each wave function is frozen. The energy for such a constrained deformation rises very steeply and soon exceeds the energy corresponding to the optimum redistribution of particles into the lowest orbitals at the given deformation. The energy corresponding to this optimum redistribution is given by a rippled curve consisting of the bottom pieces of many separate parabolas. The envelope of the parabolas represents the ground-state energy of the system pretty well, except for magic number situations. For example, in the case of the Hill-Wheeler box, A = 60 is a magic number for the cube. Thus the parabola centered at $\alpha = 0$ is anomalously low if A = 60. (See Ref. (2)).

Note that at each deformation there are many parabolas (the different excited states of the total system) and that there are many crossings between them. Such crossings of the energy levels of a system are possible, in general, only because of the symmetries present. (The reflection symmetries in the case of the box).

Suppose now we go over to the Chaotic Regime by putting in dents and corrugations in the sides of the box in order to break down the symmetries. The energy spectrum of the system is now shown in the upper picture in the transparency. The ground-state energy as a function of shape is not very different from what it was before (except that the special stability of the unstretched shape with $\alpha = 0$ has been destroyed). But the excited states are now not allowed to cross and each will be a (somewhat ripply?) curve with a trend more or less like the ground state.

If you look at these two plots of $\Sigma\varepsilon_i$ against deformation, you realize that there are two characteristic stiffnesses in the problem of stretching a prototype nuclear system: the stiff curvature of each parabola, and the soft curvature of the ground-state envelope. The stiff curvature is made up of A contributions, each associated with stretching and squeezing the separate wave functions. The total is proportional to the number of particles in the system and has, therefore, the properties of a coefficient of elasticity of a solid body. It can also be readily shown that the second, soft curvature is proportional to the area of the system and has, therefore, the characteristics of a surface-energy coefficient of a fluid.

The elastic stiffness coefficient for stretching (i.e., quadrupole type) distortions turns out to have a beautifully simple form, viz

$$V(\alpha) = V_o + (\text{coeff})\,\alpha^2, \tag{1}$$

$$\text{where} \quad \text{coeff} = V_o = (\tfrac{3}{5}E_F)A = \text{Total Energy!} \tag{2}$$

The surface-energy coefficient γ can also be calculated and the result can be written as

$$4\pi r_o^2\gamma = \frac{3\pi}{40}\left(\frac{3}{\pi}\right)^{1/3} E_F \quad , \tag{3}$$

where r_o, the radius constant, is related to the density of particles. The actual numerical value of γ, as given by eq. (3), is unimportant, since an infinitely steep wall is not a realistic representation of a nuclear surface. The important result is that the stiffness is proportional to the surface area. Thus the ground-state energy in the Chaotic Regime, and the average trend of the ground state in the Ordered Regime,

both follow the potential energy of a fluid with surface tension. On the other hand, for fast deformations in the Ordered Regime (when the nodal structures remain frozen) and for magic nuclei, the system acts like an elastic solid. Thus, in the Ordered Regime, the elastic response to stretching is given by Eq. (1) and in the Chaotic Regime by

$$V(\alpha) = \text{L.D.} = -c_1(\text{Volume}) + c_2(\text{Area}) + \text{corrections}. \tag{4}$$

The nuclear potential-energy problem is fairly well understood and what I described has been known for many years. It has also been known for some time that one can do a fair job of describing phenomenologically the Transitional Regime in the potential energy by simply multiplying the shell-effect (i.e. the deviation from the Liquid Drop energy, Eq. (4)) by a damping factor

$$e^{-\theta^2} \tag{5}$$

or

$$(1-2\theta^2)\, e^{-\theta^2}\ , \tag{6}$$

where θ is a measure of the deformation from a symmetric, magic number configuration. (Refs. (2), (3)).

In the case of dynamics, the situation is much less clear. In the lower part of the transparency (Fig. 1) I have, nevertheless, made an attempt to order some of the simplest insights in a pattern paralleling the discussion of the statics.

First, in the Chaotic Regime, where there are no symmetries or regularities and the particle motions may be assumed to be randomized, there ought to be some simple limiting form of the dynamics of a large

leptodermous, dolichohodous system, based on statistical, phase-space considerations. It seems fairly certain to me that this limit is represented by combining the Liquid Drop potential energy with the Wall Formula for dissipation and disregarding inertial effects, which appear to be small compared to the dissipation. The result is an astonishingly simple equation of motion for the time evolution of a nuclear shape (Refs. (4), (5), (6)):

$$\frac{dn}{dt} = \frac{P}{\rho\bar{v}} \tag{7}$$

Here dn/dt is the rate of normal displacement of a point on the surface, P is the excess pressure at that point due to the conservative forces (surface tension and electric) and $\rho\bar{v}$ is a characteristic constant of the one-body dissipation theory (the product of the mass density of the system and the mean particle speed, about 1×10^{-22} MeV sec fm^{-4} for a nucleus). Equation (7) is, I believe, the dynamical counterpart of the Liquid Drop potential-energy equation of nuclear statics.

By way of contrast, in the dynamics of the Ordered Regime one has a more complicated situation, with all the crossing parabola-like energy levels. The discussion of this regime has centered since the work of Hill and Wheeler on estimating the probability flow at such crossings or near-crossings. There are the two limiting cases of adiabatic (slow) and diabatic (fast) motion (see, for example, Ref. (7)), where you either stay on the lowest soft envelope level or on one of the stiff parabolas with frozen nodal structure. The introduction of a "friction kernel" seems a natural way to span the two limits and recently Nörenberg has studied a particularly simple equation of motion with such a friction kernel. (Ref. (8)). It is shown in the lower

part of Fig. 1. The friction kernel, with a characteristic amplitude a and a characteristic memory time τ, collects information about the speed of the deformation, $d\alpha/dt$, from $t = o$ to $t = t$, and the force constructed in this way is balanced against an intertial force, proportional to $d^2\alpha/dt^2$. You may easily verify that if the memory is short compared to characteristic dynamical times (i.e. if the motion is slow) the equation reduces to a damped motion. If the motion is fast, the equation reduces to the harmonic oscillator equation. In this limit the system is oscillating up and down one of the stiff elastic parabolas, with the elasticity coefficient given by V_o. It is noteworthy that if this elasticity is combined with an inertia of irrotational flow one gets a resonance frequency for stretching vibrations (as given by Bertsch or Nix & Sierk, see Ref. (9)):

$$\hbar\omega = \frac{(9\pi)^{1/3}}{\sqrt{2}} \frac{\hbar^2}{m r_o^2} A^{-1/3} = 64.7\, A^{-1/3} \text{ MeV},$$

where m is the nuclear mass unit, 931.5 MeV. This is in good agreement with observed giant quadrupole oscillations. (It appears that, in effect, the Bertsch-Nix-Sierk interpretation of the giant resonances is equivalent to treating each volume element of the nucleus as a little Hill-Wheeler box, oscillating elastically with effectively frozen nodal structure.)

If my assignment of the giant resonances to the Ordered Regime, and of the wall formula dynamics to the Chaotic Regime is correct, then the analogy with the statics suggests looking for a phenomenological theory encompassing both limits. Could we do that by inserting some-

where a factor $e^{-\beta^2}$, telling the system about its proximity to a magic, highly symmetric configuration?

Perhaps my transparency may stimulate some attempts in this direction. In any case, I hope that it has helped to bring out the relation between the giant-resonance dynamics and the wall formula dynamics and that it will discourage conclusions along the lines that, if one is confirmed experimentally, the other must be wrong. They each have a place in the appropriate regime of shapes and motions. What the quantitative range of validity is for each regime, is a question not easy to answer from first principles, and we will have to rely heavily on experimental findings and further studies of the Transitional Regime.

It seems clear that we are still a long may from being able to describe quantitatively all the different aspects of nuclear macroscopic dynamics. But I am beginning to have the feeling that we are getting close to a qualitative understanding of how it will probably all come out. The framework needed to support the richness of nuclear dynamics will have to include the description of fluids (ordinary, superfluid and superviscid), as well as the elastic vibrations of solids and, perhaps, their plastic flow. In this connection I would like to finish with a paragraph from a note by Georg Süssmann, entitled "On the continuity between the solid and the liquid state." The note was written in Berkeley in 1973 and remains, I believe, unpublished. In the introduction Süssmann says:

"According to our usual experience there is a rather clear cut distinction between solids and liquids. The vast majority of condensed materials is, under normal conditions, either shape preserving and thus in a solid state, or quickly fluid and thus in a liquid state. (This fact is stressed by the remarkable discontinuity known as melting which seems to extend to very high pressures and temperatures.) Of course, we know of counter examples as tar or (silly) putty, but they are rare and show a rather complicated behavior. There are two phenomena that

bridge the gap between the solids and the fluids: viscosity tends to make a fluid somehow like a solid, whereas relaxation tends to make a solid somehow like a fluid. In the following we will give a short account of these concepts which interpolate between elastodynamics and hydrodynamics in the much broader frame of plastodynamics."

I believe that, in addition to first-principles numerical studies on the lines of TDHF with residual interactions, it will be useful to develop a phenomenological theory of nuclear dynamics. In this endeavor the mathematical structure of Süssmann's plastodynamics should be a useful background.

References

1. D.L. Hill and J.A. Wheeler, Phys. Rev. 89 (1953), 1102, especially Fig. 12.
2. W.D. Myers and W.J. Swiatecki, Nucl. Phys. 81 (1966), 1, especially Fig. 7.
3. W.D. Myers, "Droplet Model of Atomic Nuclei", IFV Plenum, 1977.
4. W.J. Swiatecki, Progr. Particle & Nucl. Phys. 4 (1980), 383.
5. J. Randrup and W.J. Swiatecki, Ann. Phys. (N.Y.) 125 (1980), 193.
6. J.P. Blocki et al., Ann. Phys. (N.Y.) 113 (1978), 330.
7. L. Wilets, "Theories of Nuclear Fission", Clarendon Press, Oxford, 1964.
8. W. Nörenberg, Phys. Lett. 104B (1981), 107.
9. J.R. Nix and A.J. Sierk, Phys. Rev. C21 (1980), 396.

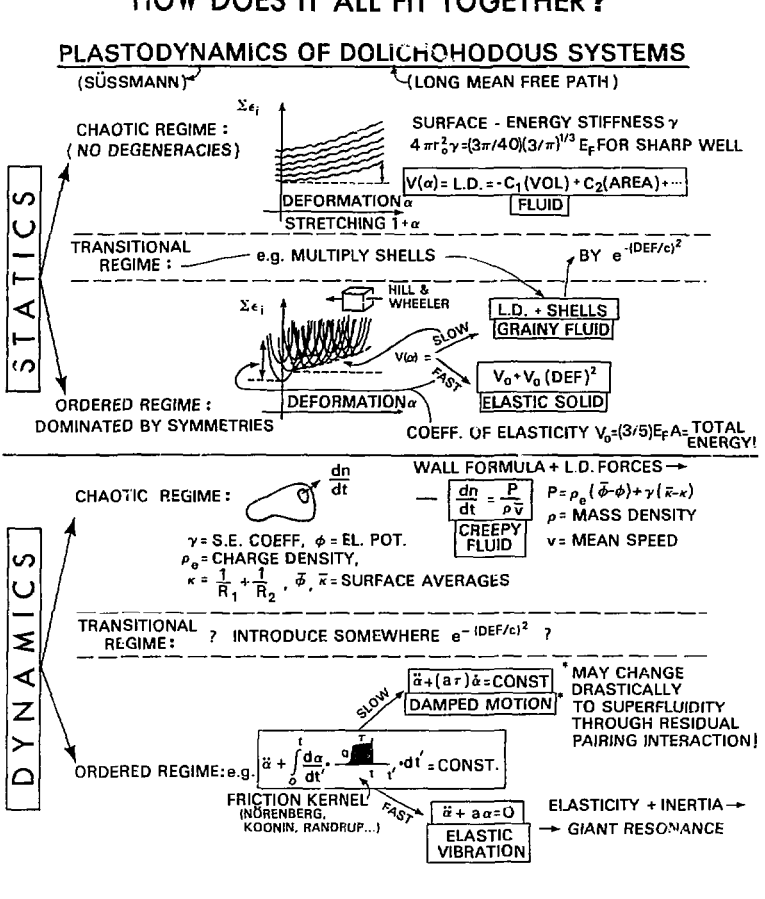

Fig. 1. An attempt to sketch the relation to each other of various limiting theories of nuclear statics and nuclear dynamics. The principal message is that the description of macroscopic nuclear dynamics may be expected to call for a rich mathematical structure, including the theory of fluids (ordinary, superfluid and superviscid) of elastic solids and of plastic flow, depending on the presence or absence of symmetries and regularities in the configurations and deformations in question.

THE VISCOELASTIC PROPERTIES OF THE NUCLEUS

Cheuk-Yin Wong
Oak Ridge National Laboratory*
Oak Ridge, TN 37830

and

Nestor Azziz
University of Puerto Rico
Mayaguez, Puerto Rico 00708

Abstract

The Maxwell solid, which has a short-time elastic behavior and a long-time viscous behavior, cannot properly describe the viscoelastic properties of the nuclear fluid in its ground state. The Voigt solid, which exhibits asymptotically an elastic behavior, is a good model for the nuclear fluid in its ground state.

* * * *

Recently, in the discussion of nuclear collective motion, nuclear giant resonances were successfully described as elastic vibrations of a nucleus,[1-4] although alternative descriptions were also presented.[5,6] In this elastic model, the widths of the giant resonances provide information on the viscoelastic properties of the nuclear fluid and are therefore of great interest.

Previously, in our study of the damping of the giant resonances, it was assumed that the stress tensor originates from both the elastic response and the viscous dissipation.[2] The stress tensor p_{ij} is then the sum of the elastic stress tensor and the viscous stress tensor, as in the dissipation of ordinary solids:[7]

$$p_{ij} = -\mu\left(\frac{\partial D_i}{\partial x_j} + \frac{\partial D_j}{\partial x_i}\right) - \lambda\delta_{ij}\nabla\cdot\vec{D}$$
$$-\eta\left(\frac{\partial u_i}{\partial x_j} + \frac{\partial u_j}{\partial x_i} - \frac{2}{3}\delta_{ij}\nabla\cdot\vec{u}\right) - \zeta\,\nabla\cdot\vec{u} \qquad (1)$$

where $\vec{D}$ is the displacement field, $\vec{u} = \frac{\partial\vec{D}}{\partial t}$ is the velocity field, λ and μ are the Lamé constants and η and ζ are the viscosity coefficients. Perturbative treatments led to reasonable agreement with experiment and the determination of the

*Operated by the Union Carbide Corporation under contract W-7405-eng-26 for the Division of Basic Energy Sciences, U.S. Department of Energy.

viscosity coefficients. Of particular interest is the result that for such a viscoelastic model of the nuclear fluid, the widths of the resonances are proportional to the second power of the resonance energy, in approximate agreement with experimental observations.

The viscoelastic property of a medium consists of a specification relating the stress tensor p_{ij} with the strain tensor $\partial D_i/\partial x_j + \partial D_j/\partial x_i$. Equation (1) is only one of the many possible relationships and represents a class of elastic media known as the Voigt (model) solid[8] which exhibits asymptotically an elastic behavior. There is a different class of media known as the Maxwell solids,[7,8,9] in which the relationship between the stress and the strain is different. Many polymers such as resin are Maxwell solids. They exhibit a short-time elastic behavior but a long-time viscous behavior. There are also media which can be represented by a combination of the Voigt solid elements and the Maxwell solid elements.[8]

We would like to examine the consequences of the nuclear fluid as a Maxwell solid to see whether a description in terms of a Maxwell solid is also consistent with experimental data. In a Maxwell solid, the stress p_{ij} is related to the strain by[7-9]

$$\left(\frac{1}{\eta} + \frac{1}{\mu}\frac{\partial}{\partial t}\right)p_{ij} = -\left(\frac{\partial u_i}{\partial x_j} + \frac{\partial u_j}{\partial x_i}\right) \quad \text{for } i \neq j, \tag{2}$$

and

$$\left(\frac{1}{\zeta} + \frac{1}{\lambda + \frac{2}{3}\mu}\frac{\partial}{\partial t}\right)\frac{1}{3}\sum_{i=1}^{3} p_{ii} = -\nabla\cdot\vec{u}. \tag{3}$$

We shall adopt the perturbative approach and examine small deviations from elastic vibrations due to the presence of viscosity. In this approach, the time dependence of p_{ij} and D_i in Eqs. (2) and (3) is approximately given by $e^{i\omega_0 t}$ where ω_0 is the frequency of the unperturbed oscillation. Thus, we have

$$p_{ij} = -\mu'(\partial D_i/\partial x_j + \partial D_j/\partial x_i) \quad \text{for } i \neq j, \tag{4}$$

and

$$\frac{1}{3}\sum_{i=1}^{3} p_{ii} = -\left(\lambda' + \frac{2}{3}\mu'\right)\nabla\cdot\vec{D}, \tag{5}$$

where

$$\mu' = \frac{\mu}{1 - i\mu/\omega_0\eta}, \tag{6}$$

and

$$\lambda' + \tfrac{2}{3}\mu' = \frac{\lambda + \frac{2}{3}\mu}{1 - i(\lambda + \frac{2}{3}\mu)/\omega_0\zeta}. \tag{7}$$

The equation of motion is

$$\frac{\partial^2\vec{D}}{\partial t^2} = -\sum_j \nabla_j p_{ij} = (\lambda'+\mu')\nabla(\nabla\cdot\vec{D}) + \mu'\nabla^2\vec{D} \tag{8}$$

with the solution

$$\vec{D}(\vec{r},t) = [A_1\vec{\mathcal{D}}_1(\vec{r}) + A_2\vec{\mathcal{D}}_2(\vec{r}) + A_3\vec{\mathcal{D}}_3(\vec{r})]e^{i\omega t} \tag{9}$$

where, as given by Lamb,[10,2] $\vec{\mathcal{D}}_1$ is a compressional and irrotational displacement and $\vec{\mathcal{D}}_2$ and $\vec{\mathcal{D}}_3$ are isovolumetric and rotational displacements.

For a solution which consists of a $\vec{\mathcal{D}}_1$-type displacement, the effect of viscosity is to change the frequency from ω_0 to

$$\omega = \omega_0 + \frac{i}{2(\lambda+2\mu)}\left[\frac{(\lambda + \frac{2}{3}\mu)^2}{\zeta} + \frac{\frac{4}{3}\mu^2}{\eta}\right] \tag{10}$$

which corresponds to a width of

$$\Gamma = \frac{\hbar}{\lambda+2\mu}\left[\frac{(\lambda + \frac{2}{3}\mu)^2}{\zeta} + \frac{\frac{4}{3}\mu^2}{\eta}\right]. \tag{11}$$

Similarly, for a $\vec{\mathcal{D}}_2$- or $\vec{\mathcal{D}}_3$-displacement, the shear viscosity changes the frequency from ω_0 to

$$\omega = \omega_0 + \frac{i\mu}{2\eta} \tag{12}$$

which corresponds to a width of

$$\Gamma = \frac{\hbar\mu}{\eta}. \tag{13}$$

We can compare the experimental giant resonance widths with Eqs. (11) and (13). The isoscalar monopole resonance involves only compressional flows represented by a $\mathcal{Y}_0$-type displacement. So, the widths of the monopole resonance are given by Eq. (11) for a Maxwell solid. On the other hand, even though the isoscalar giant quadrupole and octupole resonances involve both a $\mathcal{Y}_1$- and a $\mathcal{Y}_3$-displacement, the flow is mainly incompressible. It is reasonable to treat these modes as a purely incompressible $\mathcal{Y}_3$-displacement in evaluating the effects of damping. The widths of the 2^+ and 3^- isoscalar resonances can then be estimated by Eq. (13).

When the comparison with experimental data is made, we find that Eqs. (11) and (13) cannot agree with the experimental data, as they give widths which are independent of the resonance energies and are the same for quadrupole and octupole resonances. In contrast, experimental data show that the widths for the octupole resonances are about twice that of the quadrupole resonances and the widths for 2^+ and 3^- decrease with increasing mass numbers. The isoscalar giant resonances do not appear to behave like a Maxwell solid! They behave more like a Voigt solid as shown previously.[2]

How do we understand the viscoelastic properties of the nuclear fluid in light of the above results? Here, we shall discuss only the viscosity properties and not the elastic properties (which are found to have their origin in the quantum stress tensor).[2,11] The Voigt solid is asymptotically (in time) an elastic solid. The presence of viscosity is only to retard the realization of its elastic properties. The Maxwell solid is asymptotically a very viscous fluid but has a short-time elastic behavior. It is well known that a normal Fermi liquid at low temperatures is very viscous,[12] as the mean-free path is very large. It appears that the Maxwell solid may be a good model for the nuclear fluid. However, this need not be true at very low temperatures. Below a critical temperature of a few MeV, the pairing interaction leads to a superfluid condensate and the viscosity can become very small.[13] It is thus not surprising that the Voigt solid, which is essentially an elastic solid, is successful in describing the widths of the isoscalar giant resonances near the ground states. The Maxwell solid, which is essentially a very viscous fluid with a short-time elastic behavior, cannot describe the nuclear fluid at $T \simeq 0$. The situation may change as the temperature increases. Above the critical temperature of a few MeV, there may be a phase transition in which the nuclear fluid changes from a superfluid to a normal Fermi fluid with large shear viscosity coefficients for which a Maxwell solid may perhaps be a better description. Investigation of the widths of the giant resonances for a nucleus at a high temperature, as may be found in heavy-ion collisions, will be of interest in mapping out such a transition.

The authors would like to thank Dr. R. Hasse for critical comments and helpful discussions.

References

1. G. F. Bertsch, Ann. Phys. (N.Y.) 86, 138 (1974); Nucl. Phys. A249, 253 (1975).

2. C. Y. Wong and J. A. MacDonald, Phys. Rev. C 16, 1196 (1977); C. Y. Wong and N. Azziz, Phys. Rev. C 24, 2290 (1981).

3. J. R. Nix and A. J. Sierk, Phys. Rev. C 21, 396 (1980).

4. R. W. Hasse, A. Lumbroso, and G. Ghosh, Proceedings Workshop on Semi-classical Aspects of Description of Nuclei (Grenoble, 1981), ILL Report, Grenoble, 1981, No. 16; R. W. Hasse, A. Lumbroso, and G. Ghosh, Proceedings International Workshop IX on Gross Properties of Nuclei and Nuclear Excitations (Hirschegg, 1981), ed. H. Feldmeier, T. H. Darmstadt, 1981, p. 44; R. W. Hasse, G. Ghosh, J. Winter, and A. Lumbroso (preprint).

5. N. Auerbach and A. Yeverechyahu, Ann. Phys. (N.Y.) 95, 35 (1975).

6. G. Holzwarth and G. Eckart, Z. Phys. A284, 291 (1978).

7. L. D. Landau and E. M. Lifshitz, Theory of Elasticity, Pergamon Press, London, 1959.

8. D. R. Bland, The Theory of Linear Viscoelasticity, Pergamon Press, New York, 1960.

9. S. Middleman, The Flow of High Polymers, Interscience Publishers, New York 1968.

10. H. Lamb, Lond. Math. Soc. Proc. 13, 278 (1882).

11. C. Y. Wong, J. Math Phys. 19, 1008 (1975).

12. L. D. Landau, Zh. Eksp. Teor. Fiz. 32, 59 (1957) [Sov. Phys. JETP 5, 101 (1957)].

13. C. J. Pethick, et al., Phys. Rev. Lett. 34, 643 (1975).

LONG-MEAN-FREE-PATH NUCLEAR FLUID DYNAMICS TO ALL ORDERS IN THE MOMENTS*

Rainer W. Hasse
Institut Laue-Langevin, 156X, 38042 Grenoble Cedex, France

and

Gautam Ghosh
Sektion Physik, Universität München, Garching, Germany

After the first derivation of elastic forces in vibrating nuclei from the RPA-equations by Bertsch[1] the subject of semiclassical models of isoscalar giant resonances has gained widespread attention. Holzwarth and Eckart[2], Wong et al.[3], Nix and Sierk[4] then derived the same properties by employing the dynamical Thomas-Fermi approximation, the Madelung-Bohm quantum potential, or the collisionless Vlasov equation, respectively. In order to solve the fluid dynamical equations for the isoscalar giant resonance frequencies, these authors either used no approximation, or a sharp density, or a sharp density and potential flow, respectively, but all authors truncated the Euler or dynamical Thomas-Fermi equations after the pressure tensor, i.e. after the second moments. Later on, starting with the many-particle Schrödinger equation, Winter[5] derived a full set of fluid dynamical equations to all moments but did not solve for them. Simultaneously, Yukawa and Holzwarth[6] also put forward a similar set of equations based on Landau's theory of Fermi liquids, cf. refs.[7], and solved for the dispersion relations.

In previous papers[8], we therefore adopted Winter's scheme and solved for the isoscalar giant resonance energies including effects of the third and fourth moments and found large enhancements up to 40 % of the electric surface vibrational modes 2^+, 3^-, 4^+... In these papers we concluded that moment expansions converge very slowly by the fact that the expansion parameter is of order unity.

In this paper, we propose a new scheme based on a moment expansion of the collisionless Vlasov equation which we are able to sum up to all orders and to solve for the eigenmodes. Let $f(\vec{r},\vec{v},t)$ be the Boltzmann distribution function and $\vec{F}(\vec{r})$ be an external force, then in the limit of a large mean free path the collisionless Vlasov or Boltzmann equation reads

$$\frac{\partial f}{\partial t} + v_\alpha \frac{\partial f}{\partial x_\alpha} + \frac{F_\alpha(x)}{m} \frac{\partial f}{\partial v_\alpha} = 0 \quad . \tag{1}$$

By multiplying eq. (1) with powers of the particle velocity components and using the density ρ, fluid dynamical velocity $\vec{u}$, pressure tensor $\vec{P}$ and higher moments $P_{ij\ldots n}$ according to

* Supported by Deutsche Forschungsgemeinschaft.

$$\rho = m \int f \, d^3v$$

$$\rho u_i = m \int f \, v_i d^3v$$

$$P_{ij} = m \int f (v_i - u_i)(v_j - u_j) d^3v$$

$$P_{ij\ldots n} = m \int f (v_i - u_i)(v_j - u_j)\ldots(v_n - u_n) d^3v \quad , \tag{2}$$

we obtain the following set of equations.

$$- i\omega \rho^1 = \rho_o \frac{\partial u_\alpha}{\partial x_\alpha} \tag{3a}$$

$$- i\omega u_i = \frac{1}{\rho_o} \frac{\partial}{\partial x_\alpha} P^1_{i\alpha} - \frac{F_i}{m} \tag{b}$$

$$- i\omega \; P^1_{ij} = \frac{\partial}{\partial x_\alpha} \left[P^1_{ij\alpha} + \left\{ P^o_{ij} \, u_\alpha \right\}_{ij\alpha} \right] \tag{c}$$

$$- i\omega \; P^1_{ijk} = \frac{\partial}{\partial x_\alpha} \; P^1_{ijk\alpha} - \frac{1}{\rho_o} \left\{ P^o_{ij} \frac{\partial}{\partial x_\alpha} \; P^1_{k\alpha} \right\}_{ijk} \tag{d}$$

$$- i\omega \; P^1_{ijk\ell} = \frac{\partial}{\partial x_\alpha} \left[P^1_{ijk\ell\alpha} + \left\{ P^o_{ijk\ell} u_\alpha \right\}_{ijk\ell\alpha} \right] \tag{e}$$

$$- i\omega \; P^1_{ijk\ell m} = \frac{\partial}{\partial x_\alpha} \; P^1_{ijk\ell m\alpha} - \frac{1}{\rho_o} \left\{ P^o_{ijk\ell} \frac{\partial}{\partial x_\alpha} P^1_{m\alpha} \right\}_{ijk\ell m} \tag{f}$$

Here we treated the harmonic vibration with frequency ω as a small perturbation, $f = f^\circ + f^1$, as well as the density and moments, and linearized the results. The symbol $\{.....\}_{ij\ldots\ell}$ denotes symmetrization by cyclic permutation of the indices. The higher moment equations are easily written down by adding the appropriate number of indices. The zero order quantities are evaluated with f° being the zero temperature Fermi distribution, i.e. a step function up to the Fermi velocity v_F,

$$\rho_o = \frac{4}{3} \pi \, v_F^3 \qquad , \; p_o = \frac{1}{5} \rho_o \, v_F^2$$

$$P^\circ_{i_1 i_2 \ldots i_{2\nu}} = \frac{3}{(2\nu+3)!!} \; \rho_o \, v_F^{2\nu} \; \delta_{i_1 i_2 \ldots i_{2\nu}} \; , \tag{4}$$

where $\delta_{i_1 i_2 \ldots i_{2\nu}}$ is the totally symmetric Kronecker symbol which consists of $(2\nu-1)!!$ different terms, each being the product of ν Kronecker symbols with two indices.

In ref.[8] the fluid dynamical equations for $\vec{u}$ were obtained in treating the set (3) as an expansion in $1/i\omega$, i.e. neglecting the first terms on the r.h.s. of eqs. (3c,e), truncating after eq. (3e) and inserting the remaining equations into each other. Here we solve eq. (3b) for $\partial P^1_{i\alpha}/\partial x_\alpha$ and insert it in the odd equations (3d, f...). Subsequent insertion of a higher equation into

a lower one for the 2n-th truncation simply gives

$$(i\omega)^{2n}\,\rho_o\left(u_i - \frac{F_i}{mi\omega}\right) = \frac{\partial^{2n}}{\partial x_{\alpha_1}\cdots\partial x_{\alpha_{2n}}}\left\{P^o_{\alpha_1\cdots\alpha_{2n}}u_i\right\}_{i\alpha_1\ldots\alpha_{2n}}$$

$$+\sum_{\nu=1}^{n-1}(i\omega)^{2(n-\nu)}\frac{\partial^{2\nu}}{\partial X_{\alpha_1}\cdots\partial X_{\alpha_{2\nu}}}\left\{P^o_{\alpha_i\ldots\alpha_{2\nu}}\frac{F_i}{mi\omega}\right\}_{i\alpha_1\ldots\alpha_{2\nu}}. \qquad (5)$$

For the time being we do not consider external forces nor self-consistent potentials which, actually, should be employed in the Vlasov equation. As in ref.[8], we rather compensate for them by the introduction of an external pressure p. The eq. (5) together with (4) can easily be written as

$$\vec{u} + \frac{1}{\rho_o i\omega}\,\mathrm{grad}\;p = \left(\frac{v_F}{\omega}\right)^{2n}\left[\frac{3(-)^n}{2n+3}\,(\mathrm{grad\ div})^n + \frac{3}{(2n+1)(2n+3)}\,\mathrm{curl}^{2n}\right]\vec{u}\ . \qquad (6)$$

For incompressible nuclei, eq. (6) has the solution (case a)

$$\vec{u} = A_\ell\,\mathrm{curl}^2\,(j_\ell(kr)\,\vec{r}\,Y_{\ell o}) + B_\ell\,\mathrm{grad}\,(r^\ell\,Y_{\ell o}) \qquad (7a)$$

$$p = -\rho_o\,i\omega\,B_\ell\,r^\ell\,Y_{\ell o}\ ,$$

whereas for compressible nuclei without external pressure the normal parity solution reads (case b)

$$\vec{u} = A_\ell\,\mathrm{curl}^2\,(j_\ell(kr)\,\vec{r}\,Y_{\ell o}) + B_\ell\,\mathrm{grad}\,(j_\ell(hr)\,Y_{\ell o}). \qquad (7b)$$

On the other hand, the monopole solution is (case c)

$$\vec{u} = A_\ell\,j_1(hr)\vec{r}/r \qquad (7c)$$

and the abnormal parity solution is (case d)

$$\vec{u} = A_\ell\,\mathrm{curl}\,(j_\ell(kr)\vec{r}\ \ Y_{\ell o}). \qquad (7d)$$

With these solutions, the dispersion relations for the longitudinal velocity of sound $c_L = \omega/\hbar v_F$ and the transversal one $c_T = \omega/\hbar v_F$ relative to the Fermi velocity become

$$c_L = \left(\frac{3}{2n+3}\right)^{1/2n}\ , \qquad c_T = \left(\frac{3}{(2n+1)(2n+3)}\right)^{1/2n}\ . \qquad (8)$$

In the case of second order truncation, $2n = 2$, i.e. for the ordinary elastic model, all three truncation schemes of ref.[6], ref.[8] and of this paper, yield the same dispersion relations, $c_L = \sqrt{3/5}$, $c_T = \sqrt{1/5}$, whereas for instance for the fourth order truncation one obtains

	$\pm c_L$	$\pm c_T$
Y & H, ref.[6]	0, .54, .91	.29, .77
HGW & L, ref.[8]	.31i, .84	.37i, .58
This paper	.60(1±i), .85i, .85	.46(1±i), .65i, .65

Our schemes, hence, give only one real solution which we consider the physical one. On the other hand, for infinite truncation, $2n \to \infty$, we obtain the limits $c_L = c_T \to 1$ as required by the Landau theory[6,7].

The eigenfrequencies are determined by the Laplace boundary condition that the radial-radial pressure P^1_{rr} at the surface equals the isotropic pressure p and by the boundary condition that the radial-tangential pressure $P^1_{r\theta}$ vanishes at the surface. Furthermore, normalization is given by the Neumann boundary condition that the radial component of the fluid velocity u_r equals the boundary velocity. This pressure tensor, entering in the Euler equation of motion (3b) is given analogously to eq.(5) by

$$- (i\omega)^{2n-1} P^1_{ij} = \frac{\partial^{2n-1}}{\partial x_{\alpha_1} \cdots \partial x_{\alpha_{2n-1}}} \left\{ P^\circ_{ij\alpha_1 \cdots \alpha_{2n-2}} u_{\alpha_{2n-1}} \right\}_{ij\alpha_1 \cdots \alpha_{2n-1}}$$

$$+ \sum_{\nu=1}^{n} (i\omega)^{2(n-\nu)} \frac{\partial^{2\nu-1}}{\partial x_{\alpha_1} \cdots \partial x_{\alpha_{2\nu-1}}} \left\{ P^\circ_{ij\alpha_1 \cdots \alpha_{2\nu-2}} \frac{F_{\alpha_{2\nu-1}}}{mi\omega} \right\}_{ij\alpha_1 \cdots \alpha_{2\nu-1}} \tag{9}$$

It can be written in vector form,

$$P^1_{ij} = \frac{i\rho_o v_F^2}{\omega} \left(\frac{\partial w_i}{\partial x_j} + \frac{\partial w_j}{\partial x_i} + \frac{1}{n} \delta_{ij} \operatorname{div} \vec{w} \right), \tag{10}$$

where, for instance for case b, the vector $\vec{w}$ reads

$$\vec{w} = c_L^2 \vec{A} + \frac{n}{2n+1} c_T^2 \vec{B} \tag{11}$$

and $\vec{A}$, $\vec{B}$ are the first and second terms of the r.h.s. of eq. (7b), respectively. For the cases a, c, d, similar expressions hold and the limits $n \to \infty$ can easily be performed. Finally, we obtain the energies of isoscalar giant resonances

$$\hbar\omega = \frac{\hbar v_F x}{r_o A^{1/3}} = 45.7 \text{ MeV } A^{-1/3} x \qquad (12)$$

in terms of the dimensionless wave number x which, for the cases indicated, is the solution of one of the following characteristic equations,

$$2(\ell^2 - 1) - x^2 + 2 f_\ell(x) = 0 \qquad (13a)$$

$$x^2[(\ell-1)(3\ell+2)-x^2] - 2f_\ell(x)\,[(\ell-1)(2(\ell+1)^2+\ell)-2x^2] + 2f_\ell^2(x)\,[\ell(\ell+2)-2] = 0 \qquad (13b)$$

$$x^2 - 2f_o(x) = 0 \qquad (13c)$$

$$\ell - 1 - f_\ell(x) = 0 \quad , \qquad (13d)$$

where $f_\ell(x) = x j_{\ell+1}(x)/j_\ell(x)$. The resulting energies in units of $\text{MeV}/A^{1/3}$ are listed in the following table together with those obtained with the second and fourth truncation schemes.

Mode	exp	2nd		4th		∞ th	
		inc.	comp.	inc.	comp.	inc.	comp.
2^+	60-68	54.5	54.2	74.1	73.3	137.9	275.5
2^{+*}	-	81.8	99.5	141.7	117.8	234.1	382.8
3^-	105-120	81.9	80.1	113.1	109.8	220.7	339.9
4^+	-	105.8	102.4	146.9	140.3	303.6	401.4
0^+	75-85		90.8		92.3		95.1
1^-	126 ?		70.0		84.9		114.4
1^+	-		118.4		152.8		263.6
2^-	-		51.4		66.3		114.4

In concluding this study we note that those modes which do not involve large deformations of the Fermi sphere, namely the monopole breathing and the dipole squeezing modes, are only moderately affected by the higher moments. The monopole energy can be brought down to the experimental value by employing a surface dependent compressibility, see ref.[8]. Also the quadrupole twist mode, although not yet being observed experimentally, lies at a reasonable energy. The fact that the 1^- and 2^- modes have the same energy is accidental since they obey the same characteristic equation. The normal parity modes, on the other hand, which correspond to large deformations of the Fermi sphere, lie much too high, well above the experimental values. This gives rise to the conjecture that the higher moments or, equivalently, the higher multipole deformations of the Fermi sphere, must be damped by some mechanism. This can either be the effect of the finite nuclear mean free path which would also explain the large widths of the isoscalar giant resonances or the smooth nuclear and Fermi surfaces. All

these effects up to now have been neglected but work is under way to take into account one or the other of these effects.

References :

1. G.F. Bertsch, Ann. Phys. 86 (1974) 138; Nucl. Phys. A249 (1975) 253.
2. G. Holzwarth and G. Eckart, Z. Phys. A283 (1977) 219; Z. Phys. A284 (1978) 291; Nucl. Phys. A325 (1979) 1.
3. C.Y. Wong and J.A. MacDonald, Phys. Rev. C16 (1977) 1196; C.Y. Wong and N. Azziz, Phys. Rev. C24 (1981) 2290.
4. J.R. Nix and A.J. Sierk, Phys. Rev. C21 (1980) 396.
5. J. Winter, Proc. Workshop on Semiclassical Methods in Nuclear Physics, Grenoble 1981 (ILL-report, Grenoble, 1981) no. 15; Submitted to Ann. Phys.
6. T. Yukawa and G. Holzwarth, Nucl. Phys. A364 (1981) 29.
7. A.A. Abrikosov and I.M. Khalatnikov, Rep. Prog. Phys. 22 (1959) 329; P. Nozières, Theory of Interacting Fermi Systems (Benjamin, New York, 1964); G.E. Brown, Many-Body Problems (North-Holland/American Elsevier, Amsterdam/ New York, 1972).
8. R.W. Hasse, A. Lumbroso and G. Ghosh, Proc. Int. Workshop IX on Gross Properties of Nuclei and Nuclear Excitations, Hirschegg 1981 (TH Darmstadt-Report, Darmstadt, 1981) p. 45; R.W. Hasse and G. Ghosh, Proc. Workshop on Semiclassical Methods in Nuclear Physics, Grenoble 1981 (ILL-report, Grenoble, 1981) no. 16; R.W. Hasse, G. Ghosh, J. Winter and A. Lumbroso, Submitted to Phys. Rev. C.

A Boltzmann Equation Approach to the Damping of Zero Sound Modes in Nuclei *

P. Schuck,* Institut Laue-Langevin, Grenoble, France
J. Winter, University of Munich, Sektion Physik, Garching, Germany

Abstract

The Vlasov equation plus collision term (Boltzmann equation) represents an appropriate frame for the treatment of giant resonances (zero sound modes) in nuclei. With no adjustable parameters we seem to obtain correct positions and widths for e.g. the giant quadrupole resonances.

1. Introduction

It is well known [1] that schematic forces of the multipole-multipole type give a surprisingly good description of giant resonances within the RPA - or equivalently the TDHF-approach; this concerns for instance the position of energies and to a lesser extent transition densities but it is of course impossible within this formalism to account for the (spreading) width of the giant resonances (we treat here intermediate to heavy nuclei for which the decay or escape width should be negligible).

We will be concerned with the giant quadrupole resonance only but our theory is applicable for other multipoles as well. For our model (harmonic oscillator plus quadrupole-quadrupole force) the Vlasov equation becomes indentical to the TDHF-equation. A further helpful feature is the fact that for our (time dependent) harmonic potential moments of the Vlasov equation with respect to powers of the momentum break off after the second. This means that the coupled fluid dynamic equations for density, velocity and pressure tensor are still exact.

To account for damping we include a collision term [2] to the Vlasov equation but still break off the moments after the second, in view of what we said above certainly a very good approximation. For the collision integral we take the form of Ueling-Uhlenbeck [3] which has certain approximative features as for instance energy conservation of the quasiparticle energies during the collision process; this, however, does not seem to be a serious drawback since we will be able to explain the width of the giant quadrupole resonance quantitatively.

---

* Member of the Heisenberg fellowship.

For the two body collisions we take the s-wave part of the Gogny force which for energies around the Fermi surface is still the dominant contribution [4] . The Gogny force [5] has been chosen because it is a good phenomenological representation of a microscopic G-matrix,and also its scattering length and effective range are very close (for the s-wave part) to experimental values deduced from nucleon-nucleon scattering experiments. The fact that we use different effective forces in the collision integral and for the mean field is not contradictory since they have to describe very different processes.

In this way we arrive at a model [6] for the full description of the giant quadrupole resonance which is parameter free (the strength of the quadrupole-quadrupole force is as usual determined from the self-consistency condition of the harmonic oscillator).

2. The model

Our basic equation is the Boltzmann equation :

$$\frac{\partial f}{\partial t} - \frac{\vec{p}}{m}\frac{\partial f}{\partial \vec{R}} + \frac{\partial V}{\partial \vec{R}}\frac{\partial f}{\partial \vec{p}} = I[f] = \int d^3p' d^3p_1 d^3p_1' \; v^2(\vec{p}-\vec{p}_1)\; \delta(\vec{p}+\vec{p}'-\vec{p}_1-\vec{p}_1') \times \delta\left(\frac{1}{2m}(p^2+p'^2-p_1^2-p_1'^2)\right)\; [\bar{f}\bar{f}' f_1 f_1' - f f' \bar{f}_1 \bar{f}_1'] \tag{1}$$

where $\bar{f} = 1-f$ and $f' = f(\vec{R},\vec{p}',t)$ etc., $v(p)$ is the Fourier transform of the two body interaction and the mean field is given by

$$V(\vec{R},t) = \frac{1}{2} m \omega_o^2 R^2 - \chi q(t)\, \hat{Q} = : \frac{1}{2} m \left(\Omega_x^2(t) x^2 + \Omega_y^2(t) y^2 + \Omega_z^2(t) z^2\right)$$

$$q(t) = \mathrm{Tr}(\hat{Q}\rho(t)); \qquad \hat{Q} = 2z^2 - x^2 - y^2 \tag{2}$$

For this potential the left hand side of (1) is the exact transcription into Wigner space of $i\hbar\dot{\rho} = [h,\rho]$ and in general it is the $\hbar = 0$ limit of TDHF.

The left hand side of (1) can be solved analytically (up to classical eqs. of motion). The result is :

$$f(\vec{R},\vec{p},t) = F(\lambda - \hat{H}) \tag{3}$$

where $F(x)$ is an arbitrary function and

$$\tilde{H} = \frac{1}{2m} \sum_{i=1}^{3} (\tilde{p}_i^2 + \frac{m}{2} \Omega_i^2 \tilde{x}_i^2)$$

$$\tilde{p}_i = \xi_i (p_i - m u_i) \quad ; \quad \tilde{x}_i = \frac{x}{\xi_i} \; ; \; u_i = \dot{a}_i x_i \; ; \; a_i = \ln \xi_i \tag{4}$$

where the parameter ξ_i obey the (coupled) set of classical equations :

$$\ddot{\xi}_i - \frac{\Omega_i^2(0)}{\xi_i^3} + \Omega_i^2(t)\, \xi_i = 0 \qquad \xi_i(0) = 1 \; ; \; \dot{\xi}_i(0) = 0 \tag{5}$$

In the small amplitude limit, χ being determined from the usual oscillator self-consistency condition, this yields the well known result [1] $\omega_{2^+} = \sqrt{2}\, \omega_o = 60\, A^{-1/3}$ MeV in very good agreement with experiment.

For small amplitudes it is possible to develop (3) around equilibrium $F_o(\lambda - H)$ where F_o is now the Wigner transform of the groundstate density matrix. For what follows it is very important not to choose for F_o a step function as would be suggested by lowest order Thomas Fermi theory [7]. This would correspond to an infinite Fermi system at zero temperature ($T = 0$) and consequently no two body collisions can take place since the collision integral is proportional to T^2 [8]. Nuclei are at zero temperature but even there a smearing out of the Fermi step function is present due to either two body correlations or, most importantly the finiteness of the system. For a harmonic potential one can deduce such a fictitious "temperature" from a Strutinsky averaged Wigner transform of the density matrix [9]. One obtains a value constant over the nucleus of $T_{eff} = 4$ MeV which is a rather high value indeed. More realistic is a Woods Saxon potential for which we show in Fig. 1 the phase space distribution [10] for A = 184 and in Fig. 2 the corresponding "temperature" is extracted in fitting to the curves in Fig. 1 a Fermi distribution

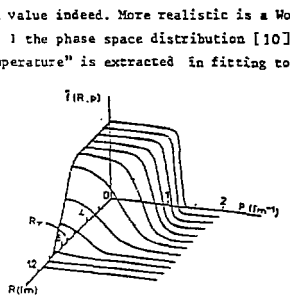

Fig. 1

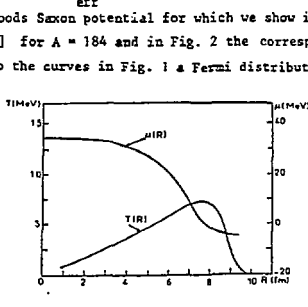

Fig. 2

of the type

$$f(R,p) = \left[1 + \exp\left(\frac{\varepsilon_p - \mu(R)}{T(R)}\right)\right]^{-1} \quad , \varepsilon_p = \frac{p^2}{2m} \tag{6}$$

We see that here the temperature is strongly varying from small values in the interior to rather high values in the surface. In spite of this fact the Fermi function (6) can be quite effectively represented by distributions

$$f = \theta(\mu - \varepsilon_p) - \frac{\pi^2}{6} T^2 \delta'(\mu - \varepsilon_p) \tag{7}$$

which then helps very much to perform the integrals in (1). Taking in addition moments of (1) with respect to $\vec{p}$ and truncating after second order we obtain [11]

$$\dot{\rho} = \mathrm{div}(\rho \vec{u})$$

$$m\left(\frac{\partial}{\partial t} + u_k \frac{\partial}{\partial x_k}\right) u_i = -\frac{\partial V}{\partial x_i} - \frac{1}{m\rho} \frac{\partial}{\partial x_k} \rho P_{ki} \tag{8(a-c)}$$

$$\left(\frac{\partial}{\partial t} - \frac{1}{\tau} + u_k \frac{\partial}{\partial x_k}\right) P_{kp} + P_{ki} \frac{\partial}{\partial x_i} u_p + (k \leftrightarrow p) = 0$$

Here we used summation convention and ρ, $\vec{U}$, $\overleftrightarrow{P}$ are the zeroeth first and second moment of f. As we said above these equations are exact in our model for vanishing collision term that can be verified with (2) and (4). In the small amplitude limit the inverse collision time turns out to be :

$$\frac{1}{\tau(R)} = \frac{\pi^2}{6} T^2(R) (3\pi^2\rho)^{-5/3} \int_0^{2(3\pi^2\rho)^{1/3}} dp\, p^2 (4(3\pi^2\rho)^{2/3} - p^2)\, v^2(p) \tag{9}$$

In the case of a superposition of Gaussians like the Gogny force even the last integral in (9) can be performed analytically and we get therefore an explicit expression for the local collision time.

If we write the pressure tensor as

$$P_{ik} = \frac{m}{\rho} p^{id} \eta_{ik} \tag{10}$$

where $p^{id} = ((3\pi^2)^{2/3}/5)\rho^{5/3}$ then we obtain for π_{ik} from (8c) in the small amplitude limit :

$$\pi_{ij} = \delta_{ij} - \int_{-\infty}^{t} dt' \, e^{-\frac{t-t'}{\tau}} \left(\frac{\partial u_i}{\partial x_j} + (i \leftrightarrow j) - \frac{2}{3} \frac{\partial u_i}{\partial x_i} \delta_{ij} \right)_{t'} \tag{11}$$

In this limit we have in our model

$$\vec{u}(t) = \delta(t) \vec{u} \; ; \qquad \vec{u} = (-x, -y, 2z) \tag{12}$$

and therefore we obtain a position independent π_{ij} if we introduce an effective inverse collision time averaged over the pressure

$$\frac{1}{\tau_{eff}} = \int d^3R \frac{p^{id}}{\tau} \Big/ \int d^3R \, p^{id} \tag{13}$$

From (8(a-c),11-13) one then obtains [11] :

$$B \ddot{\alpha} + C_0 \alpha + (C_\infty - C_0)\dot{\beta} \; ; \quad \dot{\beta} = \int_{-\infty}^{t} dt \; e^{-\frac{t-t'}{\tau_{eff}}} \dot{\alpha} \tag{14}$$

with

$$B = m \int d^3r \, \rho |\vec{u}|^2 \qquad C_0 = B \Omega_0^2 \quad ; \; C_\infty = B \Omega_\infty^2 \tag{15}$$

where Ω_0 and Ω_∞ are the well known [7] frequencies of normal sound ($\tau_{eff} = 0$) and zero sound ($\tau_{eff} = \infty$) respectively. Equation (14) is the one of a damped harmonic oscillator with a friction kernel which is non local in time, reflecting the fact that an appreciable elapse of time can occur during successful collisions. This memory effect was discussed qualitatively by Nörenberg in a recent work [12] but no determination of τ_{eff} for zero sound modes was attempted. Here we give for the first time a completely self contained theory with no adjustable parameters for giant resonances in nuclei.

In order to discuss more specifically the influence of damping it is convenient to transform (14) to a third order differential equation [11] :

$$B \dddot{\beta} + \frac{B}{\tau_{eff}} \ddot{\beta} + C_\infty \dot{\beta} + \frac{C_0}{\tau_{eff}} \beta = 0 \tag{16}$$

This equation immediately reproduces the well-known limiting frequencies of ordinary and zero sound but for finite τ_{eff}, as in our case, the characteristic equation of (16) has in general complex frequencies Ω as solution. In the limit Re $\Omega\,\tau_{eff} \to \infty$ one obtains [11] :

$$\Omega = \Omega_\infty \left[1 + \frac{3}{4}\left(\frac{1}{2} - \left(\frac{\Omega_0}{\Omega_\infty}\right)^2 + \frac{3}{2}\left(\frac{\Omega_0}{\Omega_\infty}\right)^4 \left(\frac{\Omega_\infty}{\tau_{eff}}\right)^2\right] - \frac{i}{2\tau_{eff}}\left(1 - \left(\frac{\Omega_0}{\Omega_\infty}\right)^2\right) \qquad (17)$$

From (13) and (9) we can calculate τ_{eff} with the Gogny force [5] and for intermediate and heavy nuclei we obtain a value for the width

$$\Gamma \sim 2\text{-}3 \text{ MeV} \qquad (18)$$

in quite good agreement with experimental finding as is seen from Fig. 3.

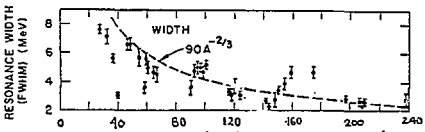

Fig. 3

More detailed numerical studies of (9,13) are necessary to obtain the detailed A-dependance of the width. However qualitatively it is clear that our fictitious temperature is related to the variance Δp^2 of the momenta which is the larger the smaller the nucleus.

3. Conclusions

We have presented a completely self contained model with no adjustable parameters to account for position and width of the giant quadrupole resonance. The model consists of a selfconsistent time dependent harmonic oscillator plus a two body collision term [6]. The model without collision term reproduces very well experimental giant resonance energies. It is well known [8] that a Fermion two body collision term goes - in the infinite matter limit - to zero with the square of the temperature. Giant resonances occur in nuclei at T = 0 nevertheless a fictitious temperature can be defined in finite Fermi systems coming from the fact that the finite real space available generates a finite diffusivity of the momentum distribution according to Heisenberg's uncertainty principle. This fictitious temperature turns out to be of the

order 5-4 MeV for intermediate to heavy nuclei and constant over the nucleus for a harmonic potential. From this it becomes also clear that the "temperature" rises going from heavy to small nuclei explaining qualitatively the increasing giant resonance widths for increasing smaller nuclei. The harmonic potential is of course quite unrealistic for most nuclei and in Fig. 2 we show that the "temperature" has a pronounced surface peak for realistic Wood Saxon potentials. In this case the other extreme view that the nucleons are moving freely in the interior and only colliding in the wall (genuine two body collisions, not collisions with the wall of the mean field) becomes approximately correct [13] . One could then introduce a "temperature" or inverse collision time which is proportional to a δ-function centered at the surface : $\tau^{-1} = \tilde{\tau}_{eff}^{-1}\ \delta(r - R_o)$. Taking all these considerations into account needs detailed numerical evaluation of the collision time (13) which are in progress [14]. Preliminary results show that the giant quadrupole width is about 2-3 MeV broad for A $\sim$ 200 in good agreement with experiment.
This indicates that our model is essentially correct, though improvements concerning for instance the energy conservation of the quasiparticles during collision should be incorporated. Investigations in this direction are in progress.

Acknowledgements

It is a pleasure for us to thank R. Hasse for comments. One of us (P.S.) is also grateful to M. Durand and V.S. Ramamurthy for their discussions and collaboration on the Wigner transform of the density matrix.

References

[1] A. Bohr and B.R. Mottelson, Nuclear Structure, Vol. II, Benjamin, New York, 1975.

[2] J. Winter, to be published.
P. Schuck, Proceedings of the Topical Conference on Heavy Ion Collisions Fall Creel Falls, Tennessee (Oak Ridge Lab.) 1977.

[3] L.P. Kadanoff and G. Baym, Quantum Statistical Mechanics, Benjamin, New York, 1962.

[4] M.A. Preston and R.K. Bhaduri, Structure of the Nucleus, Addison-Wesley, Reading. MA, 1975.

[5] J. Dechargé, D. Gogny, Phys. Rev. C21 (1980) 1568.

[6] P. Schuck, unpublished.

[7] P. Ring, P. Schuck, The Nuclear Many Body Problem, Springer 1980.

[8] G. Baym, C. Pethik, Monographs and Texts in Physics and Astronomy, Vol. XXIX, part II, p. 1, 1978.
[9] M. Prakash, S. Shlomo, V.M. Kolomietz, Nucl. Phys. A370 (1981) 30.
[10] M. Durand, V.S. Ramamurthy, P. Schuck, to be published.
[11] J. Winter, to be published.
[12] W. Nörenberg, Phys. Lett. 104B (1981) 107.
[13] G. Ghosh, H. Hasse, to be published.
[14] P. Schuck, J. Winter, to be published.

DISSIPATION AND FLUCTUATION CAUSED BY STATISTICAL EXCHANGE OF PARTICLES*

H. Feldmeier and H. Spangenberger

Institut für Kernphysik,
Technische Hochschule
Darmstadt, Germany

We calculate drift and diffusion coefficients for the dissipation caused by particle exchange between two Fermi gases. The goal is to find the probability rate $W(\vec{p},\vec{\eta})$ for the relative momentum $\vec{p}$ to change by a certain amount $\vec{\eta}$ per time. The mean value of $W(\vec{p},\vec{\eta})$ with respect to $\vec{\eta}$ determines the drift coefficient $\vec{\gamma}$ (friction force) and the record moments are the diffusion coefficients Dij which enter the Fokker-Planck equation.

$$\gamma_i = - \int d^3\eta \; W(\vec{p},\vec{\eta}) \;\; \eta_i \tag{1}$$

$$Dij = 1/2 \int d^3\eta \; W(\vec{p},\eta) \; \eta_i \eta_j \tag{2}$$

This way of calculating friction and diffusion does not a priori assume an Einstein relation. The general relation between both, the so called dissipation fluctuation theorem, manifests itself in calculating the coefficients as moments of the same probability distribution $W(\vec{p},\vec{\eta})$.

To determine $W(\vec{p},\vec{\eta})$ we have to consider the dynamical evolution of the system during a small time interval Δt. In our model we idealize the two heavy ions as two Fermi gases having different mean velocities and being in contact at a window through which they can exchange particles.

---

*Work supported by the Bundesminister für Forschung und Technologie of the Federal Republik of Germany

Since at low excitation energies the mean free path of a nucleon is long compared to a typical window size, we regard the time evolution of the two gases close to the window as a free motion of particles. To illustrate the dynamics let us even more simplify the picture and regard the particle exchange in the two-dimensional one-body phase-space. Figure 1 shows in the left part the phase-space distribution for two Fermi gases with different mean velocities $\vec{u}_1$, $\vec{u}_2$ and zero temperature in contact at a window (x=0). In the right part the shape of the distribution is shown at a small time Δt later. Due to the mismatch in velocities, occupied cells from the left enter into unoccupied phase-space on the right of the window and vice versa. Calculating now the mean velocity on one side, it obviously has slowed down. The same holds if the two gases are diverging. This case is illustrated in Figure 2. Here empty phase-space cells are moving into originally occupied space. This exchange of holes has the same dissipative effect as the exchange of particles. In the interior region fully occupied cells also cross the window replacing other occupied cells which themselves have moved away. But this is only a rearrangement in the occupied phase space and does not result in an observable change in the state of the system. Therefore only transitions close to the Fermi velocity V_F contribute to a change in observable quantities like the relative momentum or the mass number of one nucleus. Going back to the six-dimensional one-body phase-space and taking into account the different contributions from particles and holes, we arrive at the following expression for $W(p,\eta)$

$$W(\vec{p},\vec{\eta}) = \frac{1}{2}\frac{f_o}{m^3}\left|\frac{\vec{\eta}}{m}\vec{\sigma}\right|\left\{g_1\left(\frac{\vec{\eta}}{m}\right)\left(1-g_2\left(\frac{\vec{\eta}}{m}\right)\right) + g_2\left(\frac{-\vec{\eta}}{m}\right)\left(1-g_1\left(\frac{-\vec{\eta}}{m}\right)\right)\right\} \qquad (3)$$

f_o is the phase-space density of nuclear matter, m the nucleon mass and $\vec{\sigma}$ the window size and direction. g_1 and g_2 are the two velocity distributions,

which may have a diffuse Fermi-edge, and are shifted by the mean velocities $\vec{u}_1$, $\vec{u}_2$. The Pauli blocking effect shows up in the curly bracket part which allows only those velocities $\vec{n}/m$ to contribute where the phase space in one nucleus is occupied and in the other one is empty or vice versa. The negative velocities originate from the holes.

We now calculate the friction force and the diffusion coefficients as they are defined in Eqs. (1) and (2), assuming the relative velocity $\vec{u} = \vec{u}_2 - \vec{u}_1$ and the diffuseness τ of the velocity distribution to be small compared to the Fermi-velocity V_F. The resulting friction force is just the well known window friction[1]

$$\vec{Y} = -m\rho \frac{3}{16} V_F \cdot \sigma \begin{pmatrix} 1 & 0 & 0 \\ 0 & 1 & 0 \\ 0 & 0 & 2 \end{pmatrix} \vec{u} \qquad (4)$$

ρ is the nuclear density and σ the window area. In order to incorporate the effects from the diffuse Fermi surface we are parameterizing the velocity distributions $G_{1,2}(\vec{u},z)$ as shown in Figure 3. The excitation energy of a Fermi gas with the above velocity distribution is given by

$$E^*(\tau) = A \frac{m}{4} \tau^2 \left\{ 1 + \frac{3}{40} \left(\frac{\tau}{V_F}\right)^2 \right\} \qquad (5)$$

Thus Z, although it is a velocity, may be regarded as a measure of the "temperature" of the system. The excitation energy is like in the Fermi distribution proportional to the "temperature" squared.

In Figure 4 we illustrate the distribution in velocity space which enters the part in the curly brackets of Eq. (3). During the course of a heavy ion collision, initially we have a system with two sharp edged Fermi spheres displaced by the relative velocity (left part). Although the system

is cold (τ=o) we already encounter large fluctuations from the outer sickle shaped parts where the Fermi spheres do not overlap. At a later stage the relative velocity has slowed down, the Fermi spheres overlap more, and the excitation energy has smeared out the edges of the distributions so that additional transitions can take place where the edges overlap (center part of Fig. 4). At a very advanced time the relative momentum has been dissipated completely and transitions only take place due to the fact that the system has a temperature (right part of Fig. 4.).

Calculating the diffusion tensor D_{ij} according to Eq. (2) it turns out that it can be split in two parts,

$$D = |\vec{v}|\ D_u(\alpha) + \tau D_\tau(\alpha,\ \tau/|\vec{u}|) \tag{6}$$

one being proportional to the absolute value of the relation velocity $|\vec{u}|$ and the other proportional to the temperature parameter τ. D_u and D_τ are 3 x 3 matrices which depend on the angle α between the window $\vec{\sigma}$ and the relative velocity $\vec{u}$.

The matrix elements of D_u are given in Figure 5, the z-direction being the normal vector of the window. The temperature part D_τ depends on $\tau/|\vec{u}|$ as well as on α. However for $\tau >> |\vec{u}|$ the result becomes again rather simple:

$$\text{For } \tau >> |\vec{u}| \ :\ D \sim \tau \begin{vmatrix} 1 & 0 & 0 \\ 0 & 1 & 0 \\ 0 & 0 & 2 \end{vmatrix} \tag{7}$$

and the Einstein relation is obeyed (compare Eq. 4)

$$\vec{\gamma} = -\frac{D}{\tau} m \vec{u} \quad \text{for } \tau >> |\vec{u}| \tag{8}$$

Thus we obtain a description which in a natural way proceeds from a cold system far off equilibrium toward thermal equilibrium with the diffusion initially driven by the relative velocity and then gradually going over to thermal fluctuations. Based on the same physical picture Randrup[2] calculated in a different derivation rather similar diffusion coefficients.

In Figure 6 we display the double differential cross section as a function of the energy and scattering angle of the outgoing fragments for two different reactions. The calculation is the result of a moment expansion of the Liouville-Fokker-Planck equation using the above determined friction and diffusion coefficients and a conservative potential depending only on the relative distance of the two nuclei. An important result is the rather broad distribution for low energy losses. Due to the neglect of deformation the cross section does not stretch down in energy as far as in the experiment. Otherwise the calculated fluctuations do not seem to be in contradiction with the measured data.

[1] J. Blocki et al., Ann. Phys. 113 (1978) 330.

[2] J. Randrup, Nucl. Phys. A327 (1979) 490.

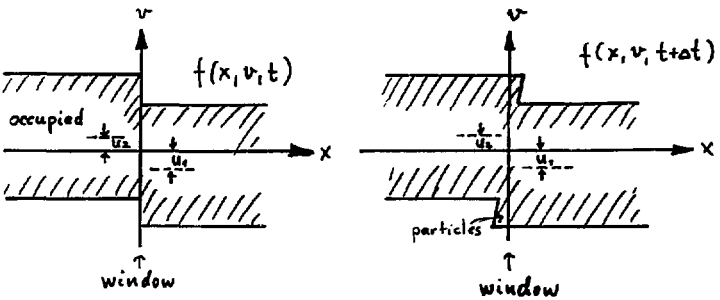

Figure 1 Time evolution of the one-body phase-space distribution for approaching Fermi gases ($u = u_2 - u_1 > 0$)

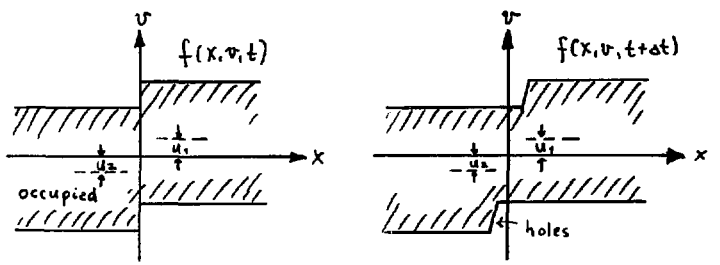

Figure 2 Same as figure 1 but for diverging Fermi gases ($u = u_2 - u_1 < 0$)

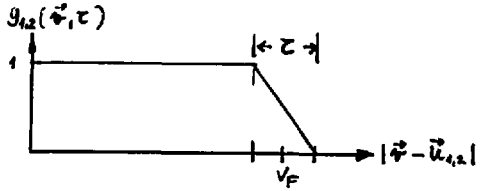

Figure 3 Velocity distribution for a system with excitation energy

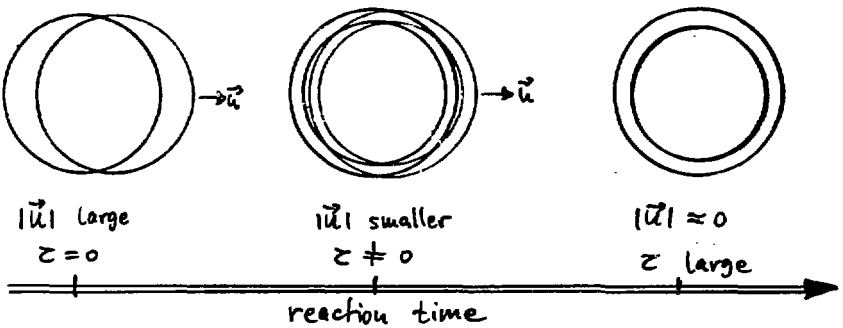

Figure 4 Fermi-spheres in velocity space as a function of decreasing relative velocity and increasing temperature

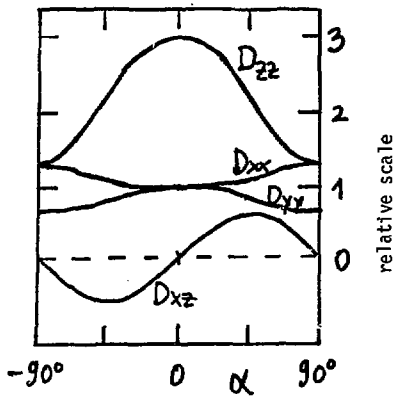

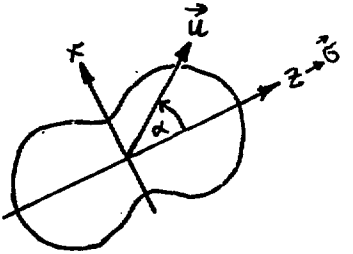

$$D \sim |\vec{u}| \cdot \begin{pmatrix} D_{xx}(\alpha) & 0 & D_{xz}(\alpha) \\ 0 & D_{yy}(\alpha) & 0 \\ D_{xz}(\alpha) & 0 & D_{zz}(\alpha) \end{pmatrix}$$

Figure 5 Diffusion coefficients as a function of the angle α between the relative velocity $\vec{u}$ and the window direction $\vec{\sigma}$ (symmetry axis of the dinuclear system) for small excitation energy ($\tau \ll |\vec{u}|$)

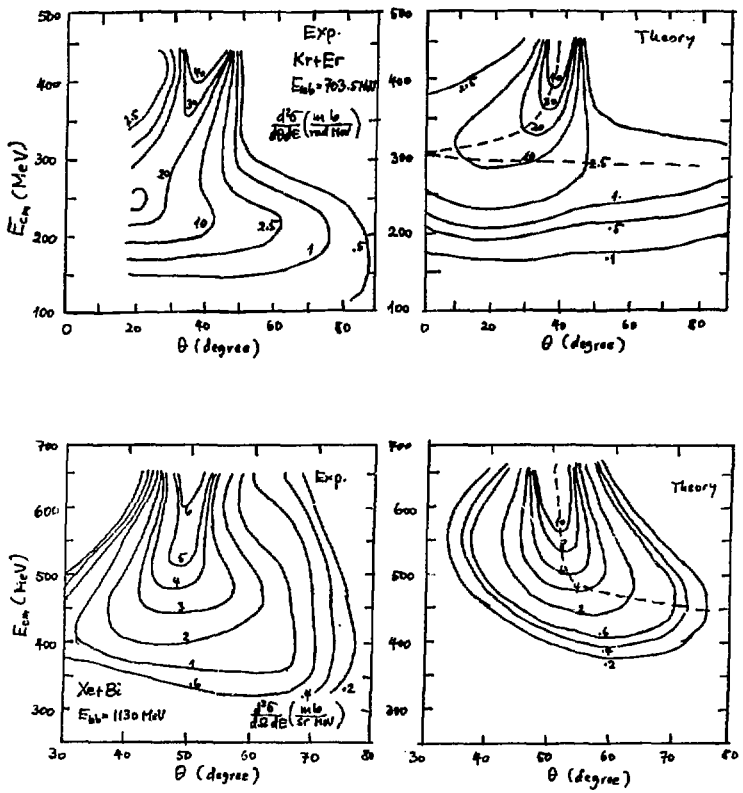

Figure 6 Comparison between measured and calculated double differential cross sections as a function of energy and scattering angle. Dashed lines result from the trajectory calculation.

THE "WALL FORMULA" FOR NUCLEAR DISSIPATION AS CLASSICAL LIMIT OF THE DAMPING OF COLLECTIVE MOTION IN THE TIME-DEPENDENT RPA†

C. Yannouleas*, M. Dworzecka, and J. J. Griffin**

Department of Physics and Astronomy
University of Maryland, College Park, Maryland 20742 U.S.A.

References 1,2 describe a microscopic model for the damping of the one-phonon RPA collective state, $|c\rangle = Q_c^\dagger|0\rangle_{S_R}$. This one-phonon RPA collective state is defined within a restricted subspace, S_R, of the discrete 1p-1h structure. Its damping is described within an extended subspace, $S = S_R + S_A$, by the time evolution of a wave packet according to the time-dependent RPA[1] and the time-dependent Second RPA[2] approximations of the complete Schrödinger equation when initialized with the one-phonon state. Here we focus on the connection of the microscopic model with the phenomenological Vibrating Potential Model for the nuclear harmonic collective motion and, thereby, with the one-body theories for nuclear dissipation, in particular the Swiatecki wall formula.[3] Since both the Vibrating Potential Model and the one-body dissipation theories utilize a phenomenological time-varying mean field, we are primarily interested in wave functions which describe the damping of coherent oscillations of the mean field. The one-phonon state, however, is unable to describe time-varying oscillations of the mean field. Such oscillations require wave packets formed by linear superposition of the RPA many-phonon eigenstates.[4,5]

Undamped Packet

We first consider undamped oscillations of the mean field, described by the following multi-phonon minimum uncertainty coherent wave packet:

$$|\phi(t)\rangle = \exp\{-\frac{\epsilon^2}{2} + \epsilon\, e^{-i(\omega_c t+\delta)} Q_c^\dagger\}|0\rangle_{S_R} \qquad (1)$$

where the many-phonon states, $|c^{(s)}\rangle$, are created through repeated action of the RPA collective operator, $Q_c^\dagger$, on the ground state.

Damping

Next, we describe the damping of the mean field oscillations by propagating in time the initial value, $|\phi(t=0)\rangle$, of the wave packet (1) according to the complete Hamiltonian, H. The complete Hamiltonian H includes all the interaction terms providing finite coupling between the restricted subspace, S_R, and the additional subspace, S_A. The wave packet, $|\Psi(t)\rangle$, describing the damping is then:

$$|\phi(t)\rangle = e^{-iHt/\hbar}|\phi(t=0)\rangle. \qquad (2)$$

Solution for Damped Time-Dependent Packet

We approximately solve the initial value problem posed in Eq. (2) by expanding the one-phonon collective state, $|c\rangle$, over the "eigenstates" $|\nu\rangle$ of H within the extended subspace, S. These stationary states, $|\nu\rangle$, are created by the action of the boson operators $\hat{Q}_\nu^\dagger$ on the ground state. The complete Hamiltonian, H, acting on $|\nu\rangle$ yields:

†Research supported by the U. S. Department of Energy.
*Research is from a thesis to be submitted to the University of Maryland Graduate School by C. Yannouleas in partial fulfillment of the requirements for Ph.D. degree in Physics.
**and Institute for Physical Sciences and Technology, University of Maryland.

$$[H,\hat{Q}_\nu^\dagger] = \hbar\omega_\nu \hat{Q}_\nu^\dagger. \tag{3}$$

The eigenstates $|\nu>$ are specified as solutions of the linearized equations of motion within the extended subspace, S. The additional subspace, S_A, might include additional states only of the lp-lh type[1] or it might be more general.[2,5] Here we restrict ourselves to the RPA approximation and include additional states only of the lp-lh structure (e.g., continuum), since we want to compare the microscopic model with one-body dissipation theories. The creation operators $\hat{Q}_\nu^\dagger$ in Eq. (3) are then given by:

$$\hat{Q}_\nu^\dagger = \sum_{mi} \{Y_{mi}(\omega_\nu)a_m^\dagger a_i - Z_{mi}(\omega_\nu)a_i^\dagger a_m\} + \sum_{\tilde{n}\tilde{j}} \{Y_{\tilde{n}\tilde{j}}(\omega_\nu)a_{\tilde{n}}^\dagger a_{\tilde{j}} - Z_{\tilde{n}\tilde{j}}(\omega_\nu)a_{\tilde{j}}^\dagger a_{\tilde{n}}\}. \tag{4}$$

Indices (m,n) refer to particles, while indices (i,j) refer to holes. The tilded indices $(\tilde{n},\tilde{j})$ refer to additional lp-lh states. The amplitudes $Y_{mi}(\omega_\nu)$, $Z_{mi}(\omega_\nu)$, $Y_{\tilde{n}\tilde{j}}(\omega_\nu)$, $Z_{\tilde{n}\tilde{j}}(\omega_\nu)$ and the eigenfrequencies ω_ν are solutions of the RPA equations-of-motion. Knowing the states $|\nu>$ we can expand the one-phonon state $|c>$ as:

$$|c> = \sum_\nu f_{\nu c}^* |\nu>. \tag{5}$$

Then the wave packet (2) describing the damping is approximated by:

$$|\Psi(t)> \approx e^{-iE_0t/\hbar} \exp\{-\frac{\epsilon^2}{2} + \epsilon\, e^{-i\delta} \sum_\nu f_{\nu c}^*\, e^{-i\omega_\nu t}\, \hat{Q}_\nu^\dagger\}|0>_S. \tag{6}$$

In refs. 1,2, it is shown that when

(1) the variations are slow (i.e., when the coupling matrix elements, $K_{\tilde{m}i}(\omega_c)$, in Eq. (9) below, and the level spacing $d_{\tilde{m}\tilde{i}}$ vary slowly with the states $|\tilde{m}i>$ of the additional space S_A);

(2) the coupling is weak (i.e., sufficiently weak to cause only a small collective energy shift and mixing of the collective state into eigenstates $|\nu>$ in a narrow energy band);

(3) subspace S_A is dense (in the sense that coupling matrix elements much exceed level spacing, $(|K_{\tilde{m}\tilde{i}}(\omega_c)|/d_{\tilde{m}\tilde{i}} >> 1)$,

then the coefficients $f_{\nu c}$ can be calculated approximately in closed form. In particular, their counterparts, $f_c(\omega)$, for the continuous S_A case are found:

$$|f_c(\omega)|^2 \approx \frac{1}{2\pi\hbar} \frac{\Gamma(\omega_c)}{(\omega-\omega_0)^2 + [\frac{\Gamma(\omega_c)}{2}]^2} \tag{7}$$

where the continuous index ω is substituted for the discrete index ν. ω_0 is the perturbed value of the collective frequency, ω_c. The width $\Gamma(\omega_c)$ is given by

$$\Gamma(\omega_c) = \frac{2\pi}{\hbar} \iint d\tilde{m}\, d\tilde{i}\ |K(\tilde{m},\tilde{i};\omega_c)|^2\, \delta(\hbar\omega_c - \epsilon(\tilde{m}) + \epsilon(\tilde{i})). \tag{8}$$

where

$$K(\tilde{m},\tilde{i};\omega_c) = \sum_{nj} \{V_{\tilde{m}j\tilde{i}n}\, y_{nj}(\omega_c) + V_{\tilde{m}n\tilde{i}j}\, z_{nj}(\omega_c) \tag{9}$$

and the coefficients $y_{nj}(\omega_c)$, $z_{nj}(\omega_c)$ are the RPA amplitudes determining the collective operator $Q_c^\dagger$. Then the energy dissipation is associated, in the case of a finite-A nucleus, entirely with the escape width, $\Gamma^\dagger$, for direct particle emission in the continuum.

We concentrate now on demonstrating the time decay of the collective energy. To do this we first define the explicit collective variables associated with the collective phonon.

By analogy with the quantal harmonic oscillator we define the operator, $\hat{\sigma}_c$, for the collective coordinate as:

$$\hat{\sigma}_c = Q_c^\dagger + Q_c = \sum_\nu \{f_{\nu c}^* \hat{Q}_\nu^\dagger + f_{\nu c} \hat{Q}_\nu\}. \tag{10}$$

To define the momentum operator, $\hat{p}_c$, for the collective degree of freedom within the extended subspace, S, we use the general definition for the time derivative of an operator in the Schrödinger picture:

$$\hat{p}_c = \frac{iM_c}{\hbar}[H, \hat{\sigma}_c] = iM_c \sum_\nu \omega_\nu \{f_{\nu c}^* \hat{Q}_\nu^\dagger - f_{\nu c} \hat{Q}_\nu\}, \tag{11}$$

where the inertial parameter, M_c, is taken to be

$$M_c = \frac{\hbar}{2\omega_0} \tag{12}$$

in order to guarantee that $\hat{\sigma}_c$ is canonical to $\hat{p}_c$:

$$[\hat{\sigma}_c, \hat{p}_c] = i\hbar. \tag{13}$$

The time-dependent expectation value of this collective coordinate, calculated with the damped wave packet solution (6) becomes:[4]

$$\langle\Psi(t)|\hat{\sigma}_c|\Psi(t)\rangle = \epsilon(e^{-i\delta} F(t) + e^{i\delta} F^*(t)), \tag{14}$$

where

$$F(t) = \int_{-\infty}^{+\infty} |f_c(\omega)|^2 e^{-i\omega t} d(\hbar\omega). \tag{15}$$

With the approximate coefficients $f_c(\omega)$ given by (7), the quantity F(t) reduces to the form:[1,2]

$$F(t) \approx e^{-i\omega_0 t - [\Gamma(\omega_c)t]/2} \qquad 0 < t < \infty. \tag{16}$$

Then the expectation value of $\hat{\sigma}_c$ oscillates and decays, as follows:

$$\langle\Psi(t)|\hat{\sigma}_c|\Psi(t)\rangle = 2\epsilon e^{-\Gamma t/2} \cos(\omega_0 t + \delta). \tag{17}$$

Likewise, we calculate the expectation values of the momentum,[4]

$$\langle\Psi(t)|\hat{p}_c|\Psi(t)\rangle = M_c \frac{d}{dt}\langle\Psi(t)|\hat{\sigma}_c|\Psi(t)\rangle, \tag{18}$$

using Eq. (17) to obtain the relation,

$$\langle\Psi(t)|\frac{d\hat{p}_c}{dt}|\Psi(t)\rangle = -\Gamma\langle\Psi(t)|\hat{p}_c|\Psi(t)\rangle - M_c(\omega_0^2 + \frac{\Gamma^2}{4})\langle\Psi(t)|\hat{\sigma}_c|\Psi(t)\rangle. \tag{19}$$

This relation (19) for the expectation values of $\hat{\sigma}_c$ and $\hat{p}_c$ has the same form as Newton's equation of motion for a classical damped harmonic oscillator. We can thus interpret (19) as describing two kinds of collective forces: a conservative force proportional to the collective coordinate and a frictional force proportional to the corresponding momentum.

We can also define a frictional Hamiltonian constructed to prescribe precisely the same time behavior for the collective variables as the exact Hamiltonian, H, produces in the time-dependent RPA approximation. Thus we define $\mathcal{H}_F$ by requiring that its substitution for H in Eqs. (11) and (19) leaves those equations unaltered. We find that such a frictional Hamiltonian must be non-linear; i.e., it must depend not only upon $\hat{\sigma}_c$ and $\hat{p}_c$ but also upon $|\Psi(t)\rangle$ through their time-dependent expectation values, as follows:

$$\mathcal{H}_F = \frac{\hat{p}_c^2}{2M_c} + \frac{M_c}{2}(\omega_0^2 + \frac{\Gamma^2}{4})\hat{\sigma}_c^2 + \Gamma\,\hat{\sigma}_c\langle\Psi(t)|\hat{p}_c|\Psi(t)\rangle, \tag{20}$$

up to an arbitrary additive function of time alone.

The conservative collective Hamiltonian, $\mathcal{H}_c$, is defined as the sum of the collective kinetic and collective potential energy parts of the frictional Hamiltonian, i.e.,

$$\mathcal{H}_c = \frac{\hat{p}_c^2}{2M_c} + \frac{M_c}{2}(\omega_0^2 + \frac{\Gamma^2}{4})\hat{\sigma}_c^2, \tag{21}$$

and its expectation value with the wave packet $|\Psi(t)\rangle$, less the zero point energy of the collective degree of freedom, is defined as the collective excitation energy:

$$\mathcal{E}_c(t) = \langle\Psi(t)|\mathcal{H}_c|\Psi(t)\rangle - {}_S\langle 0|\mathcal{H}_c|0\rangle_S. \tag{22}$$

Straightforward algebraic calculation yields the remarkable result that the collective excitation energy depends only upon the squares of the expectation values, rather than upon the expectation values of the squares of $\hat{\sigma}_c$ and $\hat{p}_c$:[4]

$$\mathcal{E}_c(t) = \frac{\langle\Psi(t)|\hat{p}_c|\Psi(t)\rangle^2}{2M_c} + \frac{M_c}{2}(\omega_0^2 + \frac{\Gamma^2}{4})\langle\Psi(t)|\hat{\sigma}_c|\Psi(t)\rangle^2. \tag{23}$$

The rate of dissipation of the collective energy, $\dot{\mathcal{E}}_{diss}(t)$, is defined as the time derivative of the collective energy (23), and calculated using (17) and (18) to be:

$$\dot{\mathcal{E}}_{diss}(t) = -2\Gamma\,\frac{\langle\Psi(t)|\hat{p}_c|\Psi(t)\rangle^2}{2M_c} \approx -2\,\epsilon^2\,\Gamma\hbar\omega_0\,e^{-\Gamma t}\,\sin^2(\omega_0 t+\delta). \tag{24}$$

The last step in (24) follows because the damping is weak, so that $\Gamma/2 << \omega_0$. The energy dissipation rate (24) is proportional to the kinetic collective energy as for a classical damped harmonic oscillator, but in contrast with the decay of a single collective eigenstate.[1,2]

From an appropriate limit of the expression (24), one can extract the coefficient which Swiatecki's classical "wall formula" would imply for the energy loss rate of a spherical droplet oscillating in a pure (sufficiently small) multipole model.

We use the following two-body schematic interaction which accounts for the motion of the nuclear surface:

$$V_{mjin} = -\kappa D_{mi} D_{nj} \tag{25a}$$

where

$$D_{ss'} = -\langle s'|r\frac{du^{(0)}(r)}{dr}Y_{\lambda 0}(\theta)|s\rangle \tag{25b}$$

and

$$u^{(0)}(r) \approx u_0\,\theta(r-R). \tag{25c}$$

$u^{(0)}(r)$ is the shell model potential, $(\lambda,0)$ the multipolarity of the surface vibration and R, the nuclear radius. With the schematic interaction (25) the collective variable, $\langle\Psi(t)|\hat{\sigma}_c|\Psi(t)\rangle$, becomes proportional to the deformation parameter, $\alpha_{\lambda 0}(t)$, of the average nuclear surface:

$$\langle\Psi(t)|\hat{\sigma}_c|\Psi(t)\rangle = c\,\alpha_{\lambda 0}(t). \tag{26}$$

Then

$$\dot{\mathcal{E}}_{diss}(t) = -\gamma\,\dot{\alpha}_{\lambda 0}^2(t), \qquad \text{where } \gamma = c^2 M_c \Gamma. \tag{27}$$

To establish a comparison with the constant coefficient of the wall formula, we consider the limit of large nuclear radius and infinite square well shell model potential. Then a lengthy but straightforward calculation[4] yields for all $\lambda << 2k_FR/\pi$:

$$\gamma_{limit} = \frac{\hbar(k_FR)^4}{8\pi^2}\frac{1}{\eta}\{(1+\eta)^{3/2} - (1-\eta)^{1/2} + (\tfrac{3}{2}\eta-1)[\sqrt{1+\eta} - \sqrt{1-\eta}] + (\tfrac{3}{2}\eta-1)\eta\,\ell n[\frac{1+\sqrt{1+\eta}}{1+\sqrt{1-\eta}}]\}, \quad \eta = \frac{\hbar\omega_c}{\epsilon_F}. \tag{28}$$

Expanding (28) in a Taylor series we get

$$\gamma_{limit} = \frac{\hbar(k_FR)^4}{8\pi^2}(1 + \frac{3}{2}\eta + \ldots). \tag{29}$$

The low frequency limit of this expression agrees exactly with the classical Swiatecki wall formula.[3] The present result thus allows one to recognize explicitly certain limitations of the classical wall formula.

REFERENCES

1. C. Yannouleas, M. Dworzecka, J. J. Griffin, U. of Md. PP #82-010 (ORO 5126-143), Nuclear Physics A (in press).
2. C. Yannouleas, M. Dworzecka, J. J. Griffin, U. of Md. PP #82-095 (ORO 5126-153), in preparation.
3. J. Blocki, et al., Ann. Phys. 113, 330 (1978).
4. C. Yannouleas, M. Dworzecka, J. J. Griffin, U. of Md. PP #82-017 (ORO 5126-146), in preparation.
5. C. Yannouleas, M. Dworzecka, J. J. Griffin, X Gross Properties of Nuclei and Nuclear Excitations Workshop, Hirschegg, Kleinwalsertal, Austria (January 18-23, 1982).

LINEAR MOMENTUM TRANSFER IN

NUCLEUS-NUCLEUS COLLISIONS

V. E. Viola, Jr., Indiana University, Bloomington, IN 47405
B. B. Back and K. L. Wolf, Argonne National Laboratory, Argonne, IL 60439
T. C. Awes and C. K. Gelbke, Michigan State University, East Lansing, MI 48824
H. Breuer, University of Maryland, College Park, MD 20742

A useful overview of the global features of non-relativistic nucleus-nucleus collisions can be obtained from studies of the linear-momentum-transfer distribution which characterizes the target-projectile interaction. For reactions involving highly fissionable target nuclei, where essentially the total reaction cross section is accompanied by fission, information of this type is provided by measurements of the angular correlation between binary fission fragments.[1] Recently, we have investigated the reaction between ^{238}U and ^{16}O ions at 8.75- and 19.7-MeV/nucleon[2] in order to study the evolution of heavy-ion reaction mechanisms as a function of increasing bombarding energy. Angular correlation results from these experiments have been incorporated with earlier such data in the hope of deriving a more systematic understanding of the distribution of strength of the reaction cross section as the bombarding energies increase well above the interaction barrier. The primary objectives of this analysis are: (1) to summarize the systematic features that characterize nucleus-nucleus reaction cross sections for the experimentally-known region extending well above the interaction barrier and (2) to project these results to energies up to 100-MeV/nucleon range where new accelerator technology will soon make extensive experimental studies possible.

In Fig. 1 in-plane correlation data for the $^{16}O + ^{238}U$ system are shown for several bombarding energies from 110 to 315 MeV (6.9 to 19.7 MeV/u).

Except for the lowest ^{16}O energy, two components are apparent in the data. At all energies the major fraction of the cross section is concentrated in a well-defined peak corresponding approximately to complete linear momentum transfer. The second component appears at correlation angles slightly smaller than 180°, where one observes the systematic growth of a broad distribution of relatively low momentum-transfer events. The arrow on each peak indicates the angular correlation centroid angle for complete linear momentum transfer, θ°_{AB}, calculated from kinematics which assume symmetric mass division and the most probable total kinetic energy release in fission predicted by systematics.

Two systematic features of the angular correlation data in Fig. 1 stand out. The first of these is the growth of the low-momentum-transfer component with increasing bombarding energy. These events are assumed to be associated with peripheral collisions and we define this component of the cross section as σ_P. In order to evaluate the importance of the peripheral component relative to the total reaction cross section, σ_P/σ_R, complete angular correlation data including all out-of-plane events are required. The results of fragment correlations in both θ and ϕ dimensions demonstrate the existence of large non-planar contributions due to partial linear momentum transfer processes.

The low momentum-transfer component of the reaction cross section can best be described in terms of peripheral reactions involving a significant target-projectile interaction during the collision stage in which only a part of the projectile is absorbed. Fig. 2 shows angular correlation data for the 315-MeV $^{16}O + ^{238}U$ system in which projectile-like and lighter fragments have been observed in coincidence with correlated fission fragments.

These data show that Be-O fragments are strongly associated with the peripheral portion of the reaction cross section, presumably associated with nucleon-transfer, projectile breakup and damped reaction mechanisms. Further, it is noted that the mass of the projectile residue appears to decrease as the linear momentum transfer increases. This suggests that at least a fraction of the missing projectile mass has been transferred to the target nucleus. In contrast, the proton- and alpha-particle-gated correlations appear to consist of two components: one related to peripheral processes associated with breakup of excited projectile-like fragments, and the other correlated with the large momentum-transfer component.

A second systematic feature of the data in Fig. 1 is the energy-dependence of the deviation between the calculated centroid for complete momentum transfer and the experimental centroid for this component of the distribution. Shown in Fig. 3 are values of the percentage linear-momentum transfer, $\% \vec{p}$, defined in terms of the ratio of the observed linear-momentum transfer to the beam momentum, $\% \vec{p} = 100 p_{exp}/p_I$, as determined from measured $\Delta\theta^{\circ}_{AB}$ values. The results below 10 MeV/nucleon based on this centroid analysis are consistent with complete momentum transfer within accuracy of the technique, which would not be sensitive to massive transfer or prompt nucleon emission processes at the $\leq$ 10 percent level. For projectile energies above 10 MeV/nucleon it is apparent that on the average complete momentum transfer becomes increasingly less probable and scales approximately with the velocity $\sqrt{E/A}$ of the projectile. In addition, as the beam energy/nucleon increases, the fraction of linear momentum transfer decreases systematically. This "missing momentum" has been shown to be carried off by promptly-emitted light ions, (Fig. 2).

From these results it is clear that above 10 MeV/nucleon the complete

fusion mechanism is not well-defined from an experimental point of view. For this reason we have proposed the term central collisions as a more appropriate term for discussing these large momentum transfer events. It is observed that the ratio σ_C/σ_R can be correlated with an effective beam momentum corresponding to an energy E in excess of the Coulomb barrier V, $p_I^{eff} \approx \sqrt{2M(E-V)}$. This dependence is shown in Fig. 4. Extrapolation of the results for σ_C/σ_R leads to the conclusion that the central collision component of the cross section, at least for light heavy ions, should become negligible in the region of 50-70 MeV/u, respectively.

The systematics of Fig. 4 are found to be in good agreement with angular correlation results with 30 MeV/A and 60 MeV/A ^{12}C beams incident on a ^{238}U target. The implication of these results is that somewhere in the region of 50-70 MeV/nucleon, the central collision component of the reaction cross section no longer can be described in terms of a coherent projectile-target interaction, at least for ^{12}C-to-^{20}Ne ions. This behavior, coupled with the observation of prompt light-ion emission for 20 MeV/u ^{16}O ions[4] suggests that nucleon-nucleon collisions begin to dominate nucleus-nucleus collisions in this energy range at the expense of coherent mean-field processes. The mass dependence of these simple extrapolations implies that for heavier ions, mean field behavior may disappear at even lower energies.

References

1. V. E. Viola, Jr., et al, submitted to Physical Review.
2. B. B. Back, et al, Phys. Rev. C22, 1927 (1980).
3. R. Bimbot, et al, Proc. Bad Hof Conference on Fission, Heavy Ions and Related Phenomena, (Oct., 1981).
4. T. C. Awes, et al, Phys. Rev. C24, 89 (1981).

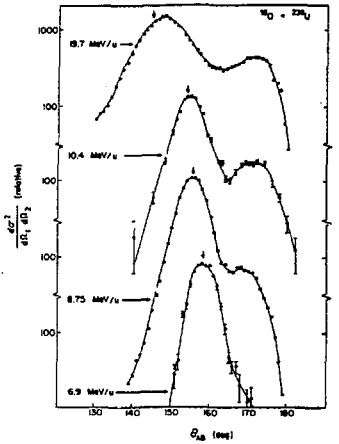

Figure 1 - In-plane angular correlation probabilities for the $^{18}O + ^{238}U$ system at energies ranging from 19.7 MeV/u (top) to 6.9 MeV/u (bottom). Arrows indicate expected centroid for complete linear momentum transfer and symmetric mass division.

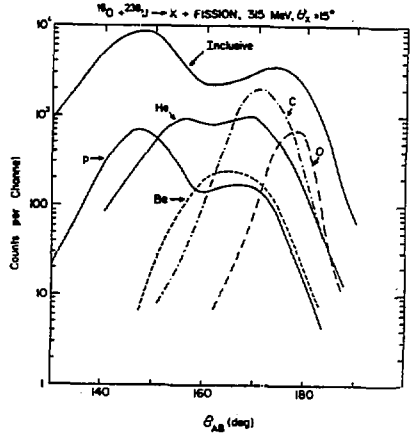

Figure 2 - Angular correlation functions for reactions associated with a third fragment. The inclusive curve includes all events. Lower curves are for protons, alpha particles, Be, C and O ions in coincidence with fission fragments, as labeled.

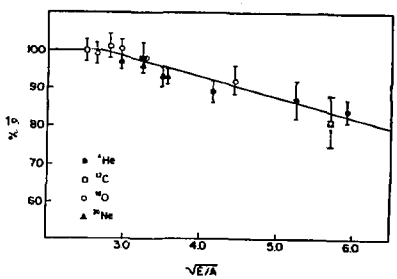

Figure 3 - Plot of percent of full-momentum-transfer for central collisions, % $\vec{p}_c$, as a function of $\sqrt{E/A}$ projectile.

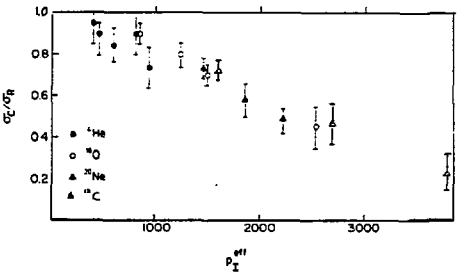

Figure 4 - Plot of the ratio σ_C/σ_R as a function of projectile momentum in excess of the Coulomb barrier, p_I^{eff}.

Preequilibrium Light-Particle Emission in ^{16}O-Induced Reactions

T. C. Awes,* C. K. Gelbke, G. Poggi,† S. Saini,**
D. Cha, R. Legrain,†† and G. D. Westfall

Cyclotron Laboratory,
Michigan State University, East Lansing, Michigan 48824

The dependence of light-particle emission on target and incident energy has been investigated through inclusive measurements[1] of p, d, t, and α particles in ^{16}O-induced reactions on ^{27}Al, ^{90}Zr, and ^{197}Au at 140, 215, and 310 MeV. The light particles were measured in two ΔE-E telescopes, each subtending a solid angle of about 20 msr and consisting of a 400-μm-thick surface barrier detector followed by a 7.6-cm-thick NaI detector. For each system the light-particle distributions were measured at many laboratory angles typically covering the range between 20 and 155°.

Recently the precompound model of nucleon emission has been generalized to heavy-ion-induced reactions.[2] In this generalization, the modified Boltzmann equation approach is applied with an additional term included to account for the time-dependent addition of nucleons from the projectile to the equilibrating system. Only s-wave collisions are considered, and the fusion rate is determined by the relative velocity at the point of contact. The angle-integrated proton energy spectra[1] for the $^{197}Au(^{16}O,p)$ reaction at 140-, 215-, and 310-MeV incident energies are compared in Figure 1 to three different precompound calculations.[2] In the first case, an energy-independent initial exciton number of $n_0 = 20$ was assumed. From this calculation it is seen that it is not possible to simultaneously reproduce the shape of the proton spectra at all three incident energies with a single energy-independent initial exciton number. Instead, values of $n_0 = 18$, 25, and 30 are required to reproduce the spectral shapes at 140, 215, and 310 MeV, respectively. The effect of the restriction to s-wave collisions was investigated by decreasing the available excitation energy by the rotational energy for fusion occurring at the angular momentum limit. These calculations, which use an initial exciton number of 16, are shown by the dotted curves of Figure 1. The effect of decreasing the available excitation energy by the

rotational energy is the same as sharing the excitation energy among more excitons. As a result, the energy dependence of n_o does not appear to be due to the restriction to s-wave collisions. It was also found that varying the rate of the fusion process had little effect on the required initial exciton number. The energy dependence of n_o is apparently due to other assumptions of the precompound model.

In order to study the target dependence and evolution of the light-particle emission with incident energy, we have used the moving source parameterization[3] to extract the characteristics of the light-particle spectra with a minimum number of parameters. The distributions are then given by

$$\frac{d^2\sigma}{dEd\Omega} = N_o E^{1/2} \exp[-(E + E_1 - 2E^{1/2}E_1^{1/2} \cos\theta)/T] ,$$

where E and θ are the laboratory energy and angle of the detected particle, $E_1 = \frac{1}{2}mv^2$ is the kinetic energy of a particle at rest in the frame having velocity v, T is the source temperature, and N_o is an overall normalization constant. This parameterization provides a very satisfactory description of the light-particle distributions.[1]

The energy and target dependence of the velocity and temperature parameters is shown in Figure 2. For comparison the dependences expected for emission from the completely fused systems are also shown by the dotted curves. For the case of reactions on ^{27}Al, the temperatures and source velocities are consistent with emission from the compound nucleus. However, the parameters for reactions on the ^{90}Zr and ^{197}Au targets are not consistent with compound nucleus emission, but instead follow the same trend as the ^{27}Al parameters. The lack of dependence of the light-particle spectra on target nucleus suggests that the particles are emitted at an early stage of the reaction before appreciable equilibration has occurred. The moving source fits indicate that the preequilibrium particles are not emitted from the compound nucleus frame as assumed in the precompound model. This may account for the energy dependence of the initial exciton number of the precompound model.

The dependence of the nonequilibrium charged-particle emission observed here perhaps clarifies the situation for nonequilibrium neutron emission. Typically, those reactions in which preequilibrium neutrons have been observed

are ones with compound nucleus temperatures and velocities which are much different from the preequilibrium values expected according to Figure 2. In these cases the nonequilibrium neutrons have spectral shapes which are distinctly different from the much more abundant evaporation neutrons and, therefore, are easily identified. On the other hand, those systems which have been reported to be consistent with equilibrium emission are generally found to have compound nucleus temperatures which are very similar to the expected preequilibrium values. As a result, unless the complete fusion component of the neutron spectra can be eliminated, using for example, coincidence requirements with strongly damped reaction partners, the nonequilibrium component will simply be lost in the large, similarly shaped, evaporation component.

The solid curves marked T_{nn} and v_{nn} in Figure 2 were calculated with the assumption that each interacting nucleon of the projectile interacts initially with a single nucleon of the target. In this case, the rest velocity, v_{nn}, of the interacting subsystem is about half of the relative velocity of target and projectile at contact. The temperature, T_{nn}, was calculated assuming the excitation energy of the interacting subsystem to be shared as a free Fermi gas.[3] According to the solid curves of Figure 2, the observed temperature and velocity parameters are 25% lower than the limit of equal contributions from target and projectile. The trend of the temperature parameter is shown in Figure 3 to persist toward relativistic energies.[3,4] The solid curve is again the dependence expected for a Fermi gas consisting of equal target and projectile contributions. The dashed curve is the result of a calculation for a free, strongly interacting gas in thermal and chemical equilibrium at an excitation energy determined by the most probable impact parameter.

For heavy-ion collisions at relativistic energies it has been shown that the energy spectra of composite particles can be related to the proton spectra according to a simple power law. In the coalescence model this power law is explained by the assumption that the complex particles are formed by the coalescence of free nucleons which happen to occupy the same region of momentum space. The model is a pure phase-space approach and makes no assumptions about the dynamics of the process. It involves a single parameter, the coalescence radius, P_o, which is the radius within which

coalescence occurs and which acts as an overall normalization constant. In this model the deuteron momentum distribution is expected to be proportional to the product of the proton and neutron distributions; the triton distribution is expected to be proportional to the proton distribution times the square of the neutron distribution, and so on. In practice, the neutron distributions typically are not measured, and so one assumes the proton and neutron spectra are alike and uses only the proton spectra in the coalescence calculation. The composite particle spectra of the present study are reproduced remarkably well by the coalescence relation as demonstrated in Figure 4 for the $^{16}O + ^{27}Al$ reaction at 140-MeV incident energy. The coalescence results are shown by the open squares. The success of the coalescence relation is surprising in the light of recent results which have shown differences between the nonequilibrium proton and neutron distributions,[5] presumably due to Coulomb effects. Understanding the differences in the nonequilibrium proton and neutron distributions and the reason for the success of the coalescence relation are interesting problems for future investigations.

References

*Present address: Oak Ridge National Laboratory, Oak Ridge, Tennessee.

†On leave from University of Florence, Florence, Italy.

**On leave from Bhabha Atomic Research Center, India. Present address: Argonne National Laboratory.

††On leave from C.E.N., Saclay, France.

1. T. C. Awes et al., MSU Preprint MSUCL-362.

2. M. Blann, Phys. Rev. C 23, 205 (1981).

3. T. C. Awes et al., Phys. Lett. 103B, 417 (1981).

4. G. D. Westfall et al., MSU Preprint MSUCL-365.

5. J. Kasagi et al., Phys. Lett. 104B, 434 (1981).

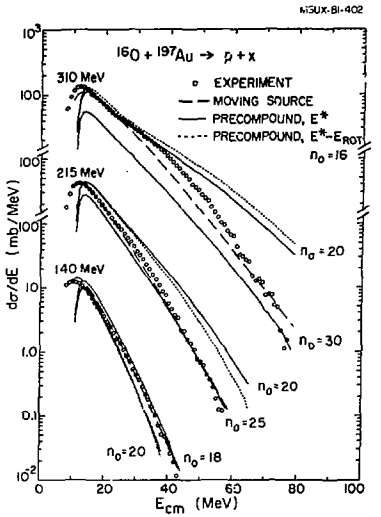

Figure 1

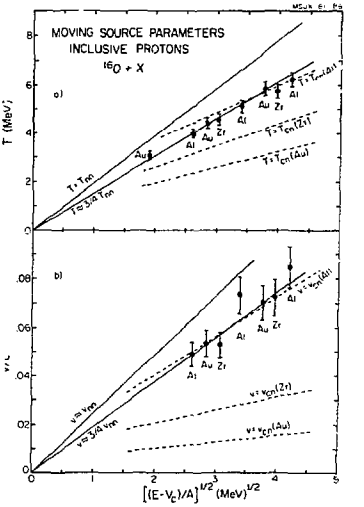

Figure 2

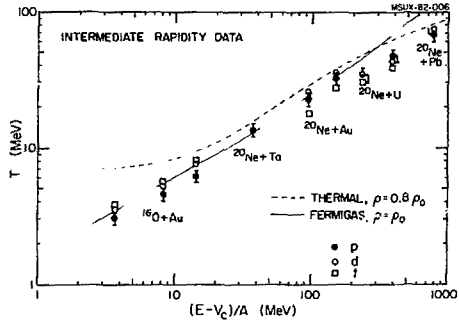

Figure 3

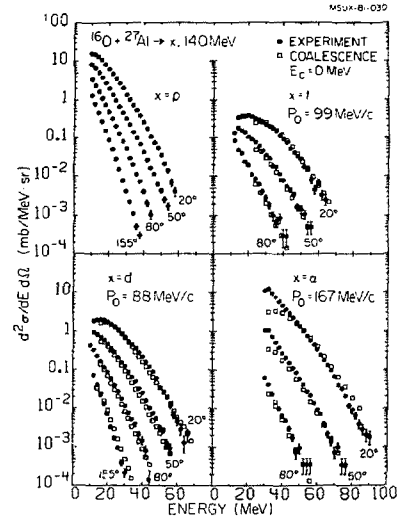

Figure 4

FRAGMENTATION at 20 to 43 MeV/NUCLEON

M. N. Namboodiri, R. K. Choudhury, J. B. Natowitz, P. L. Gonthier, L. A. Adler, R. P. Schmitt, R. L. Watson, and S. H. Simon

Cyclotron Institute
Texas A&M University, College Station, Texas 77843

Determination of the dominant nuclear reaction mechanisms in the 20 to 100 MeV/nucleon energy range is a subject of considerable current interest since it is in this transition region between low energy and high energy phenomena where interesting qualitative changes are predicted to occur.[1,2,3] These changes are expected to be associated with the achievement of relative velocities which surpass the velocity of sound in nuclear matter or the velocity of the constituent nucleons.

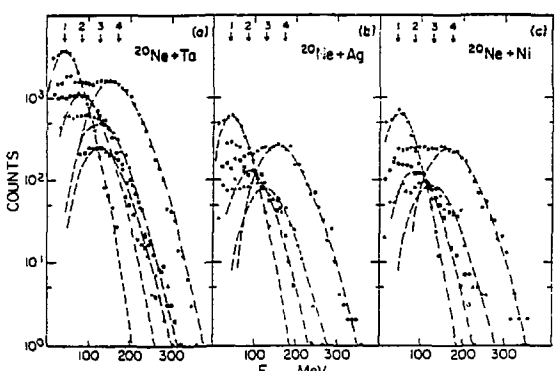

FIG. 1. Light-particle spectra observed at $\theta_L = 15°$. The spectra of H and He isotopes from (a) Ta, (b) Ag, and (c) Ni targets are shown. *p*, open circles; *d*, open squares; *t*, triangles; ^{3}He, solid squares; ^{4}He, solid circles. Dashed lines represent fragmentation model calculations with $\sigma_0 = 85$ MeV/*c*.

Our recently published study of light particle emission in the reactions of 43 MeV/nucleon ^{20}Ne with Ni, Ag and Ta targets[4] suggests that achieving a center of mass velocity above the coulomb barrier comparable to the Fermi

velocity of the projectile is a sufficient condition to assure that purely statistical projectile fragmentation processes[5,6] occur, which are entirely analogous to those observed at relativistic energies.[7] This is evidenced by the forward angle energy spectra of H and He isotopes which show components having energies per nucleon essentially equal to that of the projectile and widths which may be characterized by temperatures of 8 MeV or, alternatively, by nucleon momentum widths σ_o = 85 MeV/c. (See figures 1 and 2). Thus the spectral widths are the same as those reported for relativistic collisions but occur at (E_{cm}-V)=30 to 34 MeV/nucleon (for the different targets). The Fermi energy for the ^{20}Ne nucleus is 29 MeV.[8]

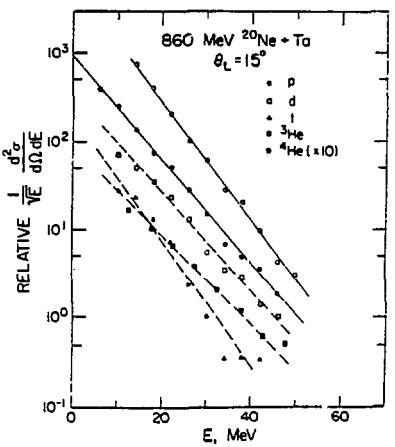

FIG. 2. Slope determinations for Ta data at θ_L=15°. The data have been transformed into the projectile frame.

Although the poor statistics for the energy spectra of projectile-like fragments collected simultaneously do not allow an accurate extraction of σ_o

from the spectra, a value of 85 MeV/c is also consistent with high energy peaks observed in the forward angle spectra for C, N and O fragments (Figure 3).

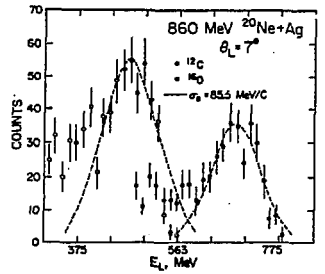

FIG. 3. High energy portions of the spectra for C and O ions observed at $\theta_L = 7°$ in the reactions of 860 MeV ^{20}Ne with Ag. The dashed lines represent fragmentation model calculations with $\sigma_0 = 85.5$ MeV/C.

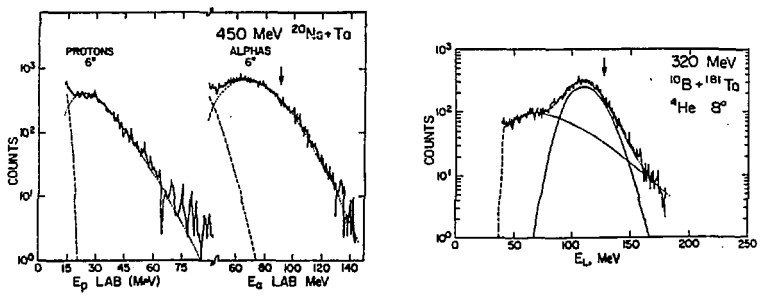

FIG. 4. Light particle spectra from the reactions of 450 MeV ^{20}Ne with Ta and 320 MeV ^{10}B with ^{181}Ta. The smooth lines represent fits assuming two moving thermal sources.

In contrast to the data obtained with 43 MeV/nucleon ^{20}Ne, extraction of the widths from projectile-like fragments observed in the reactions of ^{20}Ne with ^{197}Au at 20 MeV/μ leads to values of 30 to 40 MeV/c.[9] Taken together, these results indicate a very rapid change in the nature of the fragmentation process between 20 and 43 MeV/nucleon.

We have attempted to pursue these investigations by extracting higher energy beams from the TAMU cyclotron. Beams of 10^9 particles/second of 22.5 MeV/nucleon ^{20}Ne and 32.5 MeV/nucleon ^{10}B have been obtained and used to study light particle emission in reactions with ^{181}Ta. Spectra obtained in these studies are shown in Figure 4. Each of the spectra shows evidence of a high energy component peaking at energies somewhat below that corresponding to the projectile velocity. The highest energy component in the spectrum from the ^{20}Ne experiment is probably not from simple fragmentation. The prominent high energy component observed in the 32.5 MeV/nucleon ^{10}B experiments has a width parameter σ_o = 40 MeV/c suggesting that the major broadening occurs rapidly above that energy. The data are summarized in Figure 5. This conclusion must be viewed as tentative since there may be significant differences between ^{10}B and ^{20}Ne projectiles.

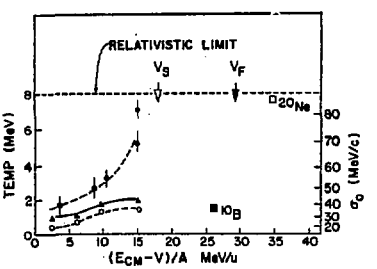

FIG. 5. Summary of width measurements as a function of $(E_{CM}-V)/A$. Circles and triangles represent data from references 2 and 9. Squares represent the current data.

Experiments scheduled in the near future should allow us to settle this question by performing measurements in the intermediate energy range with ^{20}Ne projectiles.

1. R. Stock and A. M. Poskanzer, Comments Nucl. Part. Phys., 7, 41 (1977).
2. D. K. Scott, LBL Report 8931 (1979), unpublished.
3. D. K. Scott, LBL Report 7727 (1978), unpublished.
4. J. B. Natowitz et al., Phys. Rev. Lett., 47, 1114 (1981).
5. H. Feshback and K. Huang, Phys. Lett., 47B, 300 (1973).
6. A. S. Goldhaber, Phys. Lett., 53B, 306 (1974).
7. D. E. Greiner et al., Phys. Rev. Lett., 35, 152 (1975).
8. E. J. Moniz et al., Phys. Rev. Lett., 46, 813 (1981).
9. Ch. Egelhaaf et al., Phys. Rev. Lett., 46, 813 (1981).

Heavy-Ion-Induced Fission in the Rare-Earth Region and the Statistical Model*

F. Plasil, J. R. Beene, B. Cheynis, R. L. Ferguson,
F. E. Obenshain, A. J. Sierk,† and G. R. Young
Oak Ridge National Laboratory, Oak Ridge, Tennessee 37830

A. Gavron
Los Alamos National Laboratory, Los Alamos, New Mexico 87545

G. A. Petitt
Georgia State University, Atlanta, Georgia 30303

In this work we shall consider two separate aspects of heavy-ion-induced fission in the rare-earth region. First, we will consider fission excitation functions and their relationship to fission barriers. Second, we will briefly discuss results on neutron emission associated with fission in the context of the statistical deexcitation model.

A. Fission Barriers

The extraction of fission barriers and of other statistical model parameters from measured fission excitation functions has been an active field of investigation in recent years.[1-4] In these studies the variation of fission barriers with angular momentum was based on results of the rotating liquid-drop model.[5] While the conclusions of Refs. 1-4 vary somewhat from case to case, it was found that, in all cases, the fission barriers that are consistent with the data are significantly lower than the rotating liquid-drop model predictions for the same region of angular momentum. This basic conclusion was not surprising since more realistic calculations,[6] which take into account the diffuseness of the nuclear surface and the finite range of the nuclear force, result in lower calculated fission barriers than those deduced from the liquid-drop model.

Until recently, the more realistic calculations have been available only for the case of zero angular momentum, and comparisons could only be made either by means of an arbitrary extrapolation to zero angular momentum[3] or by means of a scaling prescription.[4] In this work we make use of preliminary results of Sierk,[7] who has performed the calculations as a function

of angular momentum for a few selected cases. In these calculations the above-mentioned corrections to the surface energies[6] have been included, together with corrections to the rotational energies due to the diffuseness of the matter distribution[8] as well as corrections to the Coulomb energies due to the diffuseness of the charge distribution.[8] The parametrization has been made in terms of Legendre polynomials,[9] and the shapes have been constrained to axial symmetry as in Ref. 5.

In order to extract statistical model parameters from cross section data, it is necessary to measure both fission excitation functions and excitation functions for evaporation residues (ER). In Refs. 1-3 fits to such data have been made by means of two free parameters: the angular-momentum-dependent fission barrier, $B_f(J)$, and the ratio of the level density parameter for fission, a_f, to that for particle emission, a_ν. The fits are usually accomplished with the aid of various statistical model nuclear deexcitation computer codes. In this work, we have constrained $B_f(J)$ to the calculated theoretical values, and thus our fits involved only one free parameter, a_f/a_ν. The computer code used was a modified version of JULIAN,[10] into which the calculated $B_f(J)$ values have been incorporated.

Since our primary interest in this work involves determination of fission barriers, we have examined three cases for which measured excitation functions extend to very low fission cross sections ($\lesssim$0.1 mb). Such data are likely to provide sensitive measures of the fission barrier. The reactions studied here are $^{20}Ne + {}^{133}Cs$ and $^{12}C + {}^{141}Pr$, both leading to the ^{153}Tb compound nucleus,[3] and $^{12}C + {}^{169}Tm$. The first two reactions are of particular interest due to the additional constraint of requiring adequate fits to data from both reactions with the same values of $B_f(J)$ and of the adjustable parameter a_f/a_ν.

In Fig. 1 the calculated fission barriers are shown as a function of angular momentum for the case of $^{153}Tb^*$. The liquid-drop values are shown, together with the Sierk calculations[7] described above. $B_f(J)$ values corresponding to 80% of the liquid-drop values, $B_f^{LD}(J)$, are also indicated. In Ref. 3 the best fit to the data was obtained with $B_f(J) = 0.83\ B_f^{LD}(J)$. It can be seen from Fig. 1 that, in the region of angular momentum in which

the competition between fission and particle emission is the strongest (near 10 MeV), the $B_f(J) = 0.8\ B_f^{LD}(J)$ curve and the curve depicting the Sierk calculation are relatively close to each other. Thus we can expect an adequate fit to the data of Ref. 3 with the new fission barriers. This can be confirmed by inspecting Fig. 2, in which experimental results of Ref. 3 are compared with our calculations. The calculated results are for $a_f/a_\nu = 1.075$ (cf. $a_f/a_\nu = 1.08$ in Ref. 3). The hatched band indicates the range of computational uncertainties associated with the Monte Carlo calculation. The agreement between the experimental results and the theoretical curve is reasonably good, except at the highest excitation energies where such effects as incomplete fusion may cause the observed deviations.

The $^{12}C + {}^{169}Tm$ fission excitation function was measured by Sikkeland.[11] The excitation function for ER, however, was not available. Since the Sikkeland fission data are very suitable for our purposes (very low fission cross sections have been measured), we have measured[12] the necessary ER cross sections in order to be able to proceed with the one-parameter fit. We found that $\sigma_{ER} = 640$ mb at 74.3-MeV bombarding energy, $\sigma_{ER} = 1000$ mb at 88.1 MeV, and $\sigma_{ER} = 1320$ mb at 102.8 MeV. Our calculations are compared to Sikkeland's measurements in Fig. 3. The value of a_f/a_ν giving the fit shown was 1.04.

We conclude that, for the limited number of cases we have considered, the calculations presented here adequately represent the experimental observations and that our calculated fission barriers appear to be valid in this region of the nuclear mass table. It was pointed out by Blann[2,4] that arbitrary extrapolation of empirical B_f values to zero angular momentum may not be valid. Evidence for this can be seen in Fig. 1, where the $B_f = 0.8\ B_f^{LD}$ curve and the curve depicting the Sierk barriers intersect the zero angular momentum axis at very different energies. However, we feel that, for the first time, we have reasonable theoretical guidance as to how to make this extrapolation. Keeping in mind the above reservations, we may state that the data considered here are consistent with B_f values of 28.90 MeV for ^{155}Tb and 19.03 MeV for ^{181}Re, exclusive of any possible shell corrections.

B. Neutron Emission

Neutron emission associated with fission fragments has been reported in Ref. 13 for 192-MeV ^{12}C + ^{158}Gd and 176-MeV and 239-MeV ^{20}Ne + ^{150}Nd. It was reported that for the C reaction and for the lower energy Ne reaction, most of the neutron emission precedes fission. It was also thought that for the 239-MeV Ne bombardment, the situation changes dramatically and that most of the neutrons are emitted from the fragments. As a result of a follow-up experiment,[14] we discovered an error in the analysis of the 239-MeV data, and this conclusion turned out to be erroneous. Thus, we believe that in all cases investigated, most of the neutrons are emitted prior to fission. This conclusion is inconsistent with statistical model calculations (see Fig. 3 of Ref. 13). We may speculate, however, that the observed large pre-fission neutron emission is due in part to emission from the compound nucleus prior to fission and in part to emission from the neck, or some other region, during the scission process. Experimentally, it is not possible to distinguish between the two alternate sources of neutrons.

References

*Research supported by the Division of High Energy and Nuclear Physics, U.S. Department of Energy, under contract W-7405-eng-26 with the Union Carbide Corporation.

†Permanent address: Los Alamos National Laboratory, Los Alamos, New Mexico.

1. M. Beckerman and M. Blann, Phys. Lett. 68B, 31 (1977).
2. M. Beckerman and M. Blann, Phys. Rev. C 17, 1615 (1978).
3. F. Plasil, R. L. Ferguson, R. L. Hahn, F. E. Obenshain, F. Pleasonton, and G. R. Young, Phys. Rev. Lett. 45, 333 (1980).
4. M. Blann and T. A. Komoto, Report UCRL-87112, submitted to Phys. Rev. C, January 1982.
5. S. Cohen, F. Plasil, and W. J. Swiatecki, Ann. Phys.(N.Y.) 82, 557 (1974).
6. H. J. Krappe, J. R. Nix, and A. J. Sierk, Phys. Rev. C 20, 992 (1979).
7. A. J. Sierk, unpublished results.
8. K.T.R. Davies and J. R. Nix, Phys. Rev. C 14, 1977 (1976).
9. S. Trentalange, S. E. Koonin, and A. J. Sierk, Phys. Rev. C 22, 1159 (1980).
10. A. Gavron, Phys. Rev. C 21, 230 (1980); Y. Eyal and M. Hillman, evaporation code JULIAN (unpublished).
11. T. Sikkeland, Phys. Rev. 135, B669 (1964).
12. F. Plasil, B. Cheynis, R. L. Ferguson, F. E. Obenshain, and G. R. Young, unpublished results.
13. A. Gavron, J. R. Beene, B. Cheynis, R. L. Ferguson, F. E. Obenshain, F. Plasil, G. R. Young, G. A. Petitt, M. Jääskeläinen, D. G. Sarantites, and C. F. Maguire, Phys. Rev. Lett. 47, 1255 (1981).
14. A. Gavron, T. C. Awes, J. R. Beene, B. Cheynis, R. L. Ferguson, F. E. Obenshain, F. Plasil, G. R. Young, and G. A. Petitt, unpublished results.

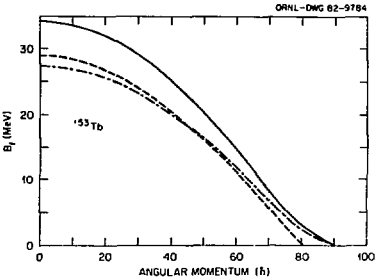

Fig. 1. Calculated fission barriers. The solid curve represents liquid-drop model values; the dash-dot curves, 80% of the liquid-drop model values; and the dashed curve, values calculated by Sierk, as described in the text.

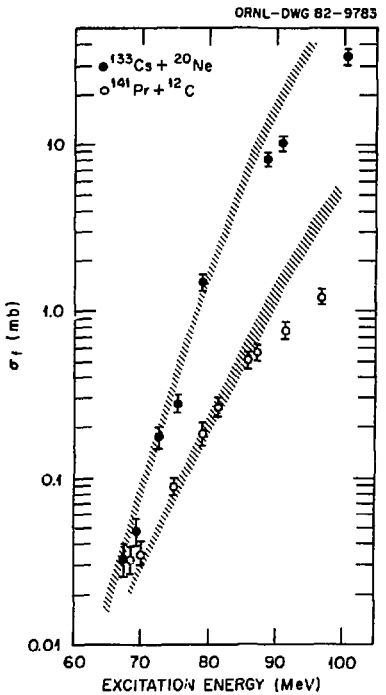

Fig. 2. Measured and calculated fission cross sections. Solid points represent measurements for ^{133}Cs + ^{20}Ne; open points are for ^{141}Pr + ^{12}C. Values are from Ref. 3. The cross-hatched bands show our results from Monte Carlo deexcitation calculations that incorporated Sierk's fission barriers. Widths of the band indicate computational uncertainties.

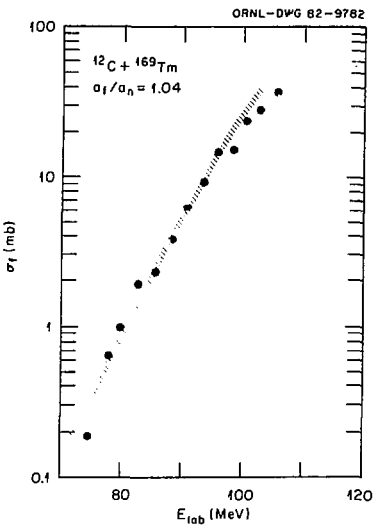

Fig. 3. Measured (points) and calculated (cross-hatched band) fission cross sections. Experimental values are from Ref. 11. See caption of Fig. 2 for remarks on calculation.

PAULI BLOCKING IN FINITE NUCLEI*

S. Shlomo and P. J. Siemens
Department of Physics and Cyclotron Institute
Texas A&M University
College Station, Texas 77843

The Pauli blocking is an important effect in describing a wide range of phenomena, such as inelastic scattering of an interacting particle (π,n,p, etc.) from a nucleus[1], propagation of a particle in nuclear matter[2] and mass transfer in heavy ion collisions[3]. We discuss here some preliminary results for the Pauli suppression factor P(q) in finite nuclei, using the harmonic oscillator (HO) model and comparing them to those obtained using the Fermi gas (FG) model. We derive an expression for P(q) in terms of the Wigner transform (WT) of the one-body density, which simplifies the calculation of P(q) for the HO model.

Within the independent particle model, the response of the nucleus to the projectile scattering probe $O(\vec{q},\vec{r})$ is given by

$$S(q,E) = \frac{\sum_{i,f} \left|\langle\Psi_i\left|O\right|\Psi_f\rangle\right|^2 \delta(E_f-E_i-E)}{\sum_i \langle\Psi_i\left|O^*O\right|\Psi_i\rangle}, \tag{1}$$

where Ψ_i and Ψ_f are occupied and unaccupied single particle states, respectively. The Pauli blocking factor is given by[1]

$$P(q) = \int S(q,E)\, dE. \tag{2}$$

In the case of no Pauli blocking ($\langle\Psi_j\left|O\right|\Psi_i\rangle = 0$ for occupied states) we have P(q) = 1. Let us first consider the Born approximation for $O(\vec{q},\vec{r})$,

$$O(\vec{q},\vec{r}) = e^{i\vec{q}\cdot\vec{r}} \qquad \text{(Born approx.)} \tag{3}$$

where $\vec{q} = \vec{k} - \vec{k}'$ is the momentum transfer. The denominator in (1) gives the nucleon number A. The Wigner transform (WT) which corresponds to a wave function $\Psi(\vec{r})$ is defined by[4]

$$f(\vec{r},\vec{p}) = (1/2\pi)^3 \int d\vec{s}\; e^{i\vec{p}\cdot\vec{s}}\; \Psi^*(\vec{r}+\vec{s}/2)\; \Psi(\vec{r}-\vec{s}/2). \tag{4}$$

Using the definition (4) one finds that

$$I_{if}(q) = \left|\langle\Psi_i\left|O\right|\Psi_f\rangle\right|^2 = \int d\vec{r}\; d\vec{p}\; f_i(\vec{r},\vec{p}+\vec{q})\; f_f(\vec{r},\vec{p}), \tag{5}$$

where $f_i(\vec{r},\vec{p})$ and $f_f(\vec{r},\vec{p})$ correspond to $\psi_i(\vec{r})$ and $\psi_f(\vec{r})$, respectively. Using (1), (2) and (3), we obtain for P(q) in (5) the result,

$$P(q) = \frac{1}{A}\int d\vec{r}\, d\vec{p}\, F_A(\vec{r},\vec{p}+\vec{q})\ [1 - \frac{(2\pi)}{4}^3 F_A(\vec{r},\vec{p})], \qquad (6)$$

where $F_A(\vec{r},\vec{p})$ is the WT of the one-body density $\rho(\vec{r},\vec{r}') = \sum_i \psi_i^*(\vec{r})\ \psi_i(\vec{r}')$. It is remarkable that (6) is of the form that one may write down for P(q), assuming that $F_A(\vec{r},\vec{p})$ is a phase space distribution function (in the classical sense). It should be pointed out, however, that $F_A(\vec{r},\vec{p})$ may acquire negative values in certain regions.

In the Fermi gas model one has

$$F(\vec{r},\vec{p}) = 4(1/2\pi)^3\ \theta(p_F^2 - p^2), \qquad (7)$$

where p_F is the Fermi momentum and the factor 4 is due to isospin-spin degeneracy. Substituting (7) in (6) one obtains the well-known result,

$$P(q) = \begin{cases} (3/4)\ x\ (1-x^2/12) & x\leq 2 \\ 1 & x>2 \end{cases} \qquad (8)$$

where $x = q/p_F$. For the HO model we make use of the result[6]

$$F(\vec{r},\vec{p}) = \sum_K n_K f_K(\vec{r},\vec{p}) = \sum n_K(4/\pi^3)(-1)^K e^{-\varepsilon} L_K^2(2\varepsilon), \qquad (9)$$

where n_K is the occupation number of the major shell K, $L_K^\alpha(x)$ is the associated Laguerre polynomial and ε is a dimensionless energy, $\varepsilon = p^2/\nu + \nu r^2 = 2E/\hbar\omega$, with $\nu = m\omega/\hbar$. Using (9), we can reduce the calculation of (6) to a one dimensional integral which is evaluated numerically. Fig. 1 shows the calculated P(q) for Fermi gas ($p_F \simeq 1.37$ fm^{-1}) model and for HO model with A = 16 and 224, respectively. Since the HO model describes the nuclear surface more realistically than the FG model, it is quite interesting to note from Fig. 1 that for low momentum transfer q, the HO results for P(q) are smaller than the corresponding FG values.

Very recent analysis of forward angle of inelastic scattering of protons with E>200 MeV from nuclei indicates[1] that for low q, the values of P(q) obtained from (8) are too small to explain the data. A similar conclusion is obtained[3] from time dependent Hartree Fock (TDHF) calculations of mass transfer between heavy ions colliding at low energy (E/A~1-2 MeV). The results presented in Fig. 1 show that this is due to the Born approximation adopted in Eq. (3) for the probe operator $O(\vec{q},\vec{r})$. In fact, significant

enhancement in P(q), for low q, is found when the distorted wave Born approximation (DWBA) with an optical potential V(r) + iW(r) is adopted to obtain the probe operator O.

*Supported in part by the National Science Foundation under contract PHY-8109010

References

1) G. F. Bertsch and O. Scholten, MSU preprint 1981.
2) C. B. Dover, D. J. Ernst and R. M. Thaler, Phys. Rev. Lett. 32 (1974)557.
3) M. Prakash, S. Shlomo, B. S. Wilsson, J. P. Bondorf and F. E. Serr, Phys. Rev. Lett. 47 (1981) 898; and to be published
4) E. P. Wigner, Phys. Rev. 40 (1932) 749.
5) S. Shlomo and P. J. Siemens, to be published.
6) S. Shlomo and M. Prakash, Nucl. Phys A357 (1981) 157.

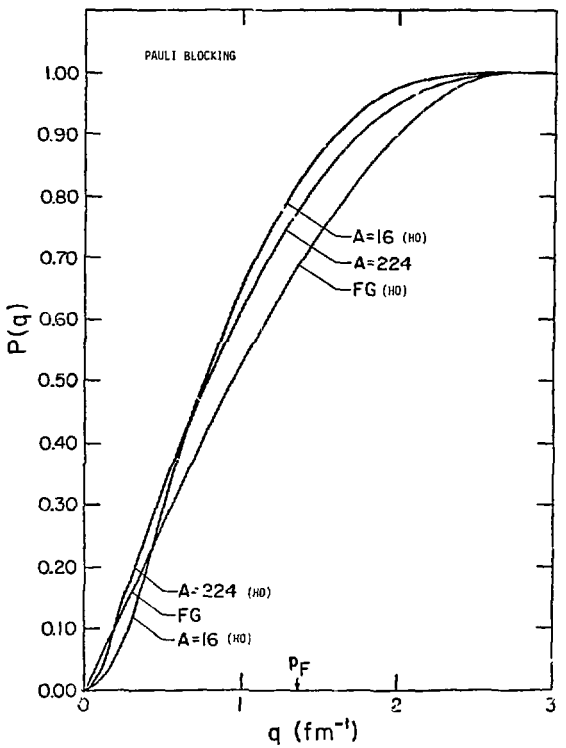

Fig. 1

MASS AND CHARGE DISTRIBUTIONS IN THE REACTIONS OF ^{40}Ca AND ^{209}Bi WITH ^{37}Cl*†

A. C. Mignerey and A. Gökmen
Department of Chemistry
University of Maryland, College Park, Maryland 20742

H. Breuer
Department of Physics and Astronomy
University of Maryland, College Park, Maryland 20742

K. L. Wolf, R. R. Betts, C. Davids, and B. G. Glagola
Argonne National Laboratory
Argonne, Illinois 60439

V. E. Viola
Department of Chemistry
Indiana University, Bloomington, Indiana 47405

The deep-inelastic reaction follows the evolution of a heavy-ion reaction system from products with quasielastic energies down to Coulomb energies corresponding to large deformations in the exit channel. The processes of charge-to-mass equilibration, nucleon exchange and relaxation of the mass asymmetry degree of freedom are intimately related to the conversion of the initial kinetic energy into internal excitation of the target and projectile. To better understand this transition, simultaneous charge and mass distributions have been measured as a function of total kinetic energy loss (TKE_{LOSS}) for the systems $^{40}Ca + {}^{37}Cl$ at $E_{Lab}(^{37}Cl) = 270$ and 221 MeV and $^{209}Bi + {}^{37}Cl$ at $E_{Lab}(^{37}Cl) = 270$ MeV The near symmetric system has N/Z ratios of the ^{37}Cl and ^{40}Ca of 1.18 and 1.0, respectively, while the N/Z ratio of ^{209}Bi is 1.52. The total kinetic energy above the entrance channel Coulomb barrier is $\sim$ 95 MeV for the 270 MeV ^{37}Cl on ^{40}Ca, $\sim$ 85 MeV for the 270 MeV ^{37}Cl on ^{209}Bi and $\sim$ 65 MeV for the 221 MeV ^{37}Cl on ^{40}Ca. The experiment was performed using ^{37}Cl beams from the Argonne Superconducting LINAC to bombard thin, self-supporting, isotopically pure targets of ^{40}Ca and ^{209}Bi. Charge and mass identification of the projectile-like fragments was achieved with two solid state detector ΔE-E time-of-flight telescope with flight paths of $\sim$ 65 cm each. The resolution was $\lesssim$ 0.5 mass and charge units over the range of products observed, with an energy resolution of $\sim$ 1 MeV. The angles at which data were taken with the ^{40}Ca target were 8° and 13° for 270 MeV ^{37}Cl, the latter being near the grazing angle, and 13° for 221 MeV ^{37}Cl, which is several degrees forward of the grazing angle. The two angles measured with the ^{209}Bi target were both in the vicinity of the grazing angle, 44° and 48°.

The measured product distributions are approximately Gaussian in the N-Z plane. The evaporation residue contribution to the $^{40}Ca + {}^{37}Cl$ reaction is

*Work supported by the United States Department of Energy.
†Support of the University of Maryland Computer Science Center is gratefully acknowledged.

cleanly separated at both bombarding energies, however sequential fission of the ^{209}Bi becomes a problem at energy losses near the Coulomb barrier. The conversion from laboratory energies to total kinetic energy (TKE) included a correction for the energy removed by particle evaporation, assuming the excitation energy is divided according to the mass of the fragments. No correction was made in the mass or charge of the measured fragments, since, especially in the $^{40}Ca + {}^{37}Cl$ reaction, both neutron and proton evaporation are probable. This is very important for the isobaric charge distributions but has a smaller effect on the widths of the overall mass and charge distributions.

The majority of available data on charge and mass distributions do not go below $\sim$ 30-40 MeV of TKE_{LOSS} and are in coarse energy bins. Since one of the goals of this work was to investigate the initial energy loss mechanism, sufficient statistics were taken to allow cuts in 2-5 MeV wide TKE bins. The excellent energy, mass and charge resolution allowed analysis of data to within 5 MeV of the elastic energy. The two-dimensional N-Z distributions were analyzed via a two-dimensional Gaussian of the form

$$P = h \exp - [a(N-N_0)^2 + b(Z-Z_0)^2 + 2c(N-N_0)(Z-Z_0)].$$

For each TKE_{LOSS} cut, six parameters describe the data: a normalization h, the centroids N_0 and Z_0 and a, b, and c representing the variances and covariance. The following provide the explicit relationships between a, b and c and the quantities discussed.[1)]

$$\sigma_Z^2 = \frac{b}{\gamma}$$

$$\sigma_N^2 = \frac{a}{\gamma}$$

$$\sigma_A^2 = \gamma(a+b+2c) \qquad \gamma = a \cdot b - c^2$$

$$\sigma_Z^2(A) = \frac{1}{a+b+2c}$$

$$\rho_{NZ} = \frac{c}{\sqrt{a \cdot b}} \qquad \sigma_{NZ} = \gamma c$$

The variances of the charge distributions σ_Z^2 are plotted in Fig. 1 as a function of TKE_{LOSS} for the reaction $^{40}Ca + {}^{37}Cl$ at the two bombarding energies. The results obtained at 8° and 20° for the 270 MeV energy are identical, further verifying the conclusion that mass and charge distributions are a function of TKE_{LOSS} and independent of angle. The widths are quite broad at energy losses in the vicinity of the Coulomb barrier but are very similar in the first 35 MeV of TKE_{LOSS}. This is consistent with the results obtained for the $^{144}Sm + {}^{84}Kr$ system at 720, 595 and 470 MeV. In fact, the results for the 470 MeV case fall on the curve[2)] defined by the 270 MeV ^{37}Cl data. These data are in contrast to

the results obtained for the $^{209}Bi + ^{37}Cl$ system which maintains a very narrow distribution, similar to that obtained in the $^{209}Bi + ^{56}Fe$ system,[3] reaching a variance of only ~ 1.4 at 60 MeV of TKE_{LOSS}.

The correlation coefficient ρ defined as $\sigma^2_{NZ}/(\sigma_N \cdot \sigma_Z)$ provides a means of measuring the correlation between the exchange of neutrons and protons. A $\rho=0$ implies independent motion while $\rho=1$ gives completely correlated transfer. The correlation coefficient for the two energies in the $^{40}Ca + ^{37}Cl$ reaction are not significantly different. Therefore only the coefficients for the 270 MeV data are plotted as a function of TKE_{LOSS} in Fig. 2. Initially the reaction shows a small amount of anticorrelated exchange which slowly increases to approaching the fully correlated limit at large TKE_{LOSS}. The anticorrelation may involve an initial alignment of the N/Z ratio along the potential energy surface. This effect is expected to be stronger in the very asymmetric system $^{209}Bi + ^{37}Cl$, however experimental verification of this is not yet available. The ratio of the neutron to proton variance σ^2_N/σ^2_Z shows that initially the neutron exchange dominates with ratios approaching 3 for 5-10 MeV of energy loss. This ratio rapidly decreases and reaches an equilibrium value at high energy losses.

The variances of the isobaric charge distributions $\sigma^2_Z(A)$ for the $^{40}Ca + ^{37}Cl$ reaction are shown in Figs. 3 and 4. Those presented in Fig. 3 have been averaged over all A values by the two-dimensional Gaussian procedure. Figure 4 shows the results of a moment analysis to individual A cuts. The widths are considerably narrower than those obtained for heavier systems. The problems of particle evaporation are very important for the lighter systems. The decrease in width at about 20 MeV of TKE_{LOSS} can be, at least partially, attributed to the particle decay channeling the secondary products along the valley of stability. The $^{209}Bi + ^{37}Cl$ system is expected to be less affected by this since, on the average, the ^{37}Cl-like fragment receives a very small fraction of the total excitation energy. It is believed that the primary distributions are quite narrow in these reactions and much narrower than for the Fe-induced reactions.[1] However, it is cautioned that any quantitative conclusions regarding the saturation of the variances must await the results of further calculations and possibly experiments to determine the widths of the excitation energy divisions in these reactions.

The results presented here represent only a portion of results from data analysis still in progress. Interested readers are invited to contact the authors for further information.

REFERENCES

1. H. Breuer, et al., Proc. Int. Workshop on Gross Properties of Nuclei and Nuclear Excitation IX, Hirschegg, Austria (January 1981), and to be published.

2. A. C. Mignerey, et al., to be published.

3. H. Breuer, et al., Phys. Rev. Lett. 43, 191 (1979).

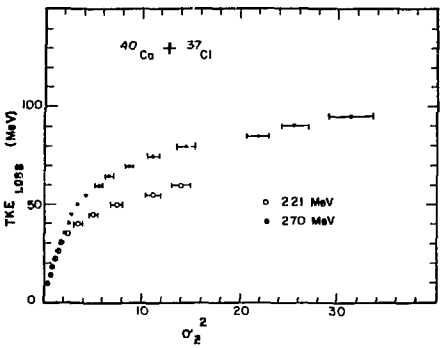

Fig. 1: Variances of the charge distributions for the reactions $^{40}Ca + 221$ and 270 MeV ^{37}Cl plotted versus total kinetic energy loss.

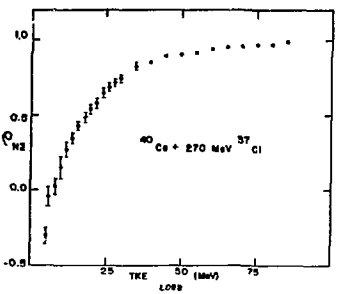

Fig. 2: Correlation coefficient for the reaction $^{40}Ca + 270$ MeV ^{37}Cl as a function of total kinetic energy loss.

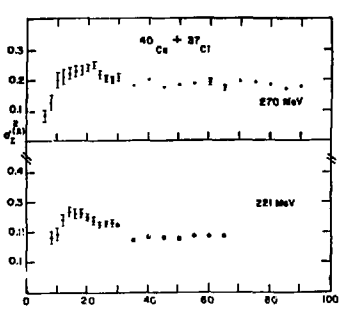

Fig. 3: Variances of the isobaric charge distributions, averaged over A value using the two-dimensional Gaussian procedure, as a function of total kinetic energy loss.

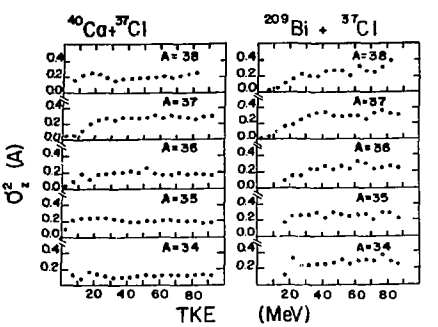

Fig. 4: Variances of the isobaric charge distributions for the systems ^{40}Ca and $^{209}Bi + 207$ MeV ^{37}Cl. Cuts were made in the mass plane for discrete A values. The variances of the resulting charge distributions were obtained through a moment analysis.

Deuteron Production in High Energy Heavy Ion Collisions*

M. Gyulassy, E. Remler, K. Frankel

Nuclear Science Division
Lawrence Berkeley Laboratory
University of California
Berkeley, CA 94720

We Apply the Wigner density formalism of Remler[1] to the production of deuterons in nuclear collisions. The theory is based on the intranuclear cascade model, which follows the space-momentum trajectories of all particles. The starting point is the transition rate formula

$$P_{12}(t) = -\frac{i}{\hbar} \mathrm{Tr}\rho_{12}[U_{12},\rho(t)] \tag{1}$$

for particles 1 and 2 to scatter into a bound state characterized by the density matrix, ρ_{12}. In eq. (1) $\rho(t)$ is the full A-body density matrix and $U_{12} = \Sigma(V_{1i} + V_{2i})$ for $i \geq 3$ is the interaction potential of particles 1 and 2 with the remainder of the system. As we are interested in the classical limit, we evaluate the trace in the Wigner representation.

In the classical limit,

$$\rho_W(x,p_1,\ldots,x_A\ _A;t) = \langle \prod_{i=1}^{A} (2\pi\hbar)^3 \delta^3[x_i - \bar{x}_i(t)]\delta^3[p_i - \bar{p}_i(t)] \rangle \tag{2}$$

in terms of the classical trajectories $\bar{x}_i(t)$ and $\bar{p}_i(t)$. The Wigner transform of the commutator in eq. (1) simplifies in the classical limit to

$$\lim_{\hbar\to 0} \frac{-i}{\hbar} [U_{12},\rho]_W = \langle \sum_{i=1}^{2} \sum_{j=3}^{A} \vec{\nabla}_{x_i} V(x_i - x_j)\cdot(\vec{p}_i - \vec{p}_j)\rho_W \rangle . \tag{3}$$

The final expression for the transition rate is

$$P_{12} = \langle \sum_{j\geq 3} \left\{ \vec{F}_{1j}\cdot\vec{\nabla}_{p_1} + \vec{F}_{2j}\cdot\vec{\nabla}_{p_2} \right\} \rho^W_{12}(x_1p_1,x_2p_2) \rangle \tag{4}$$

in terms of the Wigner transform, ρ^W_{12}, of the bound density matrix and the classical forces $\vec{F}_{ij} = -\vec{\nabla}_{x_i} V(x_i - x_j)$.

Intranuclear cascade provides a particular simple example of eqs. (2,4). The forces are impulses at discrete times t_i. The integrated probability for deuteron production is then simply given by[2]

$$P_{12} = \sum_{i=0}^{N} \frac{(2\pi\hbar)^3}{V} \delta^3[P - p_1(i) - p_2(i)] \{\rho_d[r(i),q(i)] - \rho_d[r(i+1),q(i)]\} \quad (5)$$

where $r(i) = x_1(t_i) - x_2(t_i)$, $q(i) = p_1(t_i + \varepsilon) - p_2(t_i + \varepsilon)$,

and $\rho_d(r,q) = 8 \exp(-r^2/d^2 - q^2d^2)$ for a Gaussian deuteron wave-function ($d \approx 2.1$ fm).

The brackets <...> denote an ensemble average over many cascade events. We have performed the first calculations based on eq. (5) using Cugnon's cascade code. The results are shown in Fig. 1 for the reactions 400 MeV/A Ne + U and 400 MeV/A Ar + Ca (Sandoval, et al.[3]). We show the cascade results for both the primordial sum charges and the deuterons. For the deuterons we compare both to the free deuteron data (dots) and also to the "primordial" deuteron data (solid triangles) which are important at small angles and low energy. It is necessary to compare to the primordial deuteron distribution because the total number of deuteron like correlated (n,p) pairs includes those bound in heavier fragments. We take the primordial distribution to be primordial deuterons $= \sigma_d + 3/2\ (\sigma_t + \sigma_{He^3}) + 3\sigma_{He^4}$, when we sum over experimental data. The results show the sum charges and primordial deuterons are well accounted for for deuteron energies $\gtrsim$ 20 MeV/A.

In figure two we show the results for 400 MeV Ne + U taken with a high multiplicity trigger[4]. We use an impact parameter cutoff of b_{max} = 2.1 fm, which has been adjusted to obtain the best fit. We show results for sum charges and primordial deuterons, which for this experiment contain only deuterons and tritons.

An important qualitative result that was obtained is that the unbound proton inclusive distributions can be largely modified from the summed charges inclusive yields due to deuteron production. In particular, for central collisions, the cascade code predicts a forward enhancement of the total yield. However, in the forward direction the phase space density is high and therefore most nucleons emerge as bound fragments. This nucleosynthesis process depletes the free proton spectra at forward angles. We are investigating whether the observed forward proton suppression is due to this mechanism as opposed to the hydrodynamic flow mechanisms.

This work was supported by the Director, Office of Energy Research, Division of Nuclear Physics of the Office of High Energy and Nuclear Physics of the U.S. Department of Energy under Contract DE-AC03-76SF00098.

References

1. E. Remler, Ann. Phys. (N.Y.) 136, 293 (1981).

2. M. Gyulassy, E. Remler, K. Frankel, preprint in preparation.

3. A. Sandoval, H.H. Gutbrod, W.G. Meyer, R. Stock, Ch. Lukner, A.M. Poskanzer, J. Gosset, J.-C. Jourdain, C.H. King, G. King, Nguyen VanSen, G.D. Westfall, and K.L. Wolf, Phys. Rev. C21, 1231 (1980).

4. R. Stock, H.H. Gutbrod, W.G. Meyer, A.M. Poskanzer, A. Sandoval, J. Gosset, C.H. King, G. King, Ch. Lukner, Nguyen VanSen, G.D. Westfall, and K.L. Wolf, Phys. Rev. Lett. 44, 1243 (1980)

Fig. 1 Comparison of charge inclusive data (dots) ((a) and (c)) with calculations (solid lines). In (b) and (d) the primordial deuteron distribution (lines) is compared to data (solid triangles). The free deuteron data are indicated by dots.

Fig. 2 Comparison between theory (lines) and sum charges (dots) and primordial deuterons (triangles) for impact parameters $b \leq 2.1$ fm.

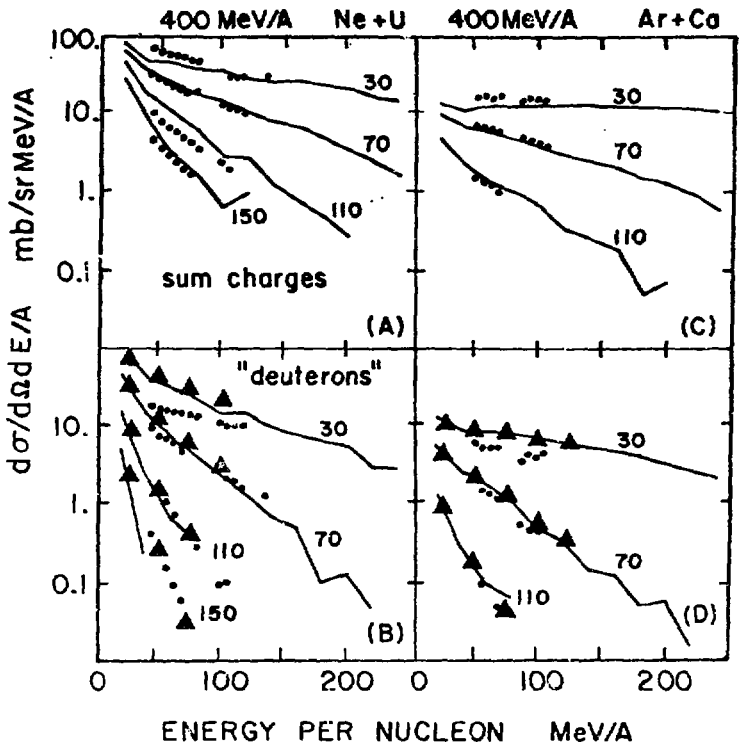
400 MeV/A Ne+U
400MeV/A Ar+Ca
100.
10.
1.
0.1
30
70
110
150
sum charges
(A)
(C)
"deuterons"
(B)
(D)
dσ/dΩdE/A mb/sr MeV/A
0
100
200
ENERGY PER NUCLEON MeV/A

Fig. 1

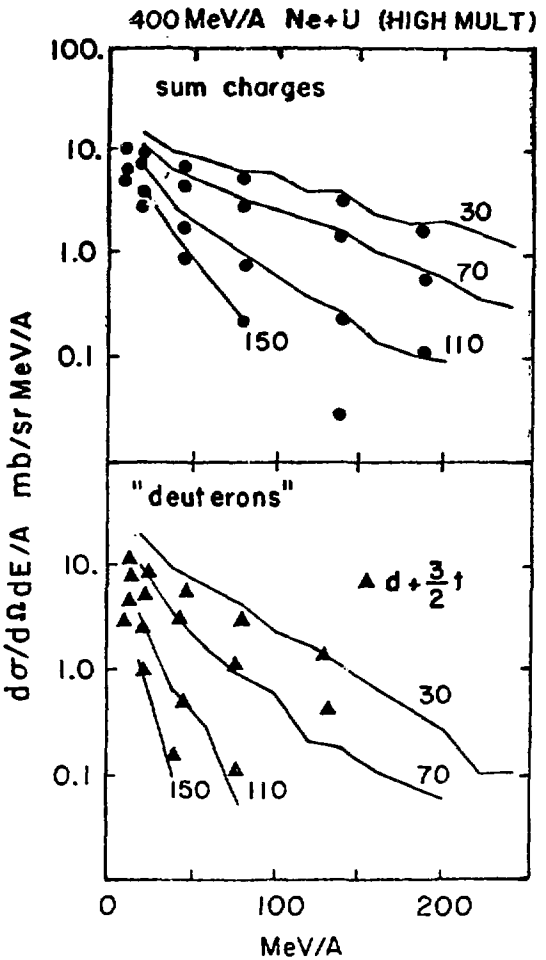
400 MeV/A Ne+U (HIGH MULT)
sum charges
100.
10.
1.0
0.1
30
70
110
150
"deuterons"
▲ d + 3/2 t
dσ/dΩdE/A mb/sr MeV/A
0
100
200
MeV/A

Fig. 2

Flow of Nuclear Matter in Heavy Ion Collisions

M. Gyulassy, K. Frankel, and H. Stöcker

Nuclear Science Division
Lawrence Berkeley Laboratory
University of California
Berkeley, CA 94720

Inclusive measurements have been unable to tell us whether hydrodynamics or intranuclear cascade provide a better model of high energy nucleus nucleus collisions. If we were to observe reactions where hydrodynamics is valid, then we would expect to observe collective flow of colliding nuclear matter. This might be expected to occur in reactions of heavy nuclei at small impact parameters. We propose a new method of global analysis to help test for hydrodynamic flow in nuclear collisions.

Consider the kinetic flow tensor[1]

$$\overleftrightarrow{F} = \sum_{\nu} \overleftarrow{P}(\nu)\,\vec{P}(\nu)/2m = f_1 e_1 e_1^{\dagger} + f_2 e_2 e_2^{\dagger} + f_3 e_3 e_3^{\dagger} \qquad (1)$$

obtained by summing over the momenta of all fragments ν on an event by event basis. The kinetic flow tensor has the advantages that it gives a full 3 dimensional description of the event, gives the correct weight to composites and the trace is fixed by energy conservation. The eigenvalues f_i and eigenvectors e_i are analytic function of F_{ij}. Furthermore, the aspect

ratios f_i/f_j and flow angles θ_i are insensitive to missed particles (neutrons). The flow tensor characterizes an event as a 3 dimensional ellipsoid in momentum space with principal axes oriented along $\hat{e}_i$ and radii $\sqrt{f_i}$. In the case of a peripheral collision we expect a prolate spheroid oriented along the beam direction. In a central collision, we would expect an oblate spheroid if hydrodynamics is valid.

Fig. 1 shows a typical charge exclusive event for 400 MeV/nucleon Ca + Ca. as measured by the plastic ball-wall[2]. The momenta of all particles are projected on the plane spanned by the beam axis and the principal axis $\hat{e}_1$, corresponding to maximum kinetic flow. The oriented ellipse that is determined by the flow analysis is also indicated. This event shows a finite deflection $\theta_{flow} \approx 19°$ and corresponds to an ellipse with aspect ratios a/b=3. Also shown in figure 1 is a flow diagram, where θ_{flow} is plotted versus $f_1/f_3=(a/b)^2$. We show results for the flow analysis using the Cugnon cascade code[3] (shaded region) and using the non-viscous hydrodynamics model[4] for 400 A MeV U+U. We observe that the hydrodynamic predictions show much more "flow" (enhanced f_1/f_3 for a given θ_{flow}) as compared to cascade. We note that flow analysis is sensitive to detector acceptance and Coulomb final state effects.

We have also investigated how the cascade code has to be altered in order to simulate the hydrodynamic flow. We have found that by running mass 2000 on 2000 the cascade flow remains close to the U+U curve and hence cascade does not converge to non-viscous hydrodynamics at large A. We also tried to make the nucleon-nucleon mean free path shorter ($\sigma_{eff} > \sigma_{NN}$) to see if we could simulate hydrodynamic flow but this also had little effect. We next tried to see if the flow was sensitive to NN scattering style. In most cascade codes

the scattering angles (θ,ϕ) are taken randomly from NN free space cross sections. We tested the effect of imposing correlations between the relative momentum transfer, $\vec{q}$, and distance, $\vec{r}$, at the point of scattering. With $\sigma_{eff} = \sigma_{NN}$ we found little effect, but with $\sigma_{eff} > \sigma_{NN}$ we find considerable dependence on scattering style. With $\sigma_{eff} = 3\sigma_{NN}$ and $\vec{q}\cdot\vec{r}>0$ (repulsive potential) scattering style we found that cascade flow became similar to the non-viscous hydrodynamic flow shown in Fig. 1.

This work was supported by the Director, Office of Energy Research, Division of Nuclear Physics of the Office of High Energy and Nuclear Physics of the U.S. Department of Energy under Contract DE-AC03-76SF00098.

References:

1. M. Gyulassy, K.A. Frankel, and H. Stöcker, Phys. Lett. (in press) [Preprint, Lawrence Berkeley Laboratory, LBL-13379 (1981)]
2. M.R. Maier, H.G. Ritter, and H.H. Gutbrod, IEEE Trans. on Nuclear Science NS-27, 42 (1980)
3. J. Cugnon, Phys. Rev. C22, 1885 (1980)
4. H. Stöcker, G. Buchwald, L.P. Csernai, G. Graßbner, J.A. Maruhn, and W. Greiner, to be published

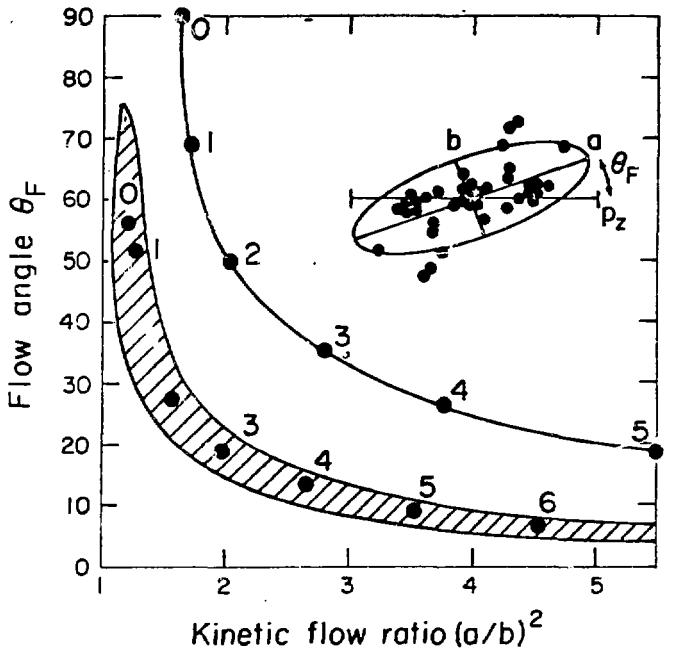

Fig. 1

Fig. 1 Flow diagram for $^{238}U+^{238}U$ at 400 MeV/nucleon. Insert shows one Ca+Ca (400 MeV/nucleon) event measured in the plastic ball. The dots represent measured and reflected momenta (about $P_{c.m.} = 0$) projected in the plane spanned by the beam axis and the principal axis e_1. The flow angle are plotted versus the kinetic flow ratio is $(f_1/f_3) = (a/b)^2$. For the event shown a/b = 3, a = 1 Gev/c, $\theta_{flow} = 19°$. The solid curve shows the results of nonviscous hydrodynamics[4]. The shaded region shows the results using intranuclear cascade[1]. The numbers along the curve indicate the impact parameter b in units of $b_{max}/10$.

Complete Events in Medium-Energy Nuclear Collisions*

George Fái and Jørgen Randrup

Nuclear Science Division, Lawrence Berkeley Laboratory
University of California, Berkeley, CA 94720

Recent developments in accelerator capability and detection technique have made it possible to obtain good-quality nearly exclusive data on multi-fragmentation processes in medium-energy collisions of heavy nuclei. A major objective of such undertakings is the search for peculiar structures in the individual event patterns, which may signal the occurrence of interesting reaction mechanisms, such as collective side-splashes or nuclear shadowing. Due to the finite multiplicity of fragments in a given event, the many-particle observables are associated with rather large fluctuations, and the identification of any structure, and the assessment of its significance, is therefore a delicate task.

Until now, no model has been able to yield sufficiently realistic exclusive events. One contender is the intra-nuclear cascade model, but it suffers from the drawback of yielding only elementary fragments (nucleons and pions) but not automatically composite nuclei. Another is the nuclear fluid-dynamical model, which, with appropriate augmentations, may yield composite fragments, but it is void of statistical fluctuations, which play an important role in practice.

As a first step towards a theory of exclusive reactions, we have found it of value to develop a model that invokes a minimum number of dynamical assumptions. Being conceptually simple, as well as practically manageable, this model provides a useful reference against which the significance of possible signals can be tested.

The work is still in progress and in this workshop contribution only some of the aspects will be dealt with. We focus on how a highly excited nuclear system disassembles into final observable fragments. In the complete theory the probability for such systems to be formed in a given collision is also addressed.

The disassembling system (or the initial state, or the source) is characterized by the following conserved quantities: its baryon number A_0, its charge number Z_0, and its four-momentum $P_0 = (\vec{P}_0, E_0)$; we denote these quantities collectively by i_0. Following the idealization introduced in ref. [2], the disassembly is assumed to proceed in two stages: First a quick explosion produces excited nuclear fragments according to the available microcanonical phase space. Subsequently, on a longer time scale, these primary fragments deexcite, first by nucleon and α-evaporation, later on by γ-decay, ultimately leading to the observed multi-fragment state.

The main novelty of the model is the calculation (in a suitable approximation) of the complete microcanonical many-fragment distribution function, rather than merely the one-fragment inclusive distributions. Thus, the calculated many-fragment states consistently incorporate the conservation laws.

With the statistical assumption, the exclusive probability for exploding into a given final many-fragment state f is given by

$$p(i_o|f) \sim \delta(i_o - i[f]) \tag{1}$$

where i[f] denotes the values of the conserved quantities associated with the state f: A_f, Z_f, P_f. The normalization constant in (1) is determined by the condition

$$\sum_f p(i_o|f) = 1 \tag{2}$$

The distribution function $p(i_o|f)$ corresponds to an exclusive measurement where the complete final state f is observed. If only some of the final fragments are observed, say $\tilde{f}$, then the corresponding inclusive probability is given by

$$\hat{p}(i_o|\tilde{f}) = \sum_{f \supseteq \tilde{f}} p(i_o|f) \tag{3}$$

where the summation includes all final states f that encompass the observed partial event $\tilde{f}$.

In general, a given final state f can be decomposed into a collection of one-fragment states $\{f_k\}$, $k \in (1, \nu_f)$ where ν_f is the multiplicity of fragments in f. It is then possible (see ref. [3]) to factorize the exclusive probability p into a product of one-fragment inclusive probabilities,

$$p(i_o|f) = \prod_{k=1}^{\nu_f} \hat{p}(i_{k-1}|f_k) \cdot p(i_{\nu_f}|0) \tag{4}$$

Here $i_k = i_{k-1} - i[f_k]$ and $\hat{p}(i_{k-1}|f_k)$ is the inclusive probability that a source characterized by the conserved quantities i_{k-1} explodes into any final state containing the specified one-fragment state f_k.

The above factorization (4) is well suited for a statistical (Monte Carlo) generation of a sample of events representative of the exclusive distribution (i.e. a sample of events f determined randomly according to the probability distribution $p(i_o|f)$). This can be done by first determining f_1 on the basis of the inclusive distribution $\hat{p}(i_o|f_1)$; then determining f_2 on the basis of the modified inclusive distribution $\hat{p}(i_1 = i_o - i[f_1]|f_2)$; and so on until no source is left.

This procedure would yield the exact multi-fragment distribution function. However, the evaluation of the microcanonical inclusive distributions is cumbersome and impractical. Therefore, we have adopted the approximation of replacing each of the inclusive probabilities in (4) by its grand canonical equivalent, truncated at the limits set by the corresponding source (so that no fragment can have A or E exceeding that of the state from which it is ejected).

The grand canonical treatment is described in refs [1,2]. It involves the evaluation of the grand partition function

$$Z[i_k] = \sum_f e^{-\beta_k(E_f - \mu_k A_f - \nu_k T_f)} \tag{5}$$

where $T_f = A_f/2 - Z_f$ is the isospin projection of the event f. The Lagrange multipliers $\beta_k \mu_k \nu_k$ appropriate for the particular source i_k are determined from the constraints:

$$\langle A_f \rangle = A_k, \ \langle Z_f \rangle = Z_k, \ \langle E_f \rangle = E_k \tag{6}$$

This approximation method proves to be quantitatively satisfactory (see ref. [3] for a detailed demonstration of this). It enables us to produce reasonably sized samples of multi-fragmentation events. (It should be added that subsequent to its formation during the explosive stage, each fragment is subjected to an evaporation treatment as described in ref. [2], so that the observed events contain only stable fragments.)

Events produced by the statistical model provide a useful testing ground for the various analysis schemes aimed at identifying peculiar structures in the emission patterns: Any search for specific dynamical effects ought to turn out negative for statistical events. This requirement can provide valuable guidance for developing the most suitable selection criteria. In this connection, it is an essential feature of the model that it contains the statistical fluctuations arising from the relative smallness of the multiplicity ν_f (finite particle number effects). Thus, as an example, even though the statistical model produces isotropic event patterns on the average (i.e. when many separate events are superimposed), each individual event usually exhibits substantial deviations from isotropy. This is clearly borne out by the illustration.

Illustration of event shapes

For this illustration we consider the disassembly into nucleons only (i.e. no composite fragments or pions are allowed). In order to obtain a global impression of an event f one may consider the Lorentz tensor

$$T_f^{\mu\nu} = \sum_{k=1}^{\nu_f} p_k^\mu \, p_k^\nu \, / 2 \, M_k \tag{7}$$

where P_k^μ is the four-momentum component of the k^{th} ejectile. Following Gyulassy et al. [4], we consider the spatial part (in the CM frame of f)

$$\vec{T}_f = \sum_{k=1}^{\nu_f} \vec{p}_k \, \vec{p}_k \, / 2 \, M_k = t_1 \vec{t}_1 + t_2 \vec{t}_2 + t_3 \vec{t}_3 \tag{8}$$

where the eigenvectors $\vec{t}_\kappa$ have been labeled so that $0 \leq t_1 \leq t_2 \leq t_3$. The three eigenvectors define an ellipsoid characterizing the distribution of ejectile momenta. In the present illustration we focus on the shape of this ellipsoid (since its overall size, given by $\mathrm{tr}\, \vec{T}$, is approximately the same for all events and its spatial orientation is entirely random in the statistical model).

Generalizing the standard description of triaxial shapes (see ref. [5]), we employ the polar coordinates (β,γ) given by

$$\beta = \left[\frac{16\pi}{15} (c_2^2 - c_1 c_3) \right]^{1/2} \in (0,\infty)$$

$$\gamma = \tan^{-1} \frac{c_2 - c_1}{\sqrt{3} c_3} \in (0, \pi/3) \tag{9}$$

where $c_K \equiv \ell n(t_K/t_0)$ with $t_0^3 = t_1 t_2 t_3$.

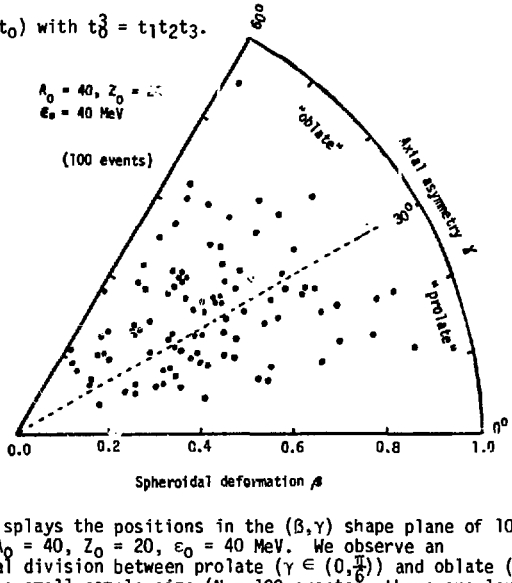

The figure displays the positions in the (β,γ) shape plane of 100 events characterized by $A_0 = 40$, $Z_0 = 20$, $\varepsilon_0 = 40$ MeV. We observe an approximately equal division between prolate ($\gamma \in (0,\frac{\pi}{6})$) and oblate ($\gamma \in (\frac{\pi}{6},\frac{\pi}{3})$) shapes. Due to the small sample size (N = 100 events), there are large fluctuations in the distribution of points. An important question is how the limiting distribution ($N \to \infty$) looks - it is clearly not uniform as a function of β (it seems to peak around $\beta = 0.5$), possibly not even as a function of γ (there seems to be some enhancement of truly triaxial shapes ($\gamma \approx \pi/6$)). An important task in the event analysis is the development of representations in which trivial dynamics (such as is assumed in the statistical model) gives rise to trivial distributions (i.e. without intriguing structures). It is therefore worthwhile noting that even though the limiting statistical event ($A_0 \to \infty$) has a spherical pattern, actual events, with their relatively small multiplicity, tend to exhibit large deviations from symmetry; this might be deceiving in the search for peculiar structure.

Finally, it should be noted that for nearly oblate shapes ($\gamma \approx \pi/3$), the event pattern has approximate symmetry around the 1-axis (rather than the 3-axis) and one might wish to take account of this feature in the possible further analysis of the event.

*This work was supported by the Director, Office of Energy Research, Division of Nuclear Physics of the Office of High Energy and Nuclear Physics of the U.S. Department of Energy under Contract DE-AC03-76SF00098.

[1] J. Randrup and S.E. Koonin, Nucl. Phys. A356 (1981) 223
[2] G. Fai and J. Randrup, Nucl. Phys. A (1982) in press
[3] J. Randrup and G. Fai, in preparation
[4] M. Gyulassy, H. Stöcker, and K. Fraenkel, LBL-13377, Phys. Lett. in press
[5] A. Bohr and B.R. Mottelson, Nuclear Structure II (1975) 677 ff

PARTICLE PRODUCTIONS IN HIGH-ENERGY, HEAVY-ION REACTIONS*

Cheuk-Yin Wong
Oak Ridge National Laboratory
Oak Ridge, TN 37830

Abstract

Results of Blankenbecler, et al. for hadron-nucleus collisions are generalized to heavy-ion collisions. Explicit expressions relating nucleon-nucleon to nucleus-nucleus partial cross sections are given.

* * * *

Recently, Blankenbecler, et al.[1] pointed out some unusual shadowing effects in particle production of nuclei in a hadron-nucleus collision at high energies. The condition for an arbitrarily defined cross section to be shadowed only by itself is given. Explicit expressions relating the nucleon-nucleon to hadron-nucleus partial cross sections were put forth. Examples were presented to illustrate the cases of interest.

We would like to generalize these results for hadron-nucleus collisions to heavy-ion collisions. We consider the scattering of a nucleus of atomic number A with a nucleus of atomic number B. The total cross section σ_{tot}^{AB} in the Glauber theory[2] is given by

$$\sigma_{tot}^{AB} = 2 \int d\vec{b} \{1 - [1 - \frac{T(b)\sigma_{tot}}{2}]^{AB}\} \tag{1}$$

where the cross section σ_{tot} without a superscript refers to that for nucleon-nucleon collisions. The profile function T(b) for heavy-ion collision is related to the nucleon-nucleon profile function $t(\vec{b})$ by

$$T(\vec{b}) = \int d\vec{q}_i d\vec{q}_j \; t(\vec{b}-\vec{b}_i+\vec{b}_j)\rho_A(\vec{q}_i)\rho_B(\vec{q}_j) \tag{2}$$

*Research sponsored by the Division of Basic Energy Sciences, U.S. Department of Energy, under contract W-7405-eng-26 with the Union Carbide Corporation.

where $\vec{b}_i$ is the transverse component of $\vec{q}_i$ and the density functions and the profile functions are normalized according to

$$\int d\vec{q}\ \rho_A(\vec{q}) = \int d\vec{q}\ \rho_B(\vec{q}) = \int d\vec{b}\ T(\vec{b}) = \int d\vec{b}\ t(\vec{b}) = 1. \tag{3}$$

Following Chou and Yang,[3] we shall take $t(\vec{b})$ to be a real function. In consequence, T(b) is also a real function.

The results of Eq. (1) indicate that for small mass numbers, $\sigma_{tot}^{AB} = AB\ \sigma_{tot}$ while for large mass numbers $\sigma_{tot}^{AB} \sim 2\pi r_o^2 (A^{1/3} + B^{1/3})^2$. Various versions of Eq. (1)[4] were found to agree well with experimental measurements of heavy-ion total cross sections.[5]

The result of Eq. (1) can be written in a different form

$$\sigma_{tot}^{AB} = 2 \int d\vec{b} \sum_{n=1}^{AB} \binom{AB}{n} \left(\frac{T(b)\sigma_{tot}}{2}\right)^n \left(1 - \frac{T(b)\sigma_{tot}}{2}\right)^{AB-n}. \tag{4}$$

Such an expansion provides a physical interpretation for each term. The general term $(T(b)\sigma_{tot}/2)^n\ (1 - T\sigma_{tot}/2)^{AB-n}$ represents the contribution from a physical process in which there are n basic nucleon-nucleon collisions and AB-n "misses" in the A × B encounters of the nucleons in the colliding nuclei. With the association of a physical process to each of the mathematical terms, mathematical expressions for different types of physical process can be conversely generated.[1]

We consider a "self-shadowing" (SS) criterion C such that the observation of a non-C event in heavy-ion collisions comes from the occurrence of non-C events in all basic nucleon-nucleon collisions.[1] We can decompose the basic total nucleon-nucleon cross section into the C-channel and non-C channel cross sections with different profile functions $t_C(\vec{b})$ and $t_N(\vec{b})$

$$t(\vec{b})\sigma_{tot} = t_C(\vec{b})\sigma_C + t_N(\vec{b})\sigma_N \tag{5}$$

where t_C and t_N are normalized in the same way as t. The cross section for the observation of the C events in heavy-ion reactions is then

$$\sigma_C^{AB} = \sigma_{tot}^{AB} - 2 \int d\vec{b} \sum_{n=1}^{AB} \binom{AB}{n} \left(\frac{T_N(b)\sigma_N}{2}\right)^n \left(1 - \frac{T(b)\sigma_{tot}}{2}\right)^{AB-n} \tag{6}$$

which leads to

$$\sigma_C^{AB} = 2 \int d\vec{b} \left\{1 - \left[1 - \frac{T_C(b)\sigma_C}{2}\right]^{AB}\right\} \tag{7}$$

with T_C (and T_N) defined in terms of t_C (and t_N) as in Eq. (2).

Many types of measurements satisfy the SS criterion. Examples are given in Ref. 1. For instance, the production of at least one particle of type P at a rapidity (or momentum) range satisfies the SS criterion. The mass dependence of σ_C^{AB} depends on the range and the elementary production cross section. If they are small, then $\sigma_C^{AB} \sim AB\sigma_C$ and if they are large, then $\sigma_C^{AB} \sim (A^{1/3} + B^{1/3})^2$. In particular, when the range is chosen to be infinitesimal, we have

$$\frac{d\sigma_C^{AB}}{dy} = AB \frac{d\sigma_C}{dy} \tag{8}$$

and

$$E \frac{d\sigma_C^{AB}}{d\vec{p}} = AB \; E \frac{d\sigma_C}{d\vec{p}} . \tag{9}$$

These equations relate the differential cross sections for heavy-ion collisions to those in nucleon-nucleon collisions. Equation (9) is approximately satisfied for π° production at large p_T in α-α collisions at a center-of-mass energy of 125 GeV.[6] Similar relations for the integrated cross section have been pointed out previously.[7,8]

We can also write down in a similar way the partial cross section for the observation of events satisfying two different SS criteria C and D. We decompose the basic cross section as

$$t(b)\sigma_{tot} = t_{CD}(b)\sigma_{CD} + t_C(b)\sigma_C + t_D(b)\sigma_D + t_N(b)\sigma_N .$$

Then, the cross section for the observation of events satisfying both C and D criteria is

$$\sigma_{CD}^{AB} = 2 \int d\vec{b} \, [\alpha + \beta - \gamma] \tag{10}$$

where

$$\alpha = 1 - \{1 - [T_{CD}(b)\sigma_{CD} + T_C(b)\sigma_C]/2\}^{AB}$$

$$\beta = 1 - \{1 - [T_{CD}(b)\sigma_{CD} + T_D(b)\sigma_D]/2\}^{AB}$$

$$\gamma = 1 - \{1 - [T_{CD}(b)\sigma_{CD} + T_C(b)\sigma_C + T_D(b)\sigma_D]/2\}^{AB},$$

and T_C, T_D, and T_{CD} are obtained from t_C, t_D, and t_{CD} as in Eq. (2). Examples of measurements satisfying two SS criteria have been given in Ref. 1. For instance, C (and D) contains events in which at least one particle of type P (and Q) are observed in a rapidity interval $\mathcal{J}_P$ (and $\mathcal{J}_Q$). Different mass dependences will be obtained depending on the product AB, the sizes of $\mathcal{J}_P$ and $\mathcal{J}_Q$, as well as the magnitude of σ_C, σ_D, and σ_{CD}. For an infinitesimal interval, we have from Eq. (10)

$$\frac{d^2\sigma}{dydy'}(AB\to PQX) = AB\,\frac{d^2\sigma}{dydy'}(NN\to PQX) \tag{11}$$

$$+\frac{AB(AB-1)}{2}\left\{\frac{1}{\pi R_1^2}\frac{d\sigma}{dy}(NN\to PX)\frac{d\sigma}{dy'}(NN\to QX) - \frac{1}{2\pi R_2^2}\left[\frac{d^2\sigma}{dydy'}(NN\to PQX)\right]^2\right\}$$

where

$$\frac{1}{\pi R_1^2} = \int d\vec{b}\; T_C(\vec{b})\; T_D(\vec{b})$$

and

$$\frac{1}{\pi R_2^2} = \int d\vec{b}\; [T_{CD}(\vec{b})]^2.$$

Clearly, such a relation is also true for the invariant cross sections.

The results we have presented are obtained in the Glauber theory without taking into account the absorption and the rescattering of produced particles and the Fermi motion of the nucleons. At high energies above 10 GeV per nucleon, particles are essentially produced outside the nucleus.[9] The incident momentum is also so high that the Fermi motion may be neglected. Thus, the results we have obtained should be a good approximation for high-energy, heavy-ion reactions such as those conducted at the Intersecting Storage Ring of CERN.

On the other hand, to apply these results to lower energies, it is necessary to correct for the effects of Fermi motion, the absorption and the rescattering of particles produced.

The author is indebted to Prof. R. Blankenbecler for stimulating discussions and helpful suggestions. He also would like to thank Prof. T. T. Chou for helpful discussions.

References

1. R. Blankenbecler, A. Capella, J. Tran Thanh Van, C. Pajares, and A. V. Ramallo, SLAC-PUB-2792, 1981.

2. R. J. Glauber, Lectures in Theoretical Physics (ed. W. E. Brittin and L. G. Dunham), Vol. 1, p. 315, Interscience, New York (1959).

3. T. T. Chou and C. N. Yang, Proceedings of the 1980 Guang-zhou Conference on Theoretical Particle Physics, Science Press, Beijing, China, 1980, p. 317 and references cited therein.

4. W. L. Wang, Phys. Lett. B52, 142 (1974); P. M. Fishbane and J. S. Refil, Phys. Rev. D10, 3128 (1974); S. Barshay, C. B. Dover, and J. P. Vary, Phys. Lett. 51B, 5 (1974); V. Franco and G. K. Varma, Phys. Rev. C15, 1375 (1977).

5. J. Jaros, A. Wagner, L. Anderson, O. Chamberlain, R. Z. Fuzesy, J. Gallup, W. Gorn, L. Schroeder, S. Shannon, G. Shapiro, and H. Steiner, Phys. Rev. C18, 2273 (1978).

6. M. Jacob, in Proceedings of Fifth High Energy Heavy Ion Study, LBL-12652, 1981, p. 581.

7. J. P. Vary, Phys. Rev. Lett. 40, 295 (1978).

8. J. Randrup and C. M. Ko, Nucl. Phys. A343, 590 (1980).

9. W. Busza, in Proceedings of the Fourth High Energy Heavy Ion Summer Study, LBL-7766, 1978, p. 253.

Quantum description of the heavy-ion collision process

P. Danielewicz*

Nuclear Science Division
Lawrence Berkeley Laboratory
University of California
Berkeley, CA 94720

There is a common belief that the high-energy heavy-ion collisions may be described classically. Is, however, the classical description really appropriate for the collisions? At the initial stage of an $E_{lab} \geq 200$ MeV/nucleon ion-collision, the mean time τ between successive NN collisions is of the order of $1/(n_0 \sigma v) \approx (1.7\text{-}3.5)$ fm/c. The value of τ implies uncertainties of nucleon energies in subsequent collisions $\hbar/\tau \approx (55\text{-}115)$ MeV. In the course of an ion collision, still higher values of the collision frequency $\hbar/\tau$ may be achieved. At the beam energies $E_{lab} < 800$ Mev/nucleon, the nucleons will have energies smaller than 200 MeV, in the equal ion-velocity frame, during the whole course of a collision. This indicates that quantum effects may be expected in the ion collision dynamics at these beam energies, because the uncertainty in nucleon energies is comparable with the energies.

Quantum effects may be even expected at much higher energies - in cases when strong kinematical restrictions occur, e.g. in the production or absorption of particles.

This paper examines the role of quantum dynamics in high-energy nuclear collisions. We have carried numerical calculations of collisions in an interpenetrating nuclear-matter model[1]. The quantum dynamics has been compared to a classical Markovian dynamics given by the Boltzmann equation. In quantum calculations, methods of nonequilibrium Green's functions have been employed.

Nonequilibrium Green's function methods, which had been initiated by Kadanoff and Baym[2], have been already proposed[3] to extend the TDHF method for low-energy nuclear collisions. The basic quantities of the approach are the 1-particle Green's functions

$$-iG^{<}(\underset{\sim}{x},t,\underset{\sim}{x}',t') = \langle \Phi_H^{+}(\underset{\sim}{x}',t')\Phi_H(\underset{\sim}{x},t)\rangle \quad ,$$

$$iG^{>}(\underset{\sim}{x},t,\underset{\sim}{x}',t') = \langle \Phi_H(x,t)\Phi_H^{+}(\underset{\sim}{x}',t')\rangle \quad ,$$

*On leave of absence from Institute of Theoretical Physics, Warsaw University, Warsaw, Poland.

with the expectation values taken with respect to some initial state at time t_0. For equal time-arguments the function $-iG^<$ is the 1-particle density matrix.

The 1-particle Green's functions satisfy the Kadanoff and Baym equations of motion

$$\left(i\frac{\partial}{\partial t_1} + \frac{\nabla_1^2}{2m}\right) G^{\gtrless}(1,1') = \int dx_2\, \Sigma_{HF}(\underset{\sim}{x}_1,\underset{\sim}{x}_2;t_1)\, G^{\gtrless}(\underset{\sim}{x}_2,t_1,1')$$

$$+ \int_{t_0}^{t_1} d2\, (\Sigma^> - \Sigma^<)(1,2)\, G^{\gtrless}(2,1')$$

$$- \int_{t_0}^{t_{1'}} d2\, \Sigma^{\gtrless}(1,2)(G^> - G^<)(2,1') \quad ,$$

and the self-energies Σ may be evaluated in terms of 1-particle Green's functions, with Feynman diagrams similar to the conventional ground-state Feynman diagrams. The second-order diagram, corresponding to the direct Born scattering with the particles of the medium, yields

$$\Sigma^{\gtrless}(1,1') = \int d\underset{\sim}{x}_2 \int d\underset{\sim}{x}_{2'}\, V(\underset{\sim}{x}_1 - \underset{\sim}{x}_2)\, V(\underset{\sim}{x}_{1'} - \underset{\sim}{x}_{2'})\, G^{\gtrless}(1,1')$$

$$\times\, G^{\gtrless}(\underset{\sim}{x}_2,t_1,\underset{\sim}{x}_{2'},t_{1'})\, G^{\lessgtr}(\underset{\sim}{x}_{2'},t_{1'},\underset{\sim}{x}_2,t_1) \quad ,$$

where V is the 2-body potential.

In the limit of slow macroscopic space and time variations in the system, as compared with characteristic momenta and energies in the system, the *Boltzmann equation*

$$\left(\frac{\partial}{\partial T} + \frac{\underset{\sim}{p}}{m}\cdot\underset{\sim}{\nabla}_R\right) f(\underset{\sim}{p};\underset{\sim}{R},T) = -i\,\Sigma^<(\underset{\sim}{p},\omega_p;\underset{\sim}{R},T)[1 - f(\underset{\sim}{p};\underset{\sim}{R},T)]$$

$$+ i\Sigma^>(\underset{\sim}{p},\omega_p;\underset{\sim}{R},T)\, f(\underset{\sim}{p};\underset{\sim}{R},T) \quad ,$$

for the evolution of the Wigner function f, may be derived from the Kadanoff and Baym equations. Here $\Sigma^{\gtrless}$ are Fourier transformed in their relative variables at fixed values of sums of the variables, and $\omega_p = p^2/2m$. In the Boltzmann equation limit, $-i\Sigma^<$ and $i\Sigma^>$ are seen as the scattering-in and scattering-out (collision frequency) rates, respectively. The characteristic

time of changes in the system is, within the Boltzmann equation, set basically by the scattering-out rate.

Both the Green's function equations of motion and the Boltzmann equation have been solved for an interpenetrating nuclear-matters system. The Boltzmann equation has been solved earlier for such a system by Randrup[4]. The self-energies in the calculation have been approximated by the direct Born term with the parameters of the potential fitted (within the Born approximation) to the NN differential cross sections.

The quantum calculations have been performed both for a two Fermi-spheres Hartree-Fock initial state and a correlated initial state of nuclear matter. The correlated initial state was prepared by an imaginary-time evolution described in Ref. 1.

Results of the calculations for E_{lab} = 400 MeV/nucleon are presented in Figs. 1 and 2. In Fig. 1 the time evolutions of the nucleon momentum distributions are shown. In the distributions resulting from the Boltzmann equation, the effects of energy conservation in binary collisions can be seen. The particles fill initially a hollow shell in momentum space, determined by the two Fermi spheres, and they cannot substantially populate the high momenta region. In quantum calculations the particles move directly into the central region between the Fermi spheres and they also spread over the whole momentum space. In contrast to what one could expect from the above, the approach to the thermodynamic equilibrium is slower by about 50% in the quantum case. This has to be attributed to the memory effects in the quantum evolution. In Fig. 2 the evolution of the momentum distribution anisotropy is depicted. In the correlated initial-state quantum calculation a value 1/2 for the anisotropy is achieved only after 10 fm/c of the evolution. The value of the time seems too large to justify the hydrodynamic description for the heavy-ion collisions at the considered beam energy.

This work was supported by the Director, Office of Energy Research, Division of Nuclear Physics of the Office of High Energy and Nuclear Physics of the U.S. Department of Energy under Contract DE-AC03-76SF00098.

References

1) P. Danielewicz, Ph.D. Thesis, Warsaw University, 1981 (to be published)
2) L.P. Kadanoff, G. Baym, Quantum Statistical Mechanics, Frontiers in Physics Series, Benjamin, New York, 1962

3) C.Y. Wong, H.H.K. Tang, Phys. Rev. Lett. 16 (1978) 1070; Phys. Rev. C20 (1979) 1419
H. Orland, R. Schaeffer, Saclay report DPh-T/78/41
C.M. Shakin, M.S. Weiss, report UCRL-80500
4) J. Randrup, Nucl. Phys. A314 (1979) 429

Figure Captions

Fig. 1. Evolution of the nucleon momentum distribution $f(p^{\perp},p^{z},t)$). Upper figures - Boltzmann equation evolution; central figures - Green's function equations of motion evolution for a two Fermi spheres Hartree-Fock initial state; bottom figures - evolution for a correlated initial state. Horizontal axes are the collision axes. The momentum space is restricted to 900 MeV/c as shown by the outer circles.

Fig. 2. Evolution of the momentum distribution anisotropy. Short-dashed line corresponds to the Boltzmann equation, long-dashed line to the Green's function equation of motion and the Hartree-Fock initial state, and the solid line to the correlated initial state. The dashed horizontal line at 0.5 is a guide to the eye representing $\langle p^{z2}\rangle = 1.5\ (\langle p^{\perp 2}\rangle/2)$.

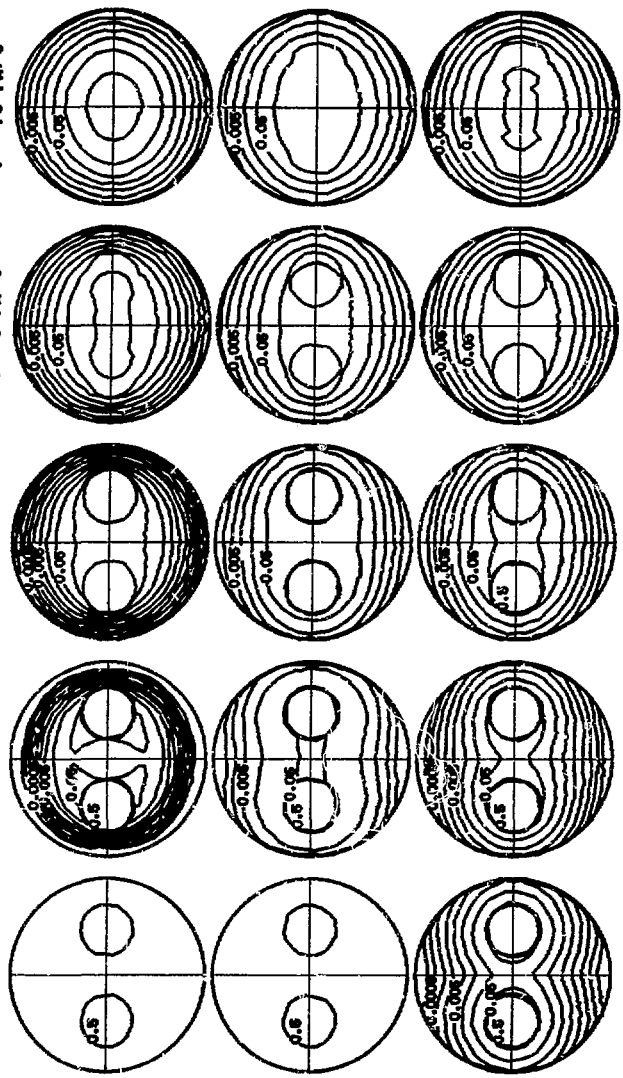

Fig. 1

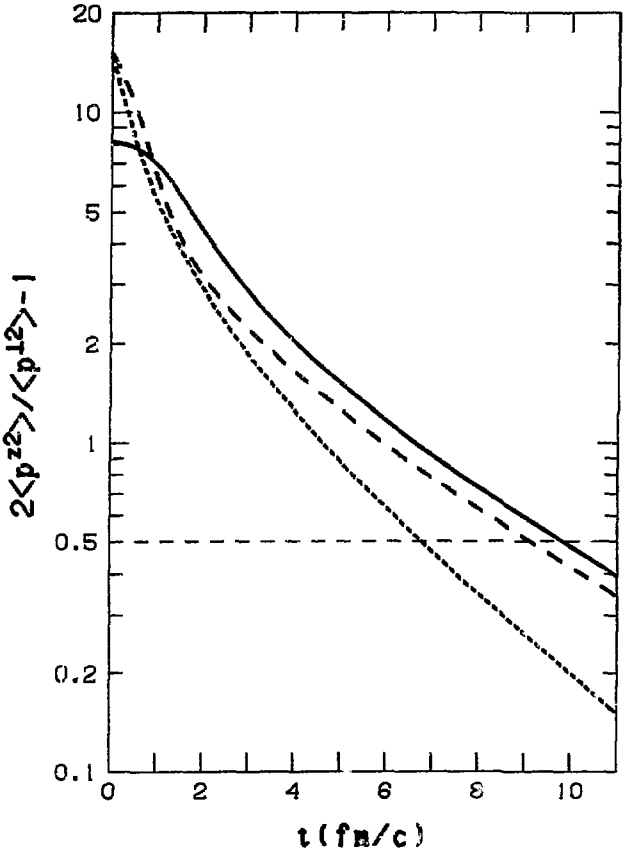

Fig. 2

A PHYSICALLY ASYMPTOTIC HARTREE-FOCK STATIONARY-PHASE APPROXIMANT TO THE MANY-BODY S-MATRIX†

James J. Griffin* and M. Dworzecka

Department of Physics and Astronomy
University of Maryland, College Park, Maryland 20742 U.S.A.

In recent years, mean field theories of many-body reaction processes have been the objects of much analysis, at first of a mostly numerical,[1] but more recently of a structural[2] Time-Dependent S-Matrix Hartree-Fock (TDSHF) and formal[3] Functional Integral Stationary Phase (FISP) type. For bound eigenstates, Gauge-Invariant Periodic Quantized (GIPQ) solutions emerged simultaneously and independently from the two distinct methodological and philosophical approaches.[4,5] The explicit development of GIPQ states as time-dependent alternatives to RPA stationary states has also begun.[6]

For continuum processes, however, the TDSHF approach yields a different description from the FISP formulation. The former assumes that Dirac's Time-Dependent Hartree-Fock theory[7] defines the time evolution of all the single-determinantal wave functions which it encompasses. It leads to the conclusion that by judicious choice of channel states, and by invoking time averaging as an interpretative procedure, the TDSHF reaction theory can be obtained, which exhibits the physically indispensable qualitative structural features of the exact Schrödinger scattering theory.[2]

The approach from functional integrals derives from the exact expression for each S-matrix element a stationary phase approximant, which is essentially different from the corresponding TDSHF-approximate S-matrix element. In particular, to describe an N-channel scattering problem, TDSHF requires only N distinct TDHF solutions, and correspondingly, N-TDHF mean fields, $\rho_i(\vec{x},t)$. For the same problem, the FISP approach determines N(N-1)/2 distinct mean fields, $\sigma_{if}(\vec{x},t)$, since each depends upon both the initial and final states. Furthermore, these fields describe non-causal time evolution (because the development of σ_{fi} at any time, t, depends upon boundary conditions imposed upon the behavior at times both infinite future and infinite past), in contrast with the causal Dirac TDHF evolution[7] upon which TDSHF is based.

Here we focus on the FISP method's lack of physical asymptoticity, which property guarantees that the predictions for all physical measurements made at great distances will be independent of the precise location of the apparatus. We note that a recent illustrative calculation[8] proposes a formulation of the FISP method which seems to circumvent the lack of asymptoticity, but its implications are not carried through to a physical statement about the predictions for measurements at distant points. When they are, we believe, it becomes clear that the alternative formulation circumvents the computational instabilities of non-asymptoticity, but not the physical non-asymptoticity of the measurable predictions. This point is currently a subject of communication with these authors.

Since asymptoticity has been explicitly structured into the TDSHF theory by an explicit choice of the allowed asymptotic channel states, we here propose a new "Asymptotic Hartree-Fock Stationary Phase" (AHFSP) approximant to the

†Research supported by the U. S. Department of Energy.
*and Institute for Physical Sciences and Technology, University of Maryland.

S matrix, obtained by imposing these assumptions about the asymptotic channel states also upon the FISP S-matrix theory. The result is a new S-matrix approximant which exhibits physical asymptoticity, but in which FISP, rather than Dirac TDHF, determines the time evolution description during the collision interval.

Consider the S-matrix element for the system, $H = H_{0,i} + V_i = H_{0,f} + V_f$, given exactly by the expression,

$$S_{fi} = \langle f|S|i\rangle = \langle \Psi_f^{(-)}(\vec{x},t_c)|\Psi_i^{(+)}(\vec{x},t_c)\rangle$$

$$= \lim_{t\to\infty} \langle f|U_{0,f}(t_0,t)U(t,t_c)U(t_c,-t)U_{0,i}(-t,t_0)|i\rangle, \qquad (1a)$$

independent of the comparison time, t_c. In (1a) the asymptotic channel "in" and "out" states are specified at $t=t_0$, and propagated to large $|t|$ via $U_{0,i}$ and $U_{0,f}$. Also, products of the propagators U in (1a) compose according to the identity,

$$U(t,t_c)U(t_c,-t) \equiv U(t,-t). \qquad (1b)$$

The new HFSP approximant is obtained from (1a) by utilizing the FISP procedure to approximate the evolution operator, $U(T_2,T_1)$, only during the collision interval, (T_1,T_2). For times outside the collision interval, the asymptotic channel states evolve via $U_0^{TDHF}(t,t')$ according to the Dirac TDHF equation, and are required to be products of well-separated sub-determinantal clusters, each of which describes a Gauge Invariant Periodic oscillation of the internal cluster structure, and translates in space along the selected asymptotic channel orbit. These conditions are discussed in detail in Ref. 2b. In this way, physical asymptoticity is guaranteed when the internal GIPQ solutions are interpreted via a time average (the specific nature of which is suggested by a recent study of exact GIPQ states[9]).

Then, instead of the FISP approximate result,[8] given by

$$S_{f,i}^{FISP} = \lim_{t\to\infty} \langle f|U_{0,f}^{FISP}(t_0,t)U^{FISP}(t,-t)U_{0,i}^{FISP}(-t,t_0)|i\rangle, \qquad (2)$$

one calculates the Asymptotic Hartree-Fock Stationary Phase (AHFSP) approximant,

$$S_{fi}^{AHFSP} = \lim_{t\to\infty} \langle f|U_{0,f}^{TDHF}(t_0,t)U_f^{TDHF}(t,T_2)U^{FISP}(T_2,T_1)U_i^{TDHF}(T_1,-t)U_{0,i}^{TDHF}(-t,t_0)|i\rangle. \qquad (3)$$

Throughout, the superscript, FISP, on U (or U_0) indicates that the propagator is to be evaluated by the Functional Integral Stationary Phase approximation[3]; whereas the superscript, TDHF, implies the use of the causal Dirac-TDHF time evolution.[7]

The time interval (T_1,T_2) in (3) is specifically chosen to be the smallest interval which includes all times during which any interaction between the two clusters is non-zero. Therefore, outside of this interval, all matrix elements of the interaction V_i (or V_f) vanish identically, and the complete TDHF propagator reduces to the unperturbed propagator, which relates the unperturbed solution at any time to the solution, β, specified at some particular time (here, t_0) by means of a dynamically trivial spatial translation. Then

$$U_\beta^{TDHF}(t',t) \equiv U_{0,\beta}^{TDHF}(t',t), \qquad (4)$$

and (3) reduces to

$$S_{fi}^{AHFSP} = \lim_{t\to\infty} \langle f|U_{0,f}^{TDHF}(t_0,t)U_{0,f}^{TDHF}(t,T_2)U^{FISP}(T_2,T_1)U_{0,i}^{TDHF}(T_1,-t)U_{0,i}^{TDHF}(-t,t_0)|i\rangle \qquad (5a)$$

$$\equiv \lim_{t\to\infty} \langle \beta'|U_{0,f}^{TDHF}(t_0,T_2)U^{FISP}(T_2,T_1)U_{0,i}^{TDHF}(T_1,t_0)|\beta\rangle \qquad (5b)$$

$$= \langle \phi_f^{(-)}(\vec{x},T_2)|U^{FISP}(T_2,T_1)|\phi_i^{(+)}(\vec{x},T_1)\rangle. \qquad (5c)$$

Here $|\phi_i^{(+)}(\vec{x},T_1)>$ denotes the TDSHF channel state which for $-\infty < t < T_1$ assumes the controlled form i labelled by a set of numbers, {i}. This set just suffices[2b] to initialize $U_{0,i}^{TDHF}$, the TDHF propagator for H_0, at time $t=t_0$ and, thereby, the asymptotic behavior of the channel state,

$$\lim_{t\to\infty} \phi_i^{(+)}(\vec{x},t) = U_{0,i}^{TDHF}(t,t_0)|i>. \qquad (6)$$

(Likewise for $<\phi^{(-)}(\vec{x},T_2)|$.)

We note that for an N-channel problem the computation of $U^{FISP}(T_2,T_1)$ by the stationary phase functional integral method will still involve $N(N-1)/2$ mean fields, $\sigma_{if}(\tau)$, defined for $T_1 \le \tau \le T_2$. Nevertheless, the new structure of expression (5c) invites a direct comparison with the time-averaged approximate S-matrix element of the TDSHF theory,[2] given by the following average over the same interval (T_1,T_2):

$$S_{fi}^{TDSHF} = (T_2-T_1)^{-1}\int_{T_1}^{T_2} <\phi_f^{(-)}(\vec{x},t')|\phi_i^{(+)}(\vec{x},t')>dt', \qquad (7a)$$

$$= (T_2-T_1)^{-1}\int_{T_1}^{T_2} <\phi_f^{(-)}(\vec{x},T_2)|U_f^{TDHF}(T_2,t')U_i^{TDHF}(t',T_1)|\phi_i^{(+)}(\vec{x},T_1)>dt'. \qquad (7b)$$

One sees that in contrast with S_{fi}^{FISP} of Eq. (2), both S_{fi}^{TDSHF} in (7) and S_{fi}^{AHFSP} in (5) are affected by nontrivial dynamical behavior *only* during the collision interval, and by the boundary conditions at its endpoints T_1,T_2. Moreover, each of these boundary conditions is directly obtained via the dynamically trivial Dirac-TDHF translational evolution from a "controlled" single-channel asymptotic state at an early (or a late) time. This structure therefore guarantees prima facie that the S matrix is not being distorted by spurious external multi-cross-channel correlations in the asymptotic regions.[10] In contrast, S_{fi}^{FISP} in (2) is influenced by its physically nontrivial dynamical evolution for all times, $-\infty < t < +\infty$, and is based upon solutions which approach no well-defined limit as $|t|$ increases indefinitely.

In summary, the Asymptotic Hartree-Fock Approximant (5) replaces the physically non-asymptotic (and dynamically nontrivial) external translation of the FISP result (2) with the asymptotic and dynamically trivial translational evolution of Dirac-TDHF by adding an explicit restriction upon the acceptable channel states. It is therefore preferable under the principle of commensurability,[10] which judges the expected output of physical descriptions in terms of the physical assumptions they incorporate. We expect that further insight into the relationship between the TDSHF and FISP methods will reward careful comparison of the respective expressions (5) and (7) in specific cases.

REFERENCES

1. (a) P. Bonche, et al., Phys. Rev. C13 (1976) 1226. (b) K. T. R. Davies, et al., ORNL Rpt. MAP-23 (1982), provide an extensive well-annotated review.
2. (a) J. J. Griffin, et al., Phys. Lett. 93E (1980) 235. (b) J. J. Griffin, et al., Phys. Rev. C21 (1980) 1351. (See especially Sec. VI.)
3. (a) H. Rheinhardt, Nucl. Phys. A331 (1979) 353. (b) S. Levit, Phys. Rev. C21 (1980) 1594.
4. K.-K. Kan, et al., Nucl. Phys. A332 (1979) 109.
5. S. Levit, et al., Phys. Rev. C21 (1980) 1603.
6. M. Dworzecka, et al., Granlibakken Workshop (1980); LBL-10688 (p. 57).
7. P. A. M. Dirac, Proc. Camb. Phil. Soc. 26 (1930) 376.
8. Y. Alhassid and S. E. Koonin, Phys. Rev. C23 (1981) 1590.
9. K.-K. Kan et al., U. of Md. Tech. Rpt. #ORO 5126-144 (Sept. 1981), *to be published.*
10. (a) J. J. Griffin, Conf. on Heavy Ion Collisions (Fall Creek Falls, TN, 1977), ORNL Rpt. #ORO-CONF-77602 (p. 1). (b) J. J. Griffin, Clustering Aspects of Nuclear..., ed. W. T. H. Van Oers (AIP, New York, 1978), p. 114. (See especially pp. 121-122.)

FRICTION AND DIFFUSION IN FEYNMAN'S PATH INTEGRAL METHOD *

E. Alek Bartnik
Institute for Theoretical Physics, Warsaw University, Warsaw, Poland;
Sektion Physik, Universität München, Garching, Germany;
Physikalisches Institut, Universität Bonn, Bonn, Germany

and

Rainer W. Hasse
Sektion Physik, Universität München, Garching, Germany;
Institut Laue-Langevin, Grenoble, France.

Feynman's path integral method[1,2] although being impractical for numerical applications proved very successful for deriving general results on coupled quantum systems[2,3]. Möhring and Smilanski[3], for instance, used this method in order to treat quite generally dissipative processes with a view on deep inelastic heavy ion collisions. Brink et al.[4] employed statistical matrix elements and derived transport coefficients. In the spirit of ref.[3], in the present paper we use the adiabatic approximation to calculate transport coefficients - which turn out to be the same as derived by time-dependent perturbation theory and calculate the influence functional, effective Lagrangian and action. Due to the present lack of communication with the first authors home country, however, the paper is still fragmentary.

In following the notation of ref.[3], the inclusive probability for a transition of a collective variable Q, from $Q_o = Q(t=0)$ to $Q_1 = Q(t=T)$ under the influence of a classical Lagrangian $L_c(Q,\dot{Q})$ coupled to an intrinsic system with coordinates ξ by the coupling operator $V(\xi,Q)$ is given by

$$P(Q_o,Q_1) = \iint D[Q]\, D[\tilde{Q}]\, F(Q,\tilde{Q})\, \exp i\left(S_c(Q) - S_c(\tilde{Q})\right). \tag{1}$$

Herein, $D[Q]\, D[\tilde{Q}]$ denotes integration over all possible paths with boundary conditions $Q(0)=\tilde{Q}(0)=Q_o$ and $Q(T)=\tilde{Q}(T)=Q_1$, the classical action is given by

$$S_c(Q) = \int_o^T L_c(Q)\,dt \tag{2}$$

and the influence functional $F(Q,\tilde{Q})$ is given by the influence phase $\phi(Q,\tilde{Q})$,

$$F(Q,\tilde{Q}) = \exp i\,\phi(Q,\tilde{Q}), \tag{3}$$

$$\phi(Q,\tilde{Q}) = i \sum_n \int_o^T dt \int_o^t ds \left[V_n(Q(t)) - V_n(\tilde{Q}(t)) \right] \times \left[e^{-iE_n(t-s)} V_n(Q(s)) - e^{iE_n(t-s)} V_n(\tilde{Q}(s)) \right] . \tag{4}$$

---

* Supported by Alexander von Humboldt-foundation and by Deutsche Forschungsgemeinschaft.

Here and in the following we set $\hbar = 1$ and use unit collective mass, E_n denotes intrinsic excitations from the ground state with $E_o = 0$ and $V_n(Q(t))$ is the matrix element of $V(\xi,Q)$ connecting the ground state and the n-th excited intrinsic state.

Eq. (4) is now evaluated for a separable coupling $V(\xi,Q) = V(\xi)Q$ in the adiabatic approximation $E_n(t-s) >> 1$ to yield

$$\phi(Q,\tilde{Q}) = \int_o^T dt[Q(t) - \tilde{Q}(t)] \times \left[\frac{\kappa^2}{2}\left(Q(t) + \tilde{Q}(t)\right) - \frac{\gamma}{2}\left(\dot{Q}(t) + \dot{\tilde{Q}}(t)\right) + iD\left(Q(t) - \tilde{Q}(t)\right) + id\left(\dot{Q}(t)\right) - \dot{\tilde{Q}}(t)\right]. \tag{5}$$

In eq. (5), the transport coefficients, κ^2 = potential correction, γ = friction constant, D = dissipative diffusion constant and d = conservative diffusion constant, turn out to be the same as those derived via time-dependent perturbation theory[5],

$$\begin{aligned} \kappa^2 &= 2\Sigma|V_n|^2/E_n \\ \gamma &= 2\pi\ \Sigma\ |V_n|^2\ \delta(E_n)/E_n \\ D &= \pi\Sigma\ V_n^2\ \delta(E_n) \\ d &= \Sigma|V_n|^2/E_n^2. \end{aligned} \tag{6}$$

With the help of eqs. (1,3-5) we can deduce an effective Lagrangian

$$L_{eff}(Q,\tilde{Q}) = \dot{\phi}(Q,\tilde{Q}) + \dot{s}_c(Q) - \dot{s}_c(\tilde{Q}), \tag{7}$$

which, for force free and harmonically oscillating motion with frequency ω, $\bar{\omega}^2 = \omega^2 - \kappa^2$, becomes

$$L_{eff} = \frac{1}{2}(\dot{Q}^2 - \dot{\tilde{Q}}^2) - \frac{1}{2}\bar{\omega}^2(Q^2 - \tilde{Q}^2) - \frac{\gamma}{2}(Q-\tilde{Q})(\dot{Q}+\dot{\tilde{Q}}) + iD(Q-\tilde{Q})^2 + id(Q - \tilde{Q})(\dot{Q}-\dot{\tilde{Q}}). \tag{8}$$

With the help of eqs (1,8), the inclusive probability can then be written entirely in terms of the collective coordinate,

$$P(Q_o,Q_1) = \iint D[Q]\ D[\tilde{Q}]\ \exp\ i\ S_{eff}(Q,\tilde{Q}), \tag{9}$$

where S_{eff} is defined analogously to eq. (2).

It remains to express S_{eff} in terms of the starting and end points Q_o, Q_1. This is most easily done by going over to the "relative" and "center-of-mass" variables

$$\begin{aligned} x &= Q + \tilde{Q}, & y &= Q - \tilde{Q} \\ x_o &= x(0),\ x_1 = x(T), & y_o &= y(0),\ y_1 = y(T), \end{aligned} \tag{10}$$

with the Lagrangian

$$L(x,y) = \frac{1}{2}\dot{x}\dot{y} - \frac{1}{2}\bar{\omega}^2 xy - \frac{1}{2}\gamma\dot{x}y + iDy^2 + i\dot{d}y\dot{y} \qquad (11)$$

and the equations of motion

$$\begin{aligned} \ddot{x} + \bar{\omega}^2 x \quad &+ \gamma\dot{x} = 4iDy \\ \ddot{y} + \bar{\omega}^2 y \quad &- \gamma\dot{y} = 0 \ . \end{aligned} \qquad (12)$$

Without going into the details of the solutions of (12) we give the final result

$$S_{eff} = \frac{\Omega}{2\sin\Omega t}\left[(x_o y_o + x_1 y_1)\cos\Omega t - \left(y_o x_1 e^{\gamma t/2} + x_o y_1 e^{-\gamma t/2}\right)\right] + \frac{\gamma}{4}(x_o y_o - x_1 y_1)$$

$$+ \frac{iD}{2\gamma\bar{\omega}^2}\left[\frac{\gamma^2}{2}(y_1^2 - y_o^2) + \frac{\gamma\Omega}{\sin\Omega t}\left(2y_o y_1 \cosh\frac{\gamma t}{2} - (y_o^2 + y_1^2)\cos\Omega t\right)\right.$$

$$\left. + \frac{2\Omega^2 \sinh\frac{\gamma t}{2}}{\sin^2\Omega t}\left(y_o^2 e^{\frac{\gamma t}{2}} - 2y_o y_1 \cos\Omega t + y_1^2 e^{-\frac{\gamma t}{2}}\right)\right], \qquad (13)$$

where $\Omega^2 = \bar{\omega}^2 - \gamma^2/4$. The limit $\bar{\omega} \to 0$ in (13) gives the force free motion result.

Work is under way to evaluate the inclusive probability (9) with the effective action (13) along the lines of ref.[3] by the saddle point method.

References

1. R.P. Feynman and A.R. Hibbs, Quantum mechanics and path integrals (McGraw-Hill, New York, 1965).
2. R.P. Feynman and F.L. Vernon Jr., Ann. Phys. 24 (1963) 118.
3. K. Möhring and U. Smilansky, Nucl. Phys. A338 (1980) 227.
4. D.M. Brink, J. Neto and M.A. Weidenmüller, Phys. Lett. 80B (1979) 170.
5. R.W. Hasse, Nucl. Phys. A318 (1979) 480.

RHI and TDHF : THE EVOLUTION OF THE TARGET

B. Grammaticos and A. Lumbroso*

Service de Physique Théorique, CRN-Strasbourg,
BP n°20, CRO 67037 Strasbourg - France

**Service de Physique Théorique, C.E.A., CEN-Saclay*
91191 Gif-sur-Yvette Cedex, France

Several models of high-energy collisions separate the role of the nucleons of the colliding systems in participants and spectators. Let us say roughly that under certain geometrical conditions (mainly the radius of the colliding nuclei and the impact parameter) the projectile pulls a cylindrical hole out of the target. At this stage the remaining nucleons of the target and/or of the projectile are called the spectators, and the compound system of the colliding nucleons constitutes the participants. The participants have been studied by several methods like the fireball (1) or the cascade (2) model. An opposite point of view is taken up by the knock-out model (8) which attributes the observed nucleons to a direct emission occurring at the collision of the nuclei. The experimental data lie between the limits set by the predictions of the two theories which may be considered as an indication that both theories are realistic up to a certain degree.

However, if the participants are well described in these models, very little is known about the spectators. On the experimental level this is due to the fact that the detection of these very low energy residues associated with a good signature for the impact parameter renders the information difficult to extract.

On the theoretical level, and as far as high energy collisions are concerned, we can surmise that the process of the target evolves on two steps. First a rapid abrasion occurs with little or no kinetic energy deposit. This seems reasonable provided that the transit time of the projectile through the target nucleus is significantly smaller than the propagation time of the disturbance inside the nucleus. Secondly the highly excited remaining target proceeds to emit particles or fragments. In a fully consistent theory one should have to treat the two stages on the same way. A step in this direction has been made by Amsden et al.(3) who treated the $^{20}Ne + ^{238}U$ collision, at very high energies, on the framework of a relativistic hydrodynamic picture. Although one could question the use of the hydrodynamic approach at such high energies, these calculations provide a fair insight into the global collision process.

In this paper we propose a quite different approach to the same question. Namely we focus our interest on the disintegration of the excited target once the projectile has bore a hole through it. The approach used here is the TDHF method (4). The initial conditions, for the time evolution of the system, correspond to a perforated in nucleus. In order to achieve this, we multiply the wave functions by a cylindrical Fermi-type cut-off factor with small thickness, the radius of which is roughly equal to the radius of the projectile.

We have preferred this type of smooth cut-off instead of a sharp step function one because it ensures the cylindrical shape of the hole, independently of the coarseness of the mesh, and does not lead into problem as far as the kinetic energy operator is concerned. We proceed further to orthogonalize the wave functions, but do not normalize them. The wave function orthogonality is essential if one wishes to evolve them according to the equation $i\dot{\varphi} = h\varphi$, which is the method used here.

Let us just remark here that at the high energies we are considering the incident nucleons perform a small number of collisions (5) before leaving the target. At these energies the nucleon-nucleon cross sections are very much forward peaked and therefore we deal with straight line trajectories and the cylindrical picture appears reasonable.

The wave functions obtained are subsequently evolved according to the TDHF equations. For this we have made a standard choice of the nuclear interactions as in Ref.(6), consisting in a contact force plus direct Yukawa and Coulomb interaction. The last one is understood to act between protons and neutrons equally, with an effective charge of 1/2, which results in a four-fold degeneracy of the single particle states. This leads to the following expression for the energy functional (with evident notations) :

$$E = \int d\vec{r}\ \frac{\hbar^2}{2m}\tau(\vec{r}) + \frac{3}{8}\,t_o\,\rho^2(\vec{r}) + \frac{1}{16}\,t_3\,\rho^3(\vec{r})$$

$$+ \frac{1}{2}\,V_o \int d\vec{r}\ d\vec{r}'\ \rho(\vec{r})\ \frac{\exp(-|\vec{r}-\vec{r}'|/a)}{|\vec{r}-\vec{r}'|/a}\ \rho(\vec{r}') + \frac{1}{8}\,e^2 \int d\vec{r}\ d\vec{r}'\ \rho(\vec{r})\ \frac{1}{|\vec{r}-\vec{r}'|}\ \rho(\vec{r}')\ .$$

The evolution of the TDHF equations is performed as described in Ref. (6). The wave functions are discretized in a box of 22 fm × 22 fm × 16 fm on a cubic mesh whose step size is taken equal to 1 fm. One has to use a full three-dimensional geometry for this kind of study with even total reflection symmetry relaxed. The only remaining symmetry is an one plane reflection one which allows to reduce the dimensions of the box to 22 fm × 22 fm × 8 fm. The time step used in the evolution of the TDHF equations is $0.6\ 10^{-23}$ sec.

In this letter we report the first results obtained with this method for a target nucleus of ^{40}Ca. The extension to heavier targets which are of greater interest from the experimental point of view is not impossible in principle (although the technical difficulties associated with that are considerable) and is currently under investigation.

In the figure we display snapshots at selected times during the evolution of the residual nucleus, obtained through the creation of a 3 fm radius hole on a ^{40}Ca target (which roughly corresponds to the hole that an ^{16}O projectile would punch in the target nucleus). Three different impact parameters are examined b=0 for a central collision and b=1.5 and 2.5 fm for peripheral collisions. The graphic corresponds to density integrated along the axis perpendicular to the plane of the drawing, which axis corresponds to the direction of the beam.

In order to have an estimation of the evaporation we have decided to count the number of nucleons through an integration of the density outside a sphere centered around the nucleus with a radius of 5 fm. It is clear that in the TDHF case that we are studying, due to the symmetries we have

imposed and to the semi-classical nature of the TDHF solutions, a coherent emission of particles with definite particle number is not to be expected. At the beginning of the evolution less than 0.5 particles lie outside this sphere, corresponding to the tails of the wavefunctions. The visualization of the evaporation is achieved by following a very low density contour. The line numbered 1 in the snapshots corresponds to a density of 0.01 fm^{-2}, and its evolution can be associated to the edge of the outgoing matter wave. An estimation of the velocity of the latter can be obtained by calculating the displacement of the low density contour between two subsequent snapshots.

i) Central collisions : an almost complete evaporation of the nucleus seems to occur in this case. The hole in the nucleus is filled up and at the same time the outgoing motion of matter depletes the center of the frame. As a result a very low density residue remains, with density lower than 0.1 fm^{-2} which corresponds to our second density contour. The evaporation proceeds further as can be judged by the motion of the very low density contour, until at the very last frame, edge effects due to finite size of our box start becoming appreciable. In the average a total number of 2.5 particles is emitted (after correction for the initial 0.5 particles lying outside the sphere). Although apparently small, this number represents roughly 40 % of the total available at the beginning of the deexcitation.

The picture of total break up, usually advocated in the case of central collisions and present in the case of relativistic hydrodynamic calculations (3), is still present in this two stage description of the collision.

ii) Peripheral collisions : as in the case of the central collisions we first observe a fast filling-up of the crescent-like hole. In this case the matter velocity which characterizes this motion is larger than in all the other cases : roughly 20 % of the velocity of light, to be compared with a value of less than 10 % in all the other cases. On the contrary the number of emitted particles is smaller than in the central case. Although 2.-2.5 particles are still emitted they represent no more than 25 % of the initially available matter.

A subsequent evolution of the remaining low density residue shows that it is still excited, and part of this excitation is manifesting itself in collective excitations of the "bending" type.

As a conclusion, we can state that the TDHF has proven itself a useful tool in the exploration of a new kind of collective motion which is of particular interest in the realm of relativistic heavy-ion physics. The simple model examined here is compatible with the main features of ^{3}HI collisions : fast collision with perforation of the target and fireball formalism sometimes followed by non-equilibrium emission from the slowly recoiling target. However, more work is needed especially in the direction of the treatment of heavier targets.

Such an extension presents two advantages. On the first hand, it would lead closer to the experimental situation, where heavy targets are used almost exclusively, allowing thus a hope for eventual quantitative comparisons. On the other hand, the validity of the approach, from a theoretical point of view, would increase with the mass of the target, the classical behaviour becoming dominant for large systems. This extension is currently investigated.

REFERENCES

(1) - J. Gosset, H. Gutbrod, W. Meyer, A.M. Poskanzer, A. Sandoval, R. Stock and G.D. Westfall, Phys. Rev. C16, 629 (1977).

(2) - J. Hüfner and J. Knoll, Nucl. Phys. A290, 460 (1977).

(3) - A. Amsden, G.F. Bertsch, F.H. Harlow and J.R. Nix, Phys. Rev. Lett. 35, 905 (1975).

(4) - P. Bonche, S. Koonin and J.W. Negele, Phys. Rev. C13, 1226 (1976).

(5) - R.L. Hatch and S. Koonin, Phys. Lett. 81B, 1 (1979).

(6) - P. Bonche, B. Grammaticos and S. Koonin, Phys. Rev. C17, 1700 (1978).

(7) - D.K. Scott, Theoretical Methods in Medium-Energy and Heavy-Ion Physics, Plenum Press 1978, eds. Mc Voy and Friedman.

(8) - S.E. Koonin, Phys. Rev. Lett. 39, 680 (1977).

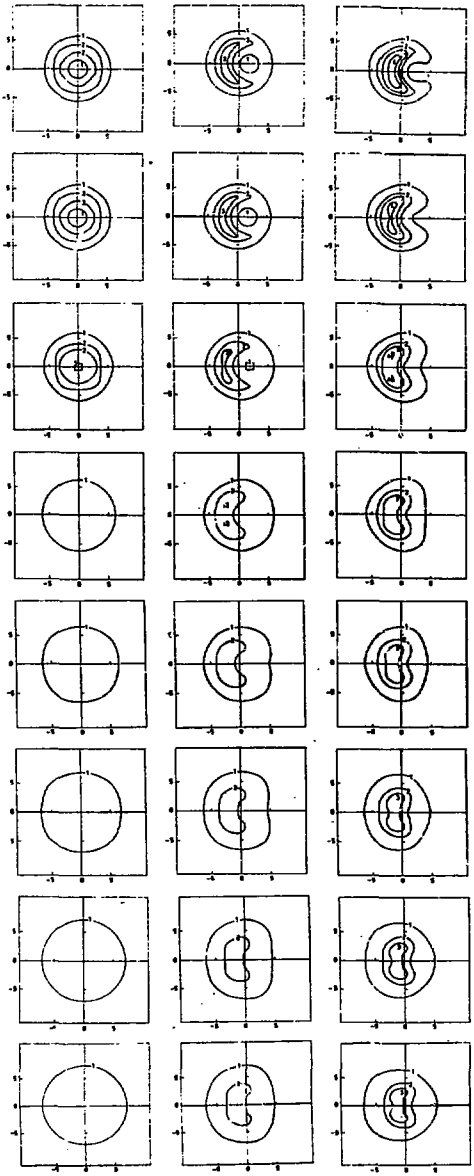

Figure caption

Selected snapshots during the time-evolution of a ^{40}Ca nucleus. Three different impact parameters (b) are shown : 0, 1.5 and 2.5 fm. Each square represents a mesh of 22×22 fm. In each column the time interval between two snapshots is 1.2×10^{-23} sec. The numbers in each equidensity contour are defined in the text.

Target Fragment Production Mechanisms in Relativistic Nuclear Collisions

A.I. Warwick, H.H. Gutbrod, M.R. Maier, H.G. Ritter, H. Stelzer, F. Weik, H.H. Wieman, S.B. Kaufman, B.D. Wilkins, E.P. Steinberg, J. Peter

Nuclear Science Division, Lawrence Berkeley Laboratory
University of California, Berkeley, CA 94720
and
Argonne National Laboratory, Argonne, IL 60439
and
Gesellschaft für Schwerionenforschung
D-6100 Darmstadt, West Germany

By studying the properties of large nuclear fragments from a heavy Au target nucleus at relativistic bombarding energies one is able to make a link between the physics of nuclear collisions at lower incident energies and the fireball-type phenomena that occur in highly excited systems at high projectile energy. We have studied collisions induced by protons, alpha particles, and Ne projectiles at total incident energies from 5 GeV to 42 GeV leading to pieces of the Au target nucleus emerging as bound nuclei with small velocities in the laboratory frame.

Figure 1 shows the experimental layout, consisting of heavy fragment detectors inside a spherical vacuum chamber and plastic scintillator detectors on the outside to count the fast charged particles emitted into the forward hemisphere from each collision.

We first consider the small cross-section leading to fission of the Au target residue. Figure 2 shows a contour plot of the yield of fragments in a mass range approximately half that of the Au target. The ordinate is simply the number of the 80 plastic scintillators which fired in the event, the abscissa is the kinetic energy of the fragment emerging at 90°

This work was supported by the Director, Office of Energy Research, Division of Nuclear Physics of the Office of High Energy and Nuclear Physics of the U.S. Department of Energy under Contract DE-AC03-76SF00098.

There are two components to the yield; the low-multifoldness high-energy component is a conventional binary fission mechanism which occurs only in the most peripheral collisions, the underlying deep spallation spectrum has its origins in more violent collisions. These findings are discussed more completely in reference 1.

For the remainder of this discussion we will examine the mechanism leading to the production of lighter fragments (A≥30). Figure 3 shows the energy spectra, observed at θ=90, for each of the different bombardments. The similarity of the spectra is obvious. They are characterized by an exponential tail (slope parameter τ between 14 MeV and 30 MeV) and a peak which is considered to arise from the Coulomb forces acting within the residue of the Au target nucleus. The evidence for the Coulomb interpretation is given in the literature[2,3] but notice in figure 3 how the peak moves to lower energies as the violence of the initial collision increases with projectile energy, consistent with the decreasing size and charge of the target residue. Also to be noted (but not shown here) is the movement of the peak to higher energies for fragments of higher Z, again as to be expected from a Coulomb effect.

Figure 4 is from reference 4 and illustrates two distinct origins of particles in these collisions. The hydrogen isotopes and ^{3}He exhibit exponential spectra indicative of emission from a high temperature source. All heavier species have an additional low temperature component at low fragment energies indicating that a considerable part of the yield of such fragments comes from a cooler source. This cooler source is essentially the only origin of fragments heavier than Be.

In figure 5 the cross section for fragment production is plotted against the fragment charge. The solid circles are measured by Nagamiya et al.[5] for high energy products and extrapolated to obtain the total yield. In this way the low temperature component is missed and these measurements represent only the yield from the fireball system. The data are fitted roughly with a statistical calculation by George Fai and Jorgen Randrup[6] using ε=155 MeV, the available energy per nucleon in the hot system. Our data is shown as solid triangles and includes the cooler component. We find that the same calculation fits the heavier fragment data with $\varepsilon \simeq 20$ MeV. The energy spectra themselves show slopes of $\tau \simeq 25$ MeV which, because of finite number effects, measure a quantity somewhat larger than the ε parameter of the calculation. Thus, the calculation of the charge yield curve seems to be consistent with the observed slopes of the energy spectra.

More discussion of the calculation would be useful, both about the technical difficulties of knowing level densities in many nuclei and about the fundamental difficulties of statistical mechanics of finite systems. However, this calculation seems to provide a description of the breakup of the target residue which does not imply a relaxed, thermalized, sequential emission of fragments from the residual system. The excitation energy ($\simeq$20 MeV/u) is too high for this relaxed mechanism to be reasonable.

Figure 6 shows the mean multiplicity of fast charge particles associated with fragments and with protons from collisions at various projectile energies. Triggering on an emerging high energy proton biases the measurement strongly towards central collisions, because it is in the most violent collision that the largest number of high energy protons is produced. Consequently, the trend shown as a solid line on the figure is that seen in the most violent collision possible as the projectile energy is varied. The

multiplicity associated with heavy fragments follows the same trend until the projectile energy gets above 10 GeV. Up to this point the most violent collisions are producing (on the average) fragments of A=10 and A=30. Above a projectile energy of 10 GeV the fragments are no longer associated with the most violent collisions and there are collisions occuring which are so violent in their initial (fireball) stages that on the average there are no bound nuclear systems produced with $A \gtrsim 10$.

This work was supported by the Director, Office of Energy Research, Division of Nuclear Physics of the Office of High Energy and Nuclear Physics of the U.S. Department of Energy under Contract DE-AC03-76SF00098.

References

1. A.I. Warwick, et al., LBL report 13831 and Phys. Rev. Lett. (to be published)

2. G.D. Westfall, et al., Phys. Rev. C17, (1978) 1368 and references therein

3. W.G. Meyer, et al., Phys. Rev. C22 (1980) 179

4. A.M. Poskanzer, et al., Phys. Rev. C3 (1971) 882

5. S. Nagamiya, et al., Phys. Rev. C24 (1981) 971

6. G. Fai and J. Randrup, LBL report 13357 and Nucl. Phys. A (to be published) see also contribution to this conference by J. Randrup

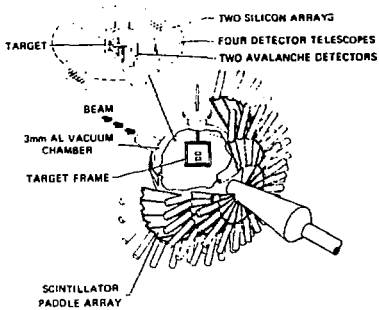

Fig. 1

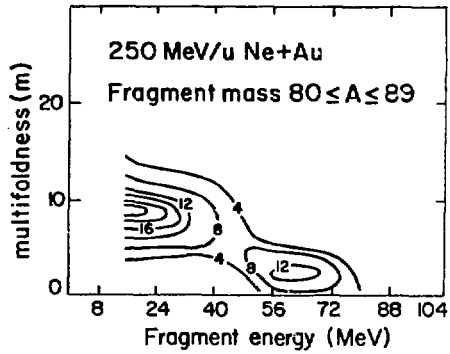

Fig. 2

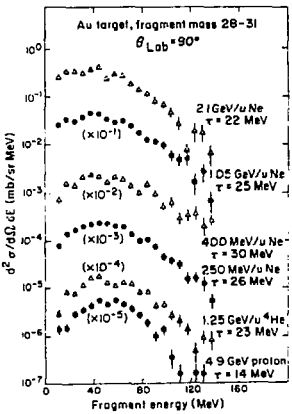

Fig. 3

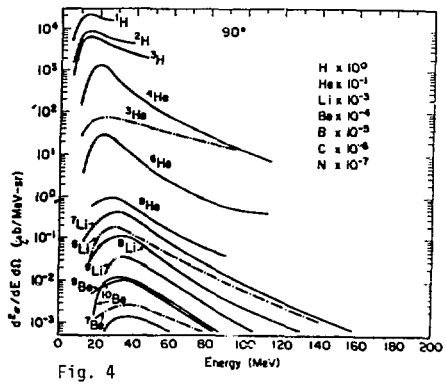

Fig. 4

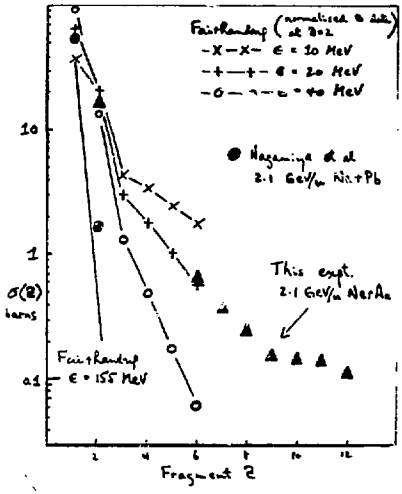
Fairbanks (normalised to data at 3e2
-X-X- ε = 10 MeV
-+-+- ε = 20 MeV
-O-O- ε = 40 MeV
Hagemann et al
2.1 GeV/u Ni+Pb
This expt.
2.1 GeV/u NerAu
Fairbanks
ε = 155 MeV
10
1
σ(Z)
barns
Fragment Z

Fig. 5

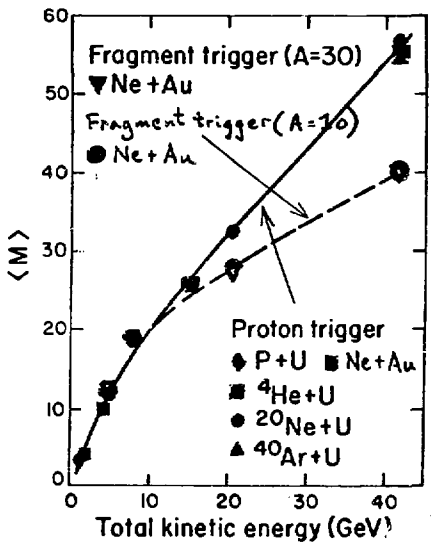
Fragment trigger (A=30)
Ne+Au
Fragment trigger(A=10)
Ne+Au
Proton trigger
P+U
Ne+Au
4He+U
20Ne+U
40Ar+U
⟨M⟩
Total kinetic energy (GeV)
0
10
20
30
40
50
60

Fig. 6

Multiplicities of Slow Target Fragments in Relativistic Heavy Ion Collisions

H. Wieman, A. Baden, M. Freedman, H.H. Gutbrod, D.J. Henderson, S.B. Kaufman, M. Maier, J. Peter, H.G. Ritter, E.P. Steinberg, H. Stelzer, A.I. Warwick, F. Weik, and B.D. Wilkins

Argonne National Laboratory, Argonne, Illinois 60439, U.S.A.
Gesellschaft für Schwerionenforschung, Darmstadt, West Germany
Lawrence Berkeley Laboratory, Berkeley, California 94720, U.S.A.

In the interaction of relativistic ^{20}Ne projectiles with Au target nuclei the production of slow, light target fragments (A = 20-40) seems to occur in the more violent central collisions.[1] Single particle inclusive energy spectra for these light fragments suggest that a reasonable amount of energy is deposited in the target nucleus, sufficient energy for multiple particle breakup of the target. In particular the energy spectra for these lower mass fragments have high energy tails with slopes of the order of 25 MeV, indicating an excitation of the target residue well above the nucleon binding energy.[2] Also, the peaks in the energy spectra, identified with the Coulomb energy, are too low to be consistent with a binary breakup of the spectator residue.[3]

In the work reported here we study this more violent type of reaction involving lighter fragments. Mean multiplicities of slow, light fragments (Z = 2-27) emitted from the same event as the measured A = 20-40 fragment have been extracted from coincidence measurements. This information, in conjunction with fast charged particle multiplicities, provides a direct measure of target destruction. These measurements were made using a gold target and neon projectiles with kinetic energies of 5, 8, 21, and 42 GeV as well as light projectiles (protons and helium-4) with 5 GeV of kinetic energy.

The apparatus used in this part of the experiment consisted of an array of 16 silicon detectors located at approximately 90° to the beam in which the A = 20-40 fragment was measured. An avalanche detector next to the target in conjunction with the silicon array provided mass identification through time of flight. In addition four ion chamber-silicon telescopes were located at 30, 62, 113, and 151 degrees relative to the beam. In these detectors coincident lighter fragments were measured. The slow fragment multiplicities were obtained from these coincidence measurements between the 16 detector

silicon array and the four ion-chamber telescopes. The fast particle multiplicities were monitored with an array of plastic scintillator paddles covering the forward hemisphere.

Associated mean multiplicities were extracted from the slow fragment coincidence measurements using the following prescription. The differential mean multiplicity of fragment 2 associated with fragment 1 is given by the relation:

$$\frac{d\langle m(\chi_1,\chi_2)\rangle}{d\chi_2} = \frac{d\sigma_{12}(\chi_1,\chi_2)}{d\chi_1 d\chi_2} \Big/ \frac{d\sigma(\chi_2)}{d\chi_1}$$

where χ_i represents variables Ω_i, E_i, and either Z_i or A_i for fragment i. In the reactions to be considered here particle 2 is a fragment detected in the ion chamber telescope with a charge ranging from 6 to 27, and particle 1, the trigger particle with which particle 2 is associated, is detected in the silicon array and has a mass range between 20 and 40. For these masses and charges the singles cross section lies within the energy dynamic range of the detectors. The four point angular dependence for the coincidence measurements is shown in Fig. 1 for 5 GeV Ne and 42 GeV Ne on Au. These distributions reflect the observed singles angular distributions--fairly isotropic for 42 GeV neon and somewhat forward peaked for 5 GeV neon. This lack of special angular correlations implies that the same sort of reaction giving rise to the singles inclusive cross sections is also responsible for the coincidence events, i.e. the coincidence requirement does not select out a rare or unusual type of event.

The associated multiplicity is found by extrapolating the four point angular distribution of Fig. 1 over 4π and depends on some assumptions about the out-of-plane dependence. Two different possible assumptions were tried, namely symmetry about the beam and symmetry about the mass 20-40 fragment detected at 90 degrees. The results were within 12% of simply averaging the four points and multiplying by 4π. Consequently the mean multiplicities we have chosen to report here are the results of this latter averaging.

In addition to measuring mean multiplicities of fragments with Z in the range 6-27 we extended our analysis below the original design limits of the detector telescope to Z = 2 thus introducing uncertainties in individual Z identification due to small delta E signals plus possible loss of higher energy fragments due to punch through. A comparison of our singles cross

sections with Ne + U data[4] at 2.1 GeV/u shows good agreement for the summed cross sections from Z = 2-5. However, the large relative cross section for ^{4}He apparently contaminates the lithium leading to a factor of 3 error in this case.

In figure 2 the resulting associated mean multiplicities are shown as a function of Z. In the region Z = 6 and above, the error bars show only statistical uncertainties while in the region Z = 2-5 the error bars also include the mentioned uncertainties due to Z misidentification. Again the trigger for these associated multiplicities is a mass 20-40 fragment at $\theta \simeq 90°$. As shown in this plot the associated multiplicity increases rapidly with decreasing Z value to approximately 3 for He particles. For comparison the Z dependence of the singles cross section is also plotted. The Z dependence for both associated mean multiplicities and the singles cross section are essentially the same, once again demonstrating that the reactions sampled in these coincidence measurements are the same reactions giving rise to the inclusive cross sections. The associated multiplicities are nearly the same for all the projectiles p, ^{4}He, and ^{20}Ne. This is apparent in figure 3 where the associated multiplicities are summed from Z = 2 to Z = 27. The summed value is ≈6, independent of projectile mass. There also appears to be only a small variation as the neon projectile kinetic energy changes over the range from 5 to 42 GeV. This is particularly interesting considering that over this energy range the associated fast particle multiplicity as measured in the scintillator paddles varies by approximately a factor of 3 (13 fast charged particles associated with the 5 GeV ^{20}Ne projectile and 42 fast charged particles associated with the 42 GeV ^{20}Ne projectile). Apparently the slow fragment associated multiplicities do not depend on the violence of the collision, as measured by the fast particle multiplicities.

Next consider a rough examination of average mass yields in the events tagged by a mass 20-40 fragment at 90 degrees. An outline of the following accounting is shown in table 1. The entry designated as slow fragment was obtained in the following manner. Each slow fragment of charge Z is assumed to have a mass of 2 x Z, giving a slow fragment mass yield = $\sum_{Z=2}^{27} \langle m(Z) \rangle \, 2\,Z$ where $\langle m(Z) \rangle$ is the mean multiplicity of charge Z fragments associated with a mass 20-40 fragment at 90°. An additional mass of 25 is added for the average of the mass 20-40 trigger particle. To estimate the fast charged particle mass contribution, it is assumed that protons constitute the full multiplicity

measured in the scintillator paddles. An estimate of the fast neutron yield was obtained by multiplying the fast charged particle multiplicity by 1.44, the total neutron/proton ratio. By this accounting there is a mean remaining mass of 51 for 42 GeV neon on gold and 115 for a neon projectile of 5 GeV. Part of this remaining mass is carried off in the form of low energy protons and neutrons. The threshold energy for protons in the scintillator paddles was 25 MeV. The below threshold contribution was estimated by scaling the low energy proton multiplicity from our measured mean helium multiplicities according to the singles cross sections for the low-energy protons and helium. The singles cross sections used for this purpose were taken from measurements of Poskanzer, et al.[5] for 5.5 GeV P plus U. The resulting estimate in this case is six protons, i.e., two times the He multiplicity. The slow neutron multiplicity was obtained from the proton estimate using the measured neutron/proton ratio of 4 in this energy range.[6] So, the total slow proton-neutron mass contribution comes to 30. Having accounted for mean mass contributions from fast particles, slow target fragments, Z = 2-27, and low-energy protons and neutrons, the remaining mass as shown in table 1 is 20 for the 42 GeV case. Part of this remaining mass should be included with the fast particles since high-energy deuterons, tritons, and helium ions were counted with only a proton mass in this analysis. But in any case for the highest energy example, 42 GeV neon, the remainder is at most 20 mass units, indicating that on the average when a mass 20-40 fragment is detected, the target has undergone complete disintegration into light fragments. At lower projectile energy, 5 GeV, a sizeable remainder is left, possibly in the form of a slow heavy fragment normally below the energy threshold of our detector.

In conclusion the average event involving a mass 20-40 fragment has a slow fragment associated multiplicity of ∿6 with half of these particles being of charge 2. This remains true independent of projectile mass and energy over the region covered in this study, namely 5 GeV protons, helium-4, and neon-20 as well as up to 42 GeV neon. The total mass involved in the reaction when including fast charged particles, on the other hand, increases with projectile kinetic energy. At the highest bombarding energy, 42 GeV neon, the average event giving rise to a mass 20-40 fragment results in complete disintegration of the target into light fragments.

This work was supported in part by the Director, Office of Energy Research, Division of Nuclear Physics of the Office of High Energy and Nuclear Physics of the U.S. Department of Energy under Contract DE-AC03-76SF00098.

References

1. A.I. Warwick, et al., LBL report 13831
2. A.I. Warwick, et al., in this Proceedings
3. A.M. Zebelman, et al., Phys. Rev. C11, 1280 (1975)
   W.G. Meyer, et al., Phys. Rev. C22, 179 (1980)
4. J. Gosset, et al., Phys. Rev. C16, 629 (1977)
5. A.M. Poskanzer, et al., Phys. Rev. C3, 882 (1971)
6. W. Schimmerling, et al., Phys. Rev. Lett. 43, 1985 (1979)

Table 1

Mass Accounting of Ne + Au Reaction

Projectile Energy (GeV)	5	8	21	42
Starting Mass	217	217	217	217
Associated Slow Fragments Z = 2-27	45	44	37	39
Trigger Fragment	25	25	25	25
Fast Charged Particles	13	19	28	42
Fast Neutrons	29	27	40	60
Slow Protons	6	6	6	6
Slow Neutrons	24	24	24	24
Remainder	85	72	57	21

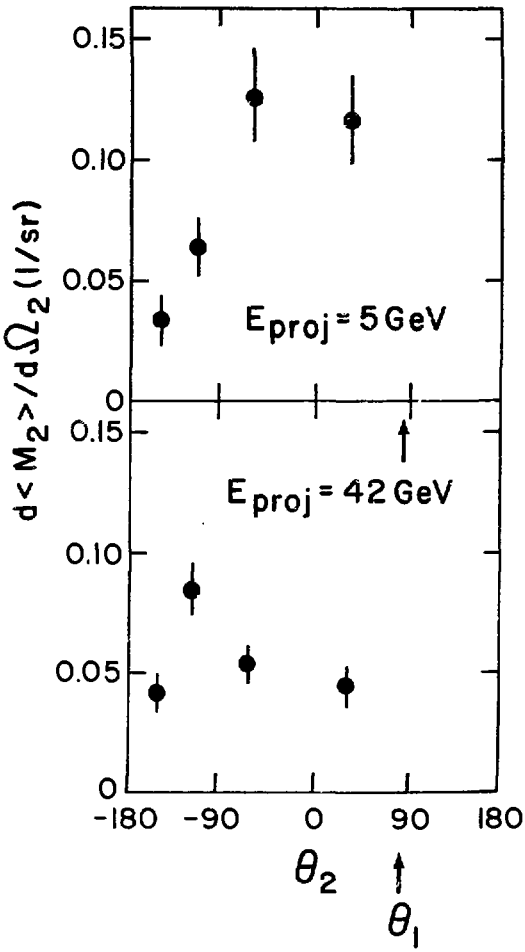

Fig. 1. Differential mean multiplicity of fragments with Z = 6-27 associated with a mass 20-40 fragment at ∿90° for Ne + Au.

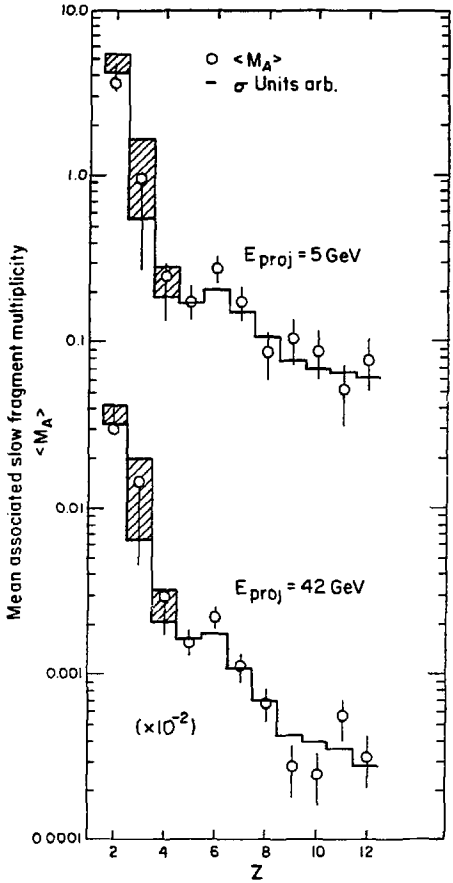

Fig. 2 Mean multiplicity of fragments with charge Z associated with a mass 20-40 fragment at ∿90° for Ne + Au. Also fragment cross sections scaled arbitrarily for comparison of Z dependence.

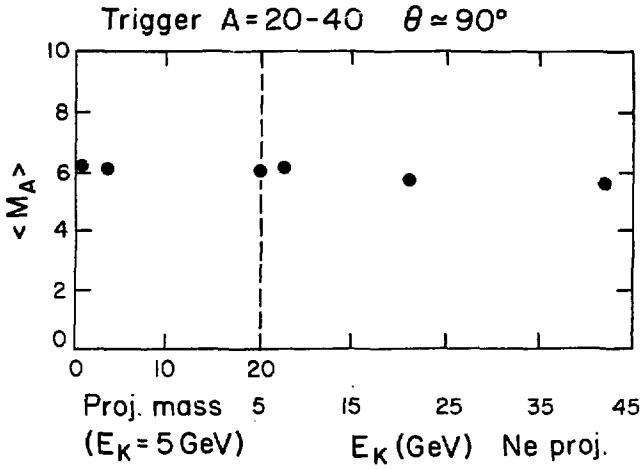

Fig. 3. Mean multiplicity of fragments with Z ranging from 2-27 associated with a mass 20-40 fragment at ∿90° shown as a function of projectile mass and projectile energy.

First Experiments with the Plastic Ball

H.G. Ritter, A. Baden, H.H. Gutbrod, H. Löhner, M.R. Maier, A.M. Poskanzer, T. Renner, H. Riedesel, H. Spieler, A.I. Warwick, F. Weik, and H. Wieman

Gesellschaft für Schwerionenforschung
Darmstadt, Germany
and
Nuclear Science Division, Lawrence Berkeley Laboratory
University of California Berkeley, CA 94720

After two and a half years of development and construction, an electronic 4π detector has been used for the first time in studying relativistic nuclear collisions. This detector complements the visual 4π detectors like emulsions, AgCl detectors, and the streamer chamber, which have been in use for many years. Only the streamer chamber has the same important feature as the Plastic Ball in being triggerable for specific event types. In a series of experiments with beams of ^{20}Ne, ^{40}Ar, and ^{40}Ca up to energies of 1.05 GeV/u, approximately three million events were measured with various trigger conditions. In contrast to the visual detectors, these events are already totally digitized and ready for immediate analysis. All multiparticle correlations of charged particles are measured in each event and do not have to be determined as an average quantity from two particle inclusive data. Besides the particle identification of the hydrogen and helium isotopes, the Plastic Ball identifies the positive pions. This makes it interesting for the study of pion production, which sets in at around 100 MeV/u incident energy, and has promise to shed some light onto the equation of state of nuclear matter. Besides the analysis of the data in the standard way of selections and of single particle inclusive data, a global analysis is in progress that should allow us to determine the reaction plane, and the event shape in phase space.

The general layout of the experiment is shown in fig. 1. The Plastic Wall, placed 6 m downstream from the target, covers the angular range from 0 to 10 degrees and measures time of flight, energy loss, and position of the reaction products. In addition, the inner counters serve together with the beam counter as a trigger.

The Plastic Ball covers the region between 10 and 160 degrees, 96% of the total solid angle. It consists of 815 detectors, where each module is a ΔE-E telescope capable of identifying the hydrogen and helium isotopes and positive

pions. The ΔE measurement is performed with a 4-mm thick CaF_2 crystal and the E counter is a 36-cm long plastic scintillator. Both signals are read out by a single photomultiplier tube. Due to the different decay times of the two scintillators, ΔE and E information can be separated by gating two different ADCs at different times. The positive pions are additionally identified by measuring the delayed $\pi^+ \rightarrow \mu^+ \rightarrow e^+$ decay. A schematic drawing of the electronics and of the timing of the different gates is shown in fig. 2.

A cluster of 13 prototype modules (a central counter and all 12 neighbors) was tested at the LAMPF low-energy pion line with monoenergetic pions and protons. The energy response curve for protons and pions and pion efficiencies could be measured in that experiment. In addition, the effect of the scattering out of particles into neighboring modules could be studied. By taking into account information from adjacent modules, this problem can be solved nearly completely[1].

Before assembling the Plastic Ball, all modules were irradiated at the Berkeley 184" cyclotron with 400 MeV and 800 MeV α beams in order to determine the high voltage for each individual photomultiplier and to measure the characteristic response of each module. A complete set of energy calibration curves for protons and all composite particles could be obtained by fragmenting the 800 MeV α beam in a thick target and by determining the energy of the fragments by a time-of-flight measurement in front of the module.

Figure 3 shows the acceptance of the Plastic Ball experiment in the plane of rapidity versus transverse momentum. In the different areas charged particles can be identified with different quality.

For the different beam-target combinations data were taken with a reaction (minimum bias) trigger and with a central trigger. The reaction trigger requests that a beam particle was identified in the start detector and that this particle lost at least one charge in a reaction with a target nucleus. The central trigger excludes reactions where particles with beam velocity (or higher velocity) are emitted within a forward cone of two degrees.

The analysis of the first experiments performed in June 1981 is in progress. Calibration factors for all detectors could be extracted from the data and test measurements so that all ΔE-E diagrams coincide. The quality of the particle separation is shown in fig. 4 for the hydrogen and helium isotopes.

Figure 5 shows the multiplicity distribution for the reaction 800 MeV/u Ne on Pb for the reaction trigger and for the central trigger (85% reduction of the trigger rate), where events with low multiplicity are strongly reduced. It is obvious that a large group of events with high multiplicity is rejected by the central trigger because in those reactions fast particles are emitted in the forward direction.

Due to the ability of identifying the particles, the Plastic Ball is well suited for investigating the emission of protons and light clusters in high energy heavy ion reactions. Such studies should yield information about the reaction mechanism and answer the question whether composite particles come from a thermalized source, or whether a coalescence process that only requires closeness in phase space of the constituents, is reponsible for cluster production. Especially the ratio of the production cross sections of deuterons to protons has been related to the entropy in the reaction zone in ref. 2. This proposition to determine the entropy from directly accessible experimental results has stimulated a vivid discussion[3-5].

Figure 6 shows that for the reaction 800 MeV/u Ne on Pb the number of protons bound in clusters increases with the multiplicity of the reaction products and equals the number of free protons in high multiplicity events. Consequently as shown in fig. 7 the deuteron to proton ratio increases with multiplicity indicating that the entropy slightly decreases.

This work was supported in part by the Director, Office of Energy Research, Division of Nuclear Physics of the Office of High Energy and Nuclear Physics of the U.S. Department of Energy under Contract DE-AC03-76SF00098.

References:

1) H.H. Gutbrod, M.R. Maier, H.G. Ritter, A.I. Warwick, F. Weik, H. Wieman, and K.L. Wolf, IEEE Trans. Nucl. Sci. Vol. NS-28 No. 1, 457 (1981)
2) P.J. Siemens and I. Kapusta, Phys. Rev. Lett. 43, 1486 (1979)
3) H. Stöcker, LBL Preprint 12302
4) J. Knoll, L. Münchow, G. Röpke, and H. Schulz, GSI Preprint 82-2
5) G. Bertsch and J. Cugnon, Phys. Rev. C24, 2514 (1981)

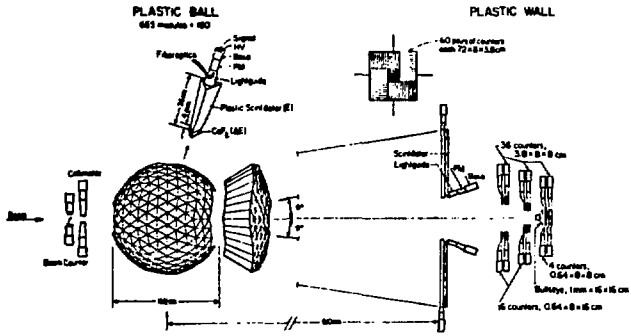

Fig. 1. General layout of the experiment

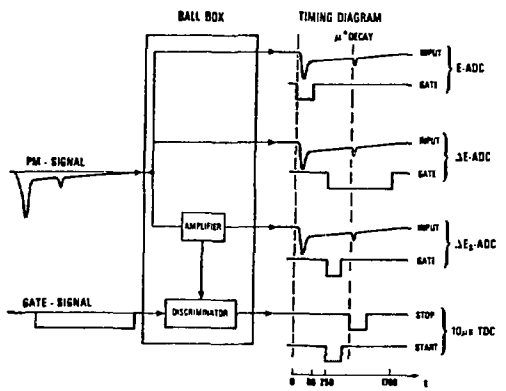

Fig. 2. Electronics scheme for one module

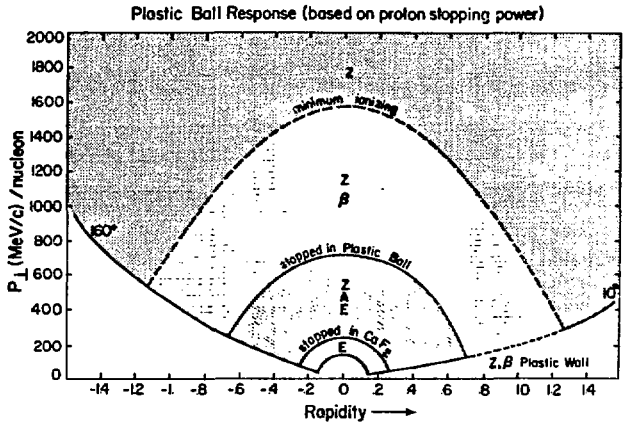

Fig. 3. Plastic Ball acceptance in the plane rapidity versus transverse momentum

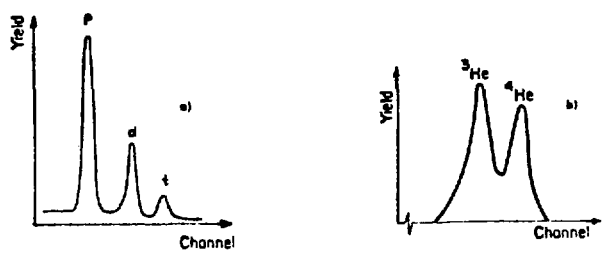

Fig. 4. Quality of the particle separation (655 modules added)
a) hydrogen isotopes, b) helium isotopes

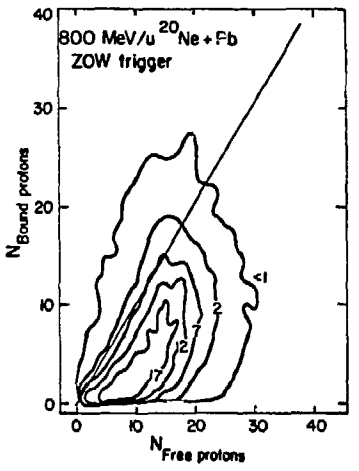

Fig. 5. Multiplicity distributions accumulated with a reaction trigger and a central trigger configuration

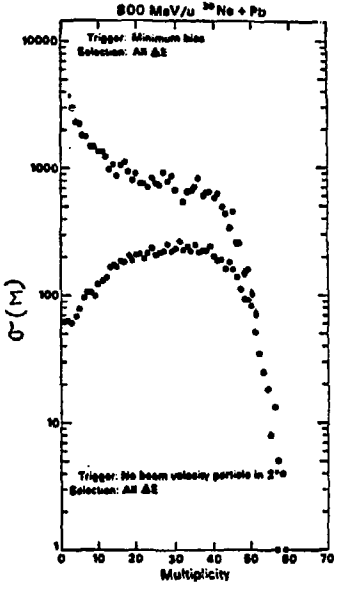

Fig. 6. Event by event contour plot of the number of free protons versus the number of protons bound in clusters

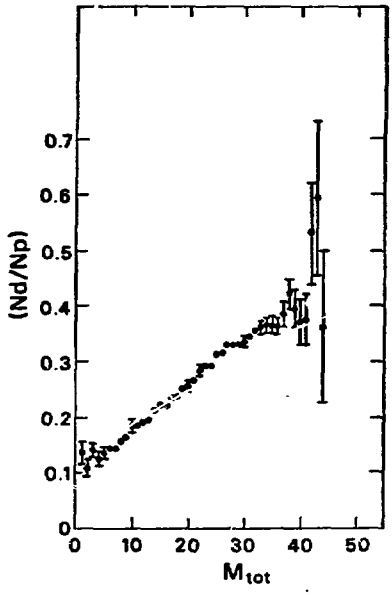

Fig. 7. Deuteron to proton ratio as a function of the total multiplicity for the reaction 800 MeV/u Ne on Pb (central trigger)

LBL-14153

Pion Production from Heavy-Ion Collisions at 80-400 MeV/N

P. Hecking

Nuclear Science Division
Lawrence Berkeley Laboratory
University of California
Berkeley, CA 94720

Pion multiplicities and spectra from heavy-ion collisions with subthreshold and/or low bombarding energies of 80-400 MeV per nucleon are not well understood. Fireball, firestreak, cascade, thermal, etc. models work better at high energies above ~800 MeV/N. The hard-scattering model is subsequently applied to explain the (few) existing pion production data in the low-energy regime.

In this model, the pions are produced by single nucleon-nucleon collisions. No clusters of nucleons, collective phenomena, pion condensation, shock waves, etc. are considered. The pion production cross section is given by:

$$\left(E\ \frac{d^3\sigma}{dp_\pi^3}\right) = \sigma_{HI}\ N_{coll}\left[\sigma_{NN}^{tot}\right]^{-1}\left(E\ \frac{d^3\sigma}{dp_\pi^3}\right)_{NN\pi}$$

Here, σ_{HI} is the (geometrical) heavy-ion cross section and N_{coll} is the number of initial nucleon-nucleon collisions, taken from a Glauber description:

$$\sigma_{HI}\ N_{coll} = \int_0^\infty 2\pi b\,db \sum_{N=1}^{A} N\ P(N,b)$$

$$P(N,b) = \binom{A}{N} P^N(b)\ [1 - P(b)]^{A-N}$$

$$P(b) = \langle\bar{\sigma}\rangle\ \sigma_{NN}^{tot}\ e^{-\langle\bar{\sigma}\rangle\sigma_{NN}^{tot}}$$

P(N,b) is the probability that N (of A) independent projectile nucleons scatter once: $\langle o \rangle$ is the thickness function. The average pion production cross section per single nucleon-nucleon collision $\left(E \frac{d^3\sigma}{dp_\pi^3}\right)_{NN\pi}$ is taken from experimental $NN\pi$ data. The center-of-mass energy of each nucleon pair is given by the initial momentum distribution, averaged over the two Fermi spheres, with nucleons assumed to be on shell. In this model, the Fermi motion is crucial for subthreshold pion production.

Pauli blocking of the final state nucleons and pion reabsorption and rescattering are included in the quantity $\left(E \frac{d^3\sigma}{dp_\pi^3}\right)_{NN\pi}$. It is assumed that the nuclei simply overlap in coordinate space and that pion production is homogeneous in the overlap region. Pion reabsorption is determined by momentum-dependent mean free paths, calculated in ref. [1]. The pions also undergo multiple scattering with nucleons from both Fermi spheres. Since nothing is known experimentally about pion-nucleon scattering in the nuclear medium, the cross section for scattering is taken to be equal to the absorption cross section, which is true in the limit of strong absorption.

Figure 1 shows a comparison of the given model with recent experimental results [2]. Older experiments [3] with low-momentum pions are well reproduced as well, fig. 2: the 380 MeV data are underestimated by a factor of 2. The angular distribution of recent low-energy data [4] seems to be well reproduced, fig. 3; the total cross section of 10 μb is overestimated by a factor of 2. However, the experimental situation is still developing, since preliminary π°-production data [5] for the same reaction yield a total cross section of ~60 μb.

Acknowledgments

This work was supported by the Director, Office of Energy Research, Division of Nuclear Physics of the Office of High Energy and Nuclear Physics of the U.S. Department of Energy under Contract DE-AC03-76SF00098 and by the Deutsche Forschungsgemeinschaft under Contract He 1155/1.

References

[1] P. Hecking, Phys. Lett. B103, 401 (1981)

[2] S. Nagamiya et al., submitted to Phys. Rev. Lett. (LBL-12123)

[3] W. Benenson et al., Phys. Rev. Lett. 43, 683 (1979) and Errata, Phys. Rev. Lett. 44, 54 (1980)

[4] T. Johansson et al., LUNFD61 (NFFK-7011) 1-4 (1981) ISSN 0348-9329

[5] E. Grosse et al., private communication

Figure Captions

Fig. 1. π^- production at $\theta_\pi^{CM} = 90^\circ$ as a function of pion center-of-mass energy for two bombarding energies. The hard-scattering model (full line) is compared with the experimental data from ref. [2].

Fig. 2. $\pi^\pm$ production at $\theta_\pi^{CM} = 0^\circ$ as a function of pion center-of-mass energy for three bombarding energies. Data taken from ref. [3].

Fig. 3. π^+ production as a function of pion center-of-mass angle for two kinetic energies. Data taken from ref. [4].

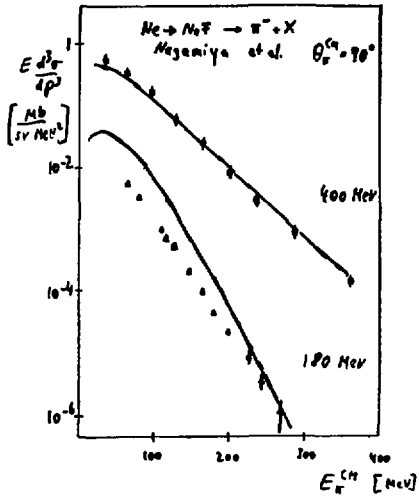

Fig. 1.

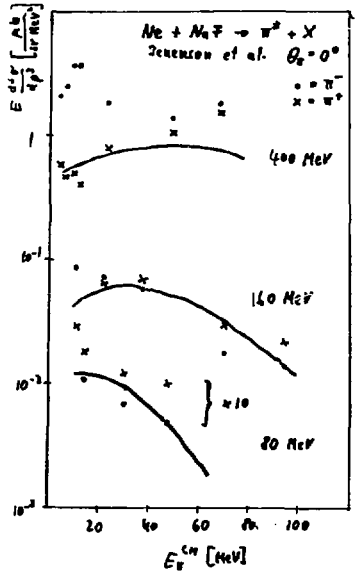

Fig. 2.

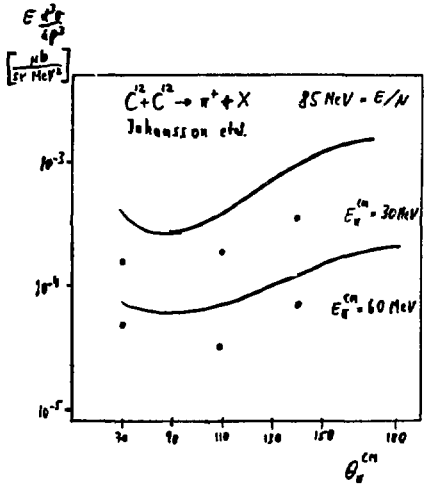

Fig. 3.

DENSITY FLUCTUATIONS IN NUCLEI: CONSEQUENCES FOR RELATIVISTIC HEAVY-ION COLLISIONS

A. Klar and J.P. Vary

Ames Laboratory - DOE and Department of Physics
Iowa State University, Ames, Iowa 50011

The exclusive measurement of all charged particles [1] which emerge from a relativistic heavy-ion collision provides the possibility to observe true many-body correlations in nuclei, because the simultaneous behavior of many nucleons is detected. In contrast with one-particle inclusive or two-particle correlation measurements, these data can be expected to yield more complete information on the A-particle density matrix of the nucleus.

How could possible many-body correlations appear in the nucleus? Our common understanding of the density of the nucleus is based mostly on the knowledge of the single-particle density we deduce from elastic electron scattering. By its nature, electron scattering measures only the behavior of a single particle in each event and the sum over events yields only the one-body density. We can think of this as observing a single particle's behavior while averaging over the behavior of the other particles. So, fluctuations of the total density around a spherical or deformed mean would be smeared out. We conclude that existing constraints on many-body correlations in nuclei are weak.

On the other hand, if there is a true many-body correlation, how could it be seen in the new experiments planned with relativistic heavy ions? We believe the exclusive data obtained event-by-event will contain the necessary information. To illustrate this we report here the results

of a model calculation.

First, we assume that the time scale for the density fluctuations is much longer than the time one nucleus needs to traverse the other. Then we invoke the popular model of abrasion [2] where the overlapping matter supplies the participants to the collision process. Thus, for our present purposes, density excursions will influence the number of participants coming from the projectile and target.

An estimate for the timescales involved could be based on the observation of the typical frequencies for giant resonances. These frequencies fall mostly in the range $\hbar\omega = 50A^{-1/3}$ to $150A^{-1/3}$ Mev. The minimum time associated with these is $T = 2\pi/\omega = 2\pi\hbar A^{1/3}/150 = R\hbar c/25c$ where R is the nuclear radius taken as approximately $1.1A^{1/3}$. This yields a minimum time of about 8R/c and is to be compared with a typical interaction time of about 2R/c for relativistic collisions. We conclude there are opportunities to see these fluctuations in these collisions.

The next question is what kind of effects could be observed? The following is intended as an illustration where we assume a conventional form for the appearance of the fluctuations. We have calculated the number of participants in a geometrical abrasion picture for the relativistic collision of ^{238}U on ^{238}U. From electromagnetic properties the one-body density is inferred to have a deformation $\beta = 0.25$. For the purpose of this illustration we have assumed a deformation of 0.6 and a spherical shape as representative of the excursions that the total density may take. With deformation the numbers of projectile and target participants then depend on the relative orientation of the two nuclei. We calculate the participants in an oriented nucleus (signified by $\vec{A}$) with the nucleon-nucleus thickness function signified by $T_{\vec{A}}(\vec{b})$ and and σ_{NN} representing the N-N total cross section via the expressions

$$N_{\vec{A}\vec{B}}^{A}(\vec{b}) = \int d^2s \; T_{\vec{A}}(\vec{b}-\vec{s})\, P_{\vec{B}}(\vec{s})$$

$$P_{\vec{B}}(\vec{s}) = \left[1 - \left(1 - \frac{\sigma_{NN} T_{\vec{B}}(\vec{s})}{B}\right)^{B}\right] \simeq 1 - e^{-\sigma_{NN} T_{\vec{B}}(\vec{s})}$$

and equivalently for $\vec{B}$. By averaging over the relative orientation we obtain the probability, P_{A-B}, that a given difference in participant number occurs. Clearly, for equal on equal spherical nuclei this probability is unity for zero difference in numbers of participants. For two U nuclei deformed by 0.6 we obtain the result shown in the figure. We find a broad distribution with a width of $\sigma = 16$, and a surprisingly long tail. These results will be used as input to calculate more directly observable quantities like exclusive momentum distributions in order to compare with planned experiments.

ACKNOWLEDGEMENTS

This work was supported by the U.S. DOE, contract No. W-7405-Eng-82, Division of High Energy and Nuclear Physics, budget code No. KB-03. One of us (AK) wishes to acknowledge the hospitality of the Lawrence Berkeley Laboratory Nuclear Science Division and the support of Studienstiftung des deutschen Volkes and the support of a NATO postdoctoral fellowship.

REFERENCES

[1] M.R. Maier, H.G. Ritter and H.H. Gutbrod, IEEE Transactions on Nuclear Science, NS27, 42(1980).

[2] J.D Bowman, W.J. Swiatecki and C.F Tsang, "Abrasion and Ablation of Heavy Ions," LBL-2908, 1973 (unpublished).

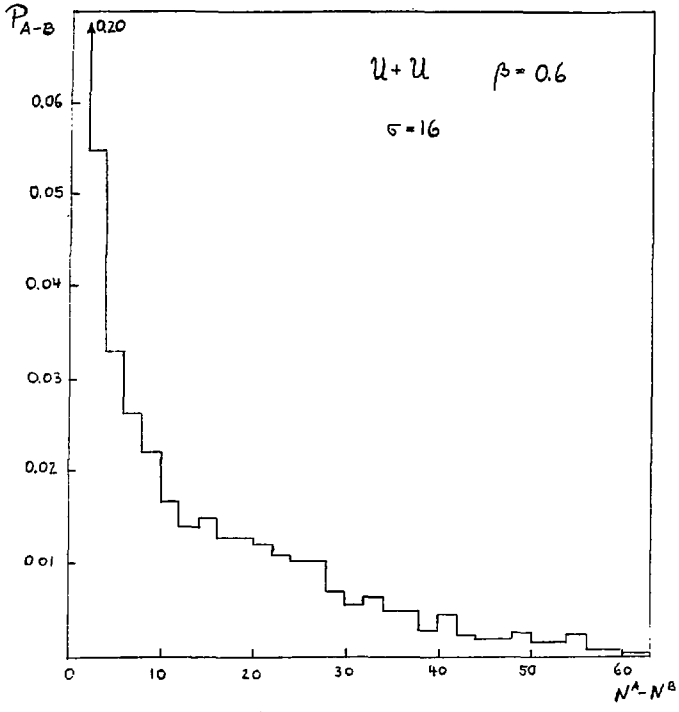

Figure

Probability for occurence of a difference N^A-N^B averaged over orientations of the nuclei, for U+U with β =0.6 .

Subthreshold K^- Production by Coherently Produced ϕ-Mesons in Nuclear Collisions

K.-H. Müller

Nuclear Science Division
Lawrence Berkeley Laboratory
University of California
Berkeley, CA 94720

In quantum field theory mesons like the π, σ, ω, or ϕ meson are described by fields that satisfy Klein-Gordon equations with source terms.[1] These fields do not only describe the virtual mesons inside the colliding nuclei during a heavy ion collision[2] but also the emission of real mesons due to the deceleration of the nucleons during such a reaction. While the σ and ω-mesons decay into pions that might be difficult to be detected in the background of pions produced via decaying Δ's, the ϕ-meson has the nice property of decaying with 47% probability into a K^+K^--pair. Recently A. Shor et al.[3] detected a surprisingly large number of subthreshold K^- mesons in the reaction ^{28}Si-^{28}Si at 2.1 GeV/nucleon. If one tries to explain these K^--mesons by the nucleon-nucleon K^- production cross section in the impulse approximation one underpredicts the measured cross section by a factor of 30.

We shall show in this contribution that there exists the possibility that these K^--mesons are created via coherently produced ϕ-mesons.

The equation that describes the vector meson ϕ of mass m_ϕ coupling to the nucleon current is in the Lorentz gauge:

$$(\Box + m_\phi^2)\, \phi_\mu(\vec{x},t) = g_\phi\, \bar{\Psi}(\vec{x},t)\, \gamma_\mu\, \Psi(\vec{x},t) \qquad (1)$$

Ψ is the nucleon field and g_ϕ the coupling constant.

To determine the number $n_{\vec{K}}^{(\alpha)}$ of ϕ-mesons with momentum K and polarization α emitted in a heavy ion collision we first assume the recoupling of the ϕ-radiation to the source to be negligible and second that the nucleons move on classical trajectories so that the nucleon current $\bar{\Psi}\Gamma_\mu\Psi$ becomes a c-number. We obtain

$$n_{\vec{K}}^{(\alpha)} = \frac{g_\phi^2}{2E\Omega}\left| U^{\mu(\alpha)} \tilde{\tilde{j}}_\mu(\vec{K},E)\right|^2 \qquad (2)$$

Here $\tilde{\tilde{j}}_\mu$ is the Fourier transformed current, $U^{\mu(\alpha)}$ the polarization vector, E the on-shell energy of the ϕ-meson and Ω a normalization volume. Including the decay of the ϕ into a relative p-state K^+K^--pair, we obtain the following invariant cross section for K^- production.

$$E\frac{d^2\sigma}{p^2dpd\Omega} = \frac{.47}{(2\pi)^2} g_\phi^2 \int db\, b \int \frac{d^3K}{2E} \sum_\alpha W_\alpha(\vec{P},\vec{K}) \left| U^{\mu(\alpha)} \tilde{\tilde{j}}_{\mu,b}(\vec{K},E)\right|^2 \qquad (3)$$

$\vec{P}$ is the c.m. momentum and E the c.m. energy of the K^--meson. $W_\alpha(\vec{P},\vec{K})$ is the probability per invariant phase space interval $\frac{d^3P}{E}$ that the decaying ϕ produces a K^- of momentum $\vec{P}$. The nucleon current depends of course on the impact parameter b.

If we restrict the momenta of the produced ϕ-mesons to momenta whose wavelengths are larger than the size of the reaction zone ($K \lesssim 1.5\ fm^{-1}$) we can talk about coherent ϕ-meson production and the production mechanism depends only on the average participant single nucleon density and not on the intrinsic granulate structure. This restricts the c.m. momentum of the K^--meson to a maximum value of about 300 MeV/c.

For the nucleon current we choose a simple fireball type of parametrization. During the initial stage of penetration the participant nucleon distribution is approximated by the sum of two Gaussian functions approaching with a certain velocity. After complete overlap is reached the Gaussian participant distribution starts to expand corresponding to nucleons whose velocities obey a Maxwell distribution. The temperature chosen is that given by the experimental proton spectrum. Figure 1 shows the predicted invariant K^--production cross section of Eq. (3) in comparison with the experimental value. The solid curve shows the case where we assumed a constant velocity of the two penetrating Gaussian distributions, namely the initial velocity. The dashed curve one gets taking into account fluctuations in the number of participants due to binomial distributions. Figure 2 displays the predicted subthreshold K^--invariant cross section at $p_{K^-}^{cm}$ = 60 MeV/c and ϑ = 0° at different bombarding energies. Even at 1 GeV/nucleon a large number of K^--mesons are to be expected.

We have demonstrated that there is the possibility of coherent ϕ-meson production in nuclear collisions. The interesting aspect of this model is that one can learn about the nuclear dynamics $j_\mu(\vec{x},t)$ by measuring more extensively subthreshold K^--mesons at small momenta.

This work was supported by the Deutsche Forschungsgemeinschaft, West Germany, and by the Director, Office of Energy Research, Division of Nuclear Physics of the Office of High Energy and Nuclear Physics of the U.S. Department of Energy under Contract DE-AC03-76SF00098.

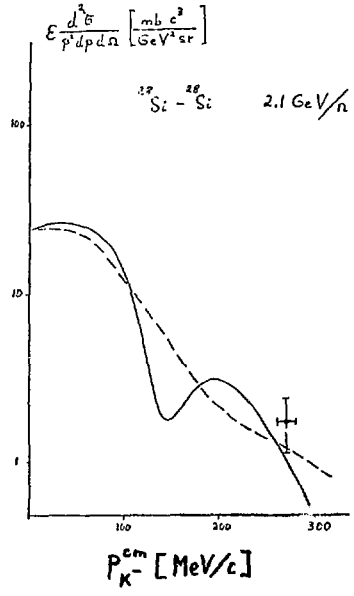

Fig. 1

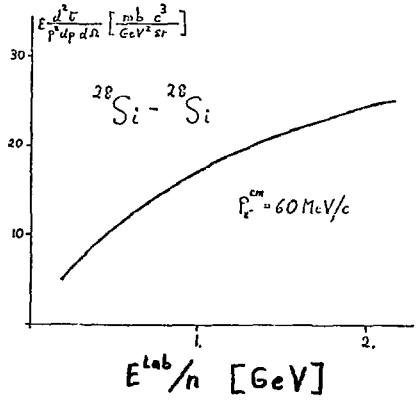

Fig. 2

References

1) J.D. Walecka, Ann. Phys. 83 (1974) 491

2) K.-H. Müller, Nucl. Phys. A372 (1981) 459

3) A. Shor, et al., submitted to Phys. Rev. Lett.